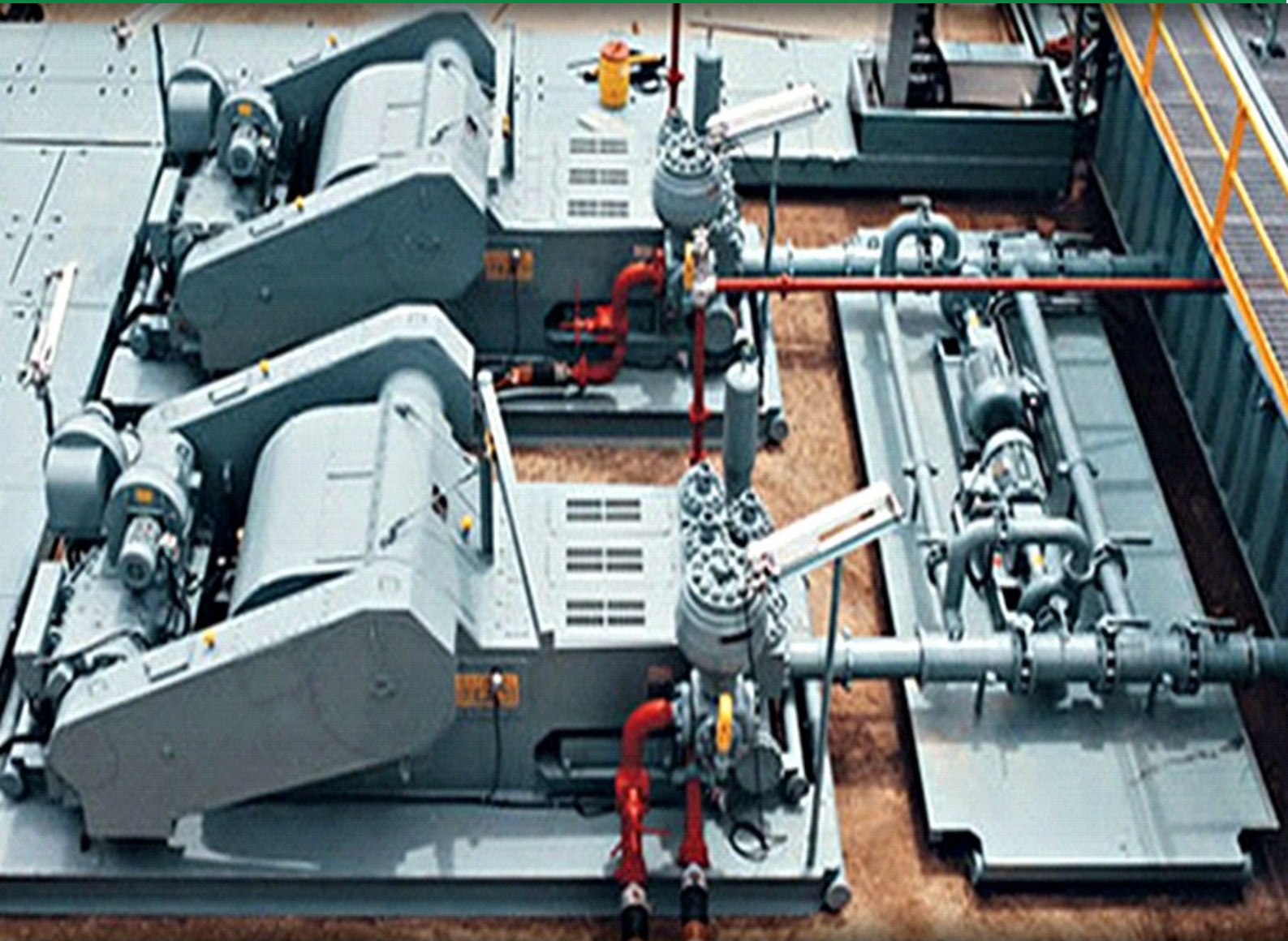


PÅL SKALLE

DRILLING FLUID ENGINEERING



Pål Skalle

Drilling Fluid Engineering

Contents

1.	Introduction	8
1.1	Nine distinct mud systems	8
1.2	The five main tasks of a drilling fluid	9
1.3	About this book	10
2.	Mud circulation loop and its components	11
2.1	The mud loop	11
2.2	The mud pump	14
3.	Drilling fluid viscosity control	16
3.1	Clay chemistry	16
3.1.1	Structure of Montmorillonite	17
3.1.2	Interaction between clay particles	19
3.2	Polymer chemistry	21
3.2.1	Fundamental structure of polymers	21
3.2.2	Classification of polymers	23
3.3	Rheology of drilling fluids	24
3.4	Additives	28
3.4.1	Viscosity control	28
3.4.2	Fluid loss control	30
3.4.3	Friction reducers	30
3.4.4	Summary of additives	31

4.	Hydraulic friction in the circulating system	32
4.1	Head loss	33
4.2	Laminar flow	34
4.2.1	Pipe flow	34
4.2.2	Annular flow	40
4.2.3	Shear rate and effective viscosity	44
4.2.4	Laminar pressure loss example	45
4.3	Turbulent pipe flow	46
4.4	Singularity losses	50
5.	Removal of cuttings from under the bit	55
5.1	Cuttings removal process	55
5.2	Boundary conditions of the drilling process	57
5.2.1	Friction loss increases with depth	57
5.2.2	Annular flow velocity limitations	59
5.3	Optimizing ROP, liner by liner	60
5.4	Optimizing the complete well	63
6.	Transport of cuttings to the surface	68
6.1	Hole cleaning in vertical wells	68
6.1.1	Slip velocity of perfect spheres	68
6.1.2	Slip velocity of imperfect spheres	71
6.2	Hole cleaning in inclined wells	74
6.2.1	Mechanistic model	75

6.2.2	Empirical model	79
6.2.3	Effect of barite segregation	80
7.	Keeping wellbore within maximum and minimum pressure; ECD-control	82
7.1	Density control	83
7.2	ECD factors	85
7.2.1	Mud density vs. temperature and pressure	85
7.2.2	Annular friction	85
7.2.3	Effect of cuttings	86
7.2.4	Surge & swab	88
7.2.5	Other effects	89
7.3	Temperature variation	91
7.3.1	Ocean and wellbore temperature profile	91
7.3.2	Conduction	93
7.4.3	Convection	94
7.4.4	Numerical solution	95
8.	Keeping the wellbore stable	97
8.1	Wellbore stability problems	97
8.2	Filtration control	98
8.3	Mechanical stability	101
8.4	Chemical stability	102
8.4.1	Swelling of shale	103
8.4.3	Bit balling	104
8.3.4	Downhole problems	105

8.5	Inhibitive muds	105
8.5.1	Oil based muds (OBM)	105
8.5.2	Water based mud (WBM)	109
9.	References	112
10.	Supportive information	113
10.1	Nomenclature	113
10.2	Abbreviations and explanations	116
10.3	Definitions	117
10.4	Continuity, momentum and energy equation in microscopic and macroscopic form	118
10.5	Hydraulic friction loss equations	120
10.6	Determine Rheological Constants – Regression Analysis	120
10.7	Unit conversion factors	125
10.8	Viscosity and density of liquids vs. temperature	125
	Endnotes	126

1. Introduction

The simplest drilling fluid is a dirty mixture of water and clay, often referred to as mud. The drilling fluid in the drilling process can be seen as the equivalent to the blood in the human body, the mud pump is the heart, and the drilled out shale (cuttings) represent the slag products. At the surface, we find the mud cleaning system which corresponds to the kidney. Here the cuttings are removed by means of a sieve, the shale shaker.

Mud is a fluid (water or oil) circulated to bring cuttings out of the wellbore. Two important qualities of the fluid are needed for mud to achieve all its tasks:

- **Viscosity:** Water and oil has a viscosity of around 1 cP (centiPoise), which is far too little to transport the cuttings out. A component is needed to increase the viscosity. The main viscosifiers are clay and polymer, presented in Chapter 3.
- **Density:** Water and oil have a density of around 1 kg/l, which in most cases is too little to counter high pore pressure. It may in fact become twice as high as the hydrostatic water pressure. The main density giver is Barite (BaSO_4), a mineral often found as evaporite (with a specific density of 4.2 kg/l), or, soluble salts (brines).

Clay and polymers react with water, while Barite does not, and is therefore referred to as the inert phase.

1.1 Nine distinct mud systems

For mud to manage its many tasks, a broad range of different fluid systems have been developed. The July issue of World Oil¹ presents all drilling fluids and additives (approximately 5000 different additives). Nine distinct mud systems are defined here. The first seven are water-based, while the eighth is oil-based. The ninth category is a specialized one in which air or gas is the continuous fluid. The 9 categories are:

1. *Non dispersed.* These may consist of spud muds, natural muds and other lightly treated systems generally used for shallow wells or top hole drilling.
2. *Dispersed.* At greater depths or where hole conditions may be problematic, muds are often dispersed, typically by means of lignosulphonates or other deflocculants. These and similar products are also effective filtrate reducers.
3. *Calcium treated.* Divalent cations such as calcium and magnesium, when added to a mud, inhibit the swelling of formation clays and shale, and are therefore added to control sloughing shale, hole enlargement and to prevent formation damage. Hydrated lime, gypsum (calcium sulphate) and calcium chloride are principal ingredients of calcium systems. *Gyp² systems* usually have a pH of 9.5 to 10.5 and an excess gyp concentration of 2 to 4 lb/bbl; *Lime systems* have an excess lime concentration of 1 to 15 lb/bbl and a pH of 11.5 to 12.0.
4. *Polymer.* Muds incorporating long-chain, high-molecular-weight chemicals are effective in increasing viscosity, flocculating muds, reducing filtrate loss and stabilizing the formation. Various types of polymers are available for this purpose, including Bentonite extenders. Bio polymers and cross-linked polymers are also used and have good shear-thinning properties at low concentrations.

5. *Low solids*. This includes systems in which the amount and type of solids are controlled. Total solids should not range higher than about 6 % to 10 % by volume (and clay < 3 % by volume). One primary advantage of low-solids systems is that they significantly improve the rate of penetration.
6. *Saturated salt*. Include several groups: *Saturated salt systems* have a chloride ion concentration of 189 000 ppm. *Saltwater systems* have a chloride content from 6 000 to 189 000 ppm, and at its lower level are usually referred to as *brackish* or *seawater systems*.
7. *Workover*. Completion and workover fluids are specialized systems designed to minimize formation damage, and be compatible with acidizing and fracturing operations (acid soluble) and capable of inhibiting swelling clays that reduce formation permeability. Density is obtained through dissolved salt to avoid long term settling.
8. *Oil/synthetic*. Oil-based fluids are used for high temperature wells, deviated holes and wells where pipe sticking and hole stabilization is a problem. They consist of two types of systems:
 - (1) *Invert emulsion muds* are water-in-oil fluids and have water as the dispersed phase and oil as the continuous phase. They may contain up to 50 % water in the liquid phase. Emulsifier (commonly fatty acids amine derivatives, high-molecular-weight soaps), and water concentrations are varied to control rheological and electrical stability;
 - (2) Synthetic fluids are designed to duplicate the performance of oil-based muds, without the environmental hazards. Primary types of synthetic fluids are esters, poly alpha olefins and food grade paraffin. They are environmentally friendly, can be discharged offshore and are non-sheening and biodegradable.
9. *Air, mist, foam and gas*. Four basic operations are included in this specialized category according to the IADC. These include (1) Dry air drilling, which involves injecting dry air or gas into the wellbore at rates capable of achieving annular velocities that will remove cuttings; (2) Mist drilling involves injecting a foaming agent into the air stream, which mixes with produced water and lifts drill cuttings; (3) Stable foam uses chemical detergents and polymers and a foam generator to carry cuttings in fast-moving air stream; (4) Aerated fluids rely on mud with injected air (which reduces the hydrostatic head) to remove drilled solids from the wellbore.

1.2 The five main tasks of a drilling fluid

Mud has many important functions and corresponding necessary properties. Chapter 5, 6, 7 and 8 will take you through the four most important ones.

Task 1 and 2: The single most important function is to remove the cuttings away from under the bit and transport them from the bottom to the surface. Flushing the cuttings from the bottom requires a high flushing effect. This is achieved by inserting small jet nozzles in the rock bit and thereby creating a large pressure drop. Typically 50 % of the pump pressure is placed here for this very purpose. The other 50 % is pure friction loss through the thin, long drill string, and the concentric hole between the wellbore and the drill pipe. The wellbore is created by the drilling bit, and the concentric hole is referred to as the annulus.

Friction loss is an important part of Task 2, but is studied separately in Chapter 4. Here it will be revealed that the viscosity of drilling fluids is not a constant parameter for a given drilling fluid; it varies with shear rate (which is created by pump flow rate). Viscosity of the mud is in fact surprisingly high at low pump rates, but decreases with increasing flow rates.

Task 3: Pump pressure loss in the annulus has an additional importance compared to other friction drops. Annular friction pressure adds itself onto the hydrostatic wellbore pressure, and may create difficult conditions from time to time. This topic will be discussed in Chapter 7.

Task 4: Maintain a stable wellbore. This task includes many sub tasks, like chemical stability, mechanical stability and filtration control. Chapter 8 will reveal the details.

The drilling fluid must be designed to take care of other tasks also, such as;

- Cool and lubricate the bit and the drill string
- Avoid losing mud into natural or induced cracks
- Bring information back to the surface

1.3 About this book

This book aims to present the procedure on how to apply fluid mechanics on drilling challenges related to drilling fluids, and to explain the related physics involved and the engineering approaches. All students with an interest in Petroleum Engineering can read this book without special preparations.

This book does not refer to any papers. Papers often deal with too specific information which at some stage tends to be outdated. Most of the information in this book is found in textbooks and web pages from major oil companies and major drilling fluid service companies. Many of the companies have their own Best Practices Manuals. Details about Pressure Control are found in such textbooks and manuals. See References for details.

2. Mud circulation loop and its components

Mud is circulated through a wellbore to bring the cuttings to the surface. Here cuttings are separated out so that clean mud can be reinjected into the well.

2.1 The mud loop

The circulation system is presented in Figure 2-1 as an example from a fixed drilling platform, while Figure 2-2 presents the circulation system from another view; on a floating drilling unit. Here mud is mixed and prepared in the mud pits consisting of several large tanks, each typically 60 m³ large. One or two of the tanks are in active use for mud circulation, while the others are for transfer and storing. One reserve pit is for kill mud, where density is kept typically at 0.25 kg/l above the density in the active pits. Both density and rheology are maintained in the active mud pits. Typical total volume of a mud pit is 200 m³, with a surface area of typically 50 m². A vertical height of two cm corresponds to a volume of 1000 liters! In the surface mud system in Figure 2-1, we see two pumps in parallel. On offshore rigs it is more common with three.

From the pumps, a high-pressure output line leads up to the drill floor, where, on the standpipe, a multi purpose junction is made, called the standpipe manifold. Here the driller can read the standpipe pressure, which is almost identical with the pump pressure, reduced only by pipe friction in the short distance between the pump and the standpipe manifold.

On its return to the surface, the mud is directed through a wide settling tank, where the largest particles are allowed to settle out: On other rigs this tank is called the sand trap, positioned in front of the shale shakers as an overflow tank.

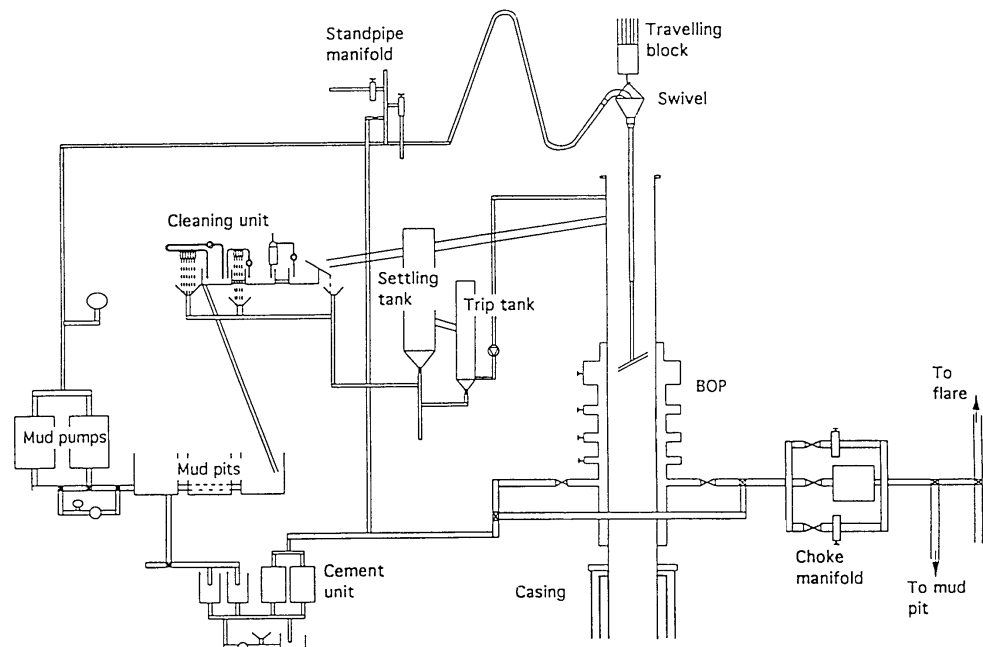


Figure 2-1: The surface mud flow path and the cleaning unit. For cementing operations and for killing operations the smaller cement pump is applied.

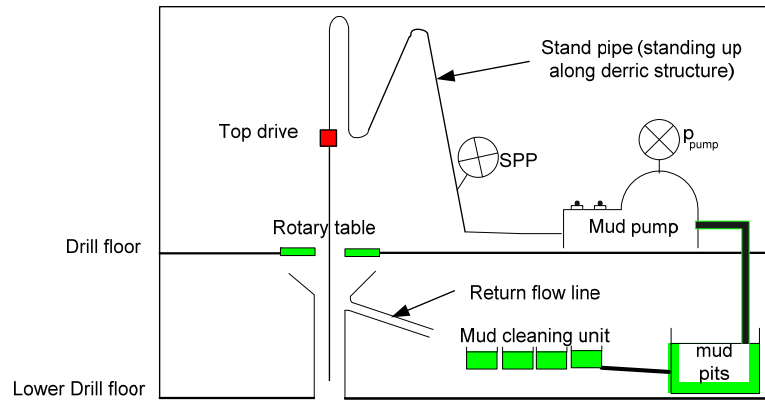


Figure 2-2: Mud circulation system on a floater.

Drilled out solids are separated from the drilling fluid and discarded in the mud-cleaning system. Figure 2-3 presents a typical mud-cleaning unit.

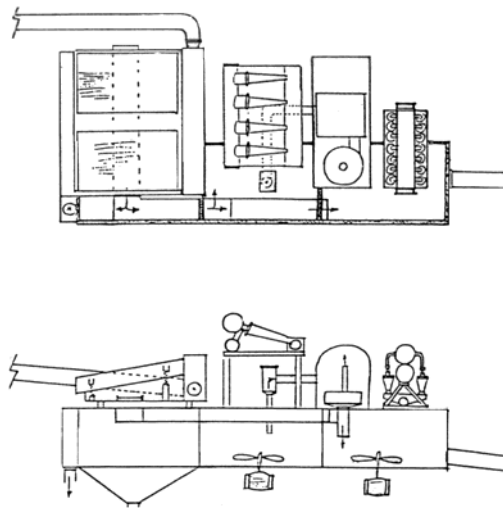


Figure 2-3: Horizontal and vertical projection of a mud cleaning unit.

In a complete mud cleaning system, the following cleaning methods may be included:

1. Settling
2. Dilution
3. Mechanical separation
4. Chemical treatment

Each method exhibits certain advantages and disadvantages. The most efficient form of solids control is a combination of several methods. Settling can remove particles down to colloidal size, but settling is time consuming and impractical. Mechanical separation can remove particles of sizes down to 5 μm as shown in Table 2-1.

Table 2-1: Mechanical cleaning equipment

Shale shaker	Can remove solids > 68 μ (200 mesh)
Desander	Dependent on size of the cone, can remove solids > 30 μ
Desilter	Dependent on size of the cone, can remove solids > 15 μ
Centrifuge	Can remove colloidal solids > 5 μ

Shakers are the most common cleaning method. With the quality and fineness of shaker filter screens available to day, other cleaning methods have become almost obsolete. With a 60 mesh and a 300 mesh filter screen in series, 99 % of the cuttings are removed. A 60 mesh filter screen removes the largest cuttings and protects the extremely fine second filter screen from wear and tear. The Mesh - size system is presented in Table 2-2.

Table 2-2: Important parameters for square Mesh shakers (#Mesh # = of openings pr. inch).

Mesh	Wire Diameter	Opening Width	Smallest particle size removed
	Inches	Microns	Microns
8	.0280	2463	2200
10	.0250	2108	2000
20	.0160	863	800
50	.0090	279	250
60	.0072	230	205
100	.0045	140	125
120	.0037	117	105
200	.0030	74	68
325	.0018	44	40

One issue with fine filter screens is filter screen wear. Filter screen monitoring and maintenance is required.

2.2 The mud pump

Pumping drilling fluids through kilometre long pipe systems will result in large hydraulic friction, and correspondingly powerful mud pumps are required. One typical pump is shown in Figure 2-3.

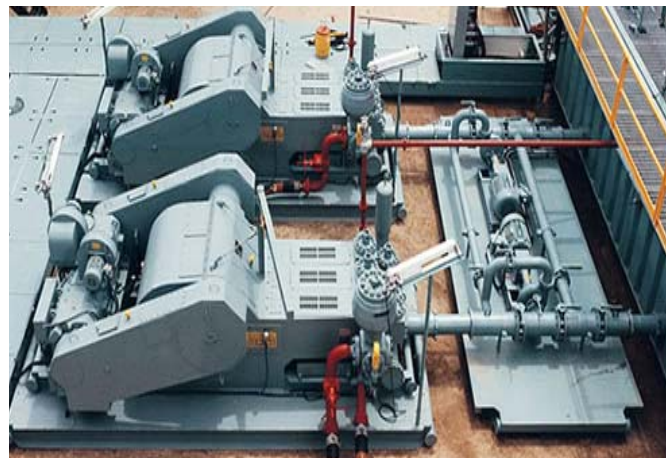
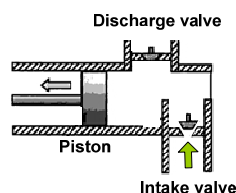


Figure 2-3: Two blue painted triplex (three triplex means three pistons working in parallel) single acting piston pumps. Single acting means acting only during one of the two stroke directions. One such piston is shown to the left.

When it comes to hydraulic friction and to Task 1, removal of crushed cuttings, it will be necessary to know the characteristics of a mud pump. Figure 2-4 shows the pumps characteristics. The pump is limited by its maximum pressure, p_{\max} , for each liner size $(p_p)_{\max}$, its maximum flow rate for each liner size, q_{\max} , and its maximum effect $(E_p)_{\max}$ (the latter is the same for all liners). The pump characteristics are divided into two different operating ranges: Range I is defined through the pump's smallest liner, and range II includes the rest of the liners. Table 2-2 presents a typical pump characteristic for large sized mud pumps.

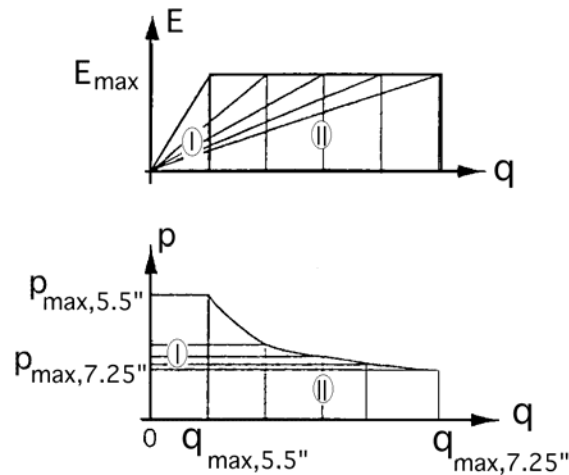


Figure 2-4: Pump characteristics. The two numbers I and II indicate the two operating ranges of the pump. Range I is represented by the smallest liner, in which the pump pressure can be manipulated to be held constant if desired, for instance at the maximum recommended pressure for the 5.5” diameter liner.

Table 2-3: Characteristics of a 1600 Hp mud pump, rated at 120 SPM (max is 140).

Parameter:	Unit:	Liner:							
		5 1/2	5 3/4	6	6 1/4	6 1/2	6 3/4	7	7 1/4
Liner size	in								
Discharge pressure	psi	5555	5085	4670	4305	3980	3690	3430	3200
	bar	383.0	350.6	322	296.8	274.4	254.4	236.5	220.6
Pump flow rate	GPM	444	486	529	574	621	669	720	772
	m ³ /s	0.0215	0.0307	.0334	.0362	.0392	.0422	.0454	.0487
Power	Hp	1439.0	1441.8	1441.3	1441.7	1442.0	1440.3	1440.8	1441.3

The effect of the pump is equal to approximately 2000 Hp when running at its maximum design speed (140 spm). It is recommended to run it at a lower maximum, e.g. 120 spm. The resulting effect, 1440 Hp, is also the nominal effect of the pump. The pumps effect can be expressed in SI units or in OFU (Watt (W) or Horsepower (Hp) respectively):

$$E_{pump} = q \cdot p_{pump} \quad (W) \tag{2.1}$$

To obtain effect in horsepower (Hp) when applying OFU, q is given in GPM and p in psi:

$$E_{pump} = \frac{q \cdot p_{pump}}{1714} \quad (Hp) \tag{2.2}$$

Other useful conversions are presented in Chapter 10.5.

3. Drilling fluid viscosity control

Clay and polymers play an important role in drilling fluid viscosity control and are therefore given special attention here. Clay plays in addition a central role for wellbore stability (Chapter 8).

3.1 Clay chemistry

The group of minerals classified as clays can be described chemically as aluminium silicates. Since the elements that constitute the clays account for more than 80 % of the earth mass (aluminium 8.1 %, silicon 27.7 % and oxygen 46.6 %) it can be readily accepted that every stage of drilling a hole brings us in contact with clay. Clay and shale thus account for more than 75 % of all sediments. Type and quantity of clay minerals is one of the most important features for chemical and mechanical properties of sedimentary rock. A compositional example of sediments vs. depth is shown in Table 3-1.

Table 3-1: Mineralogy of typical sediments at different depths. Top of the reservoir starts at 2 400 m. Mineralogy is presented in %.

Depth (m)	2 000	2 200	2 400	2 600	2 800
Quartz	10	15	55	40	75
Feldspar	12	15	8	10	6
Calcite	11	-	2	10	5
Pyrite	5	-	2	10	4
Smectite	22	25	8	5	-
Illite	22	25	10	10	5
Chlorite	10	5	6	-	-
Kaolinite	8	15	10	15	5
CEC ³	28	22	14	8	3

The selection of the drilling fluid is often related to the reactions between the fluid and the rock, as these reactions can influence the stability of the bore hole. Thus, an understanding of clay is important both in the selection of a drilling fluid system and for the optimization of bore hole stability. The most important clay properties for a drilling fluid engineer are shown in Table 3-2.

Table 3-2: Properties of common clays.

Property	Kaolinite	Mica	Montmorillonite	Attapulgite	Chlorite
<i>Crystal structure</i>	sheet	sheet	sheet	sheet	sheet
<i>Particle shape</i>	hexagonal plate	extensive	flake	needle	plate
<i>Particle size, μm</i>	5-0.5	plates	2-0.1	1-0.1	5-0.1
<i>Surface Area:</i>					
<i>BET-N₂, m²/g</i>	15-25	10 ⁵ -0.5	300-800	200	140
<i>BET-H₂O, m²/g</i>	3-15		200-800	-	-
<i>CEC, meq/100 g</i>	-	10-40	80-150	15-25	10-40
<i>Viscosity in water</i>	Low	Low	High	High	Low
<i>Effect of salt</i>	Flocculates	Flocculates	Flocculates	None	Flocculates

Bentonite is the generic name applied to a mixture of minerals that predominantly contains the mineral Montmorillonite. The associated minerals are typically other clays, such as mica, kaolinite and quartz. Clay is often formed by the *in situ* alteration of volcanic ash in the presence of water. The salinity and chemical composition of water and ash can give rise to different types of clay.

3.1.1 Structure of Montmorillonite

Montmorillonite is an aluminium silicate, in which the silicon-oxygen sandwich is a layer of aluminium hydroxide, as shown in Figure 3-2.

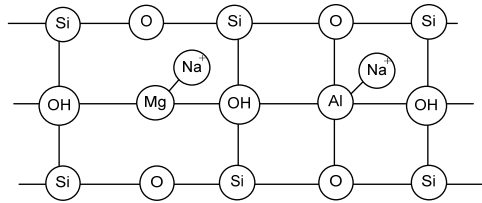
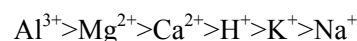


Figure 3-2: A principle and simplified structure of one unit layer of Montmorillonite, 10 Angstroms thick.

Three essential characteristics of this crystal are responsible for the special properties of Montmorillonite:

1. Some of the aluminium in the lattice structure are, during creation, replaced with ions of a lower charge (electron valence) such as magnesium (from 3 to 2). The *substitution*, without any other change of structure, creates negative surface charges in the lattice.
2. The negative charge sites created in the clay sheet by magnesium substitution are partly balanced by close association of positively charged ions (cations), normally Na^+ . When the negative charge arises in the aluminium layer, the silica layers act as a barrier that prevents effective neutralisation of either the cations or the charge sites on the clay surface. The creation of these charged ions and charged clay surfaces creates very strong attractive forces for polar water molecules that readily force themselves in between the unit layers. The unique feature of Montmorillonite is thus potential for the individual sheets to separate as more water is attracted. In other clay minerals, the bonds formed between unit layers are stronger and they do not separate. One clay particle consist normally of hundreds of stacked unit layers.
3. The loosely held cations give rise to the property known as the *cation exchange capacity*. The attached ions can be exchanged or replaced by other ions present in the surrounding water. The ability of one type of cation to replace another depends on the nature of the involved cations and their relative concentrations. The common cations will replace each other (when present in equal concentration) in the following order:



The cation exchange capacity (CEC) is easily determined by measuring the adsorption of a cationic organic dye called methylene blue.

The nature of the cations in the exchange positions can effect the hydration properties of the mineral. The most common exchangeable cations are sodium and calcium. The sodium ion has only one single positive charge. In a Montmorillonite only containing sodium exchangeable ions, the clay has a capacity for infinite expansion and even separation of the sheets down to single sheets, which are only 10 Angstroms thick. A multivalent ion, such as calcium (valence = 2), associates with two sheets, so the expansion is limited to a maximum spacing between the sheets of about 17 A, see Figure 3-3.

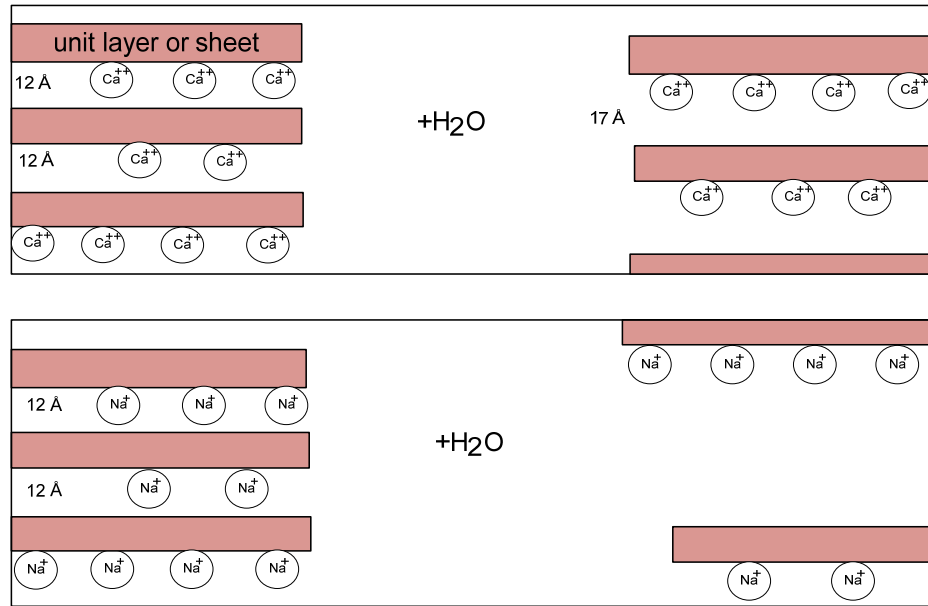


Figure 3-3: Hydration of Calcium Montmorillonite (upper) and Sodium Montmorillonite (lower)

3.1.2 Interaction between clay particles

The forces acting on the clay particles can be described as either repulsive or attractive forces. The particles may interact due to Brownian motion. Whether they will agglomerate or not will depend on the summation of the repulsive and the attractive forces.



Repulsive electrical forces

The clay particles have been described as small crystals that have a negative surplus charge (a partly compensating charge is provided by the ions in solution that are electrostatically attracted to the surface). When two negatively charged particles approach each other, there will be a repulsion between the particles that will become larger the closer the particles approach each other.

However, since thickness of the electrostatic layer can be compressed by electrolytes, then, as the electrolyte (dissolved salt) level is increased, the particles can more easily approach each other, as shown in Figure 3-4.

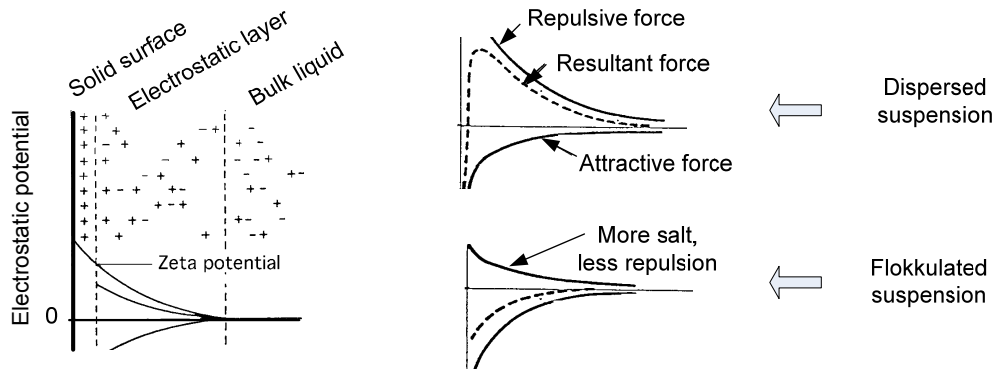


Figure 3-4: Bulk solution is neutral. Salt compresses the electrostatic layer and affects the attractive and repulsive forces between clay particles.

Attractive van der Waals forces:

van der Waals forces arise through the attraction of the spontaneous dipoles being set up due to distortion of the cloud of electrons around each atom. This is illustrated in Figure 3-5. For a large assemblage of atoms, such as in a clay platelet, this force can be significant as it is additive. The attractive force decays very rapidly with distance; inversely proportional to the distance cubed ($1/d^3$), but it is essentially independent of the electrolyte concentration.

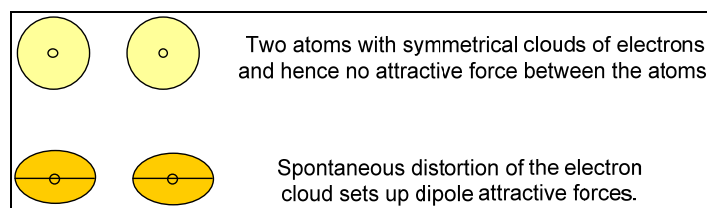


Figure 3-5: Illustration of the origins of van der Waals attractive forces in any two material close to each other.

Resulting associations

The associations between clay particles are caused by repulsive/attractive forces and are important as they affect important properties, such as viscosity, yield and fluid loss, exemplified in Figure 3-4 and 3-6. The terms describing the associations are as follows:

Deflocculated or dispersed; an overall repulsive force between clay particles, which carry the same net negative charge.

Flocculated Systems; there are net attractive forces between the particles.

Aggregated Systems; the clay consists of a basic sheet structure or unit layer, and the crystals consist of assemblages of the sheets, one upon the other.

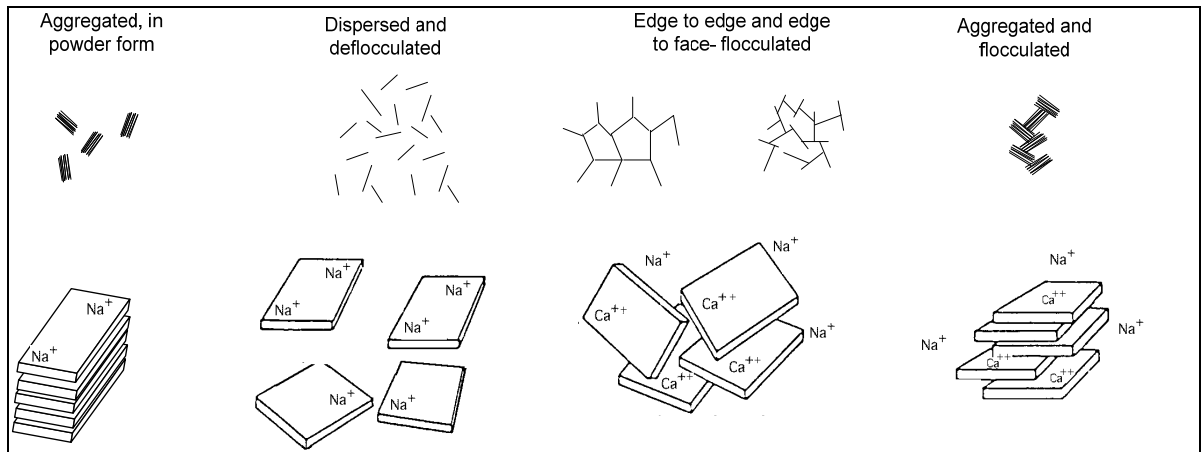


Figure 3-6: Modes of particle association of clay.

3.2 Polymer chemistry

3.2.1 Fundamental structure of polymers

A polymer consists of basic units (monomers) that are chemically joined together (polymerized), to form chains as shown in Figure 3-7.

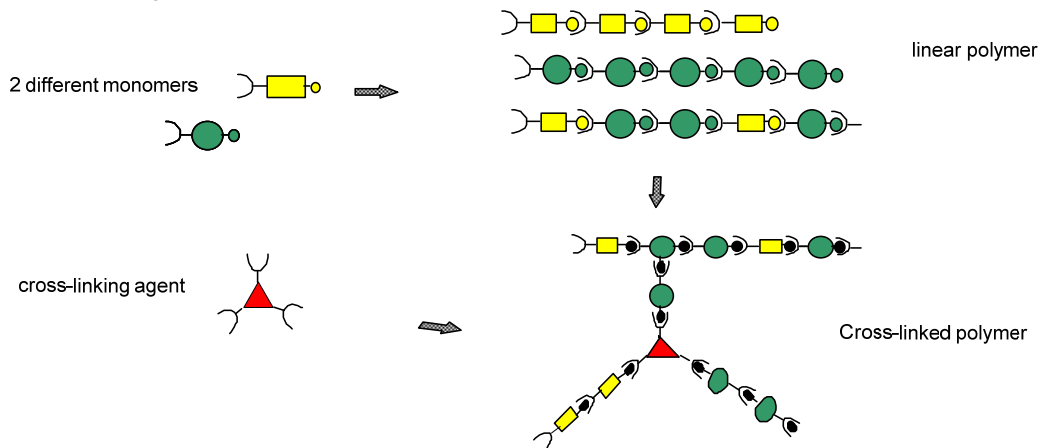


Figure 3-7: Fundamental polymer structure.

The molecular weight (MW) or chain length can be impressively long, up to 50 millions! Assuming a typical monomer diameter is 7 Å, a 50 million MW polymer is 3.5 cm long. Polymers can be divided into three groups; non-ionic, anionic (-) and cationic (+). More than one type of monomer group may be present in the same molecule. Since the groups are either weakly basic or acidic, the charged nature of most of the groups is dependent on the pH value of the drilling fluid and will change from non-ionic to cationic or anionic respectively (just like charged clay).

The ionic strength of the fluid affects the electrostatic repulsion between the charges. An increased level of electrolyte will change the balance between the repulsive and attractive forces and allows molecules of equal charges to approach each other. A negatively charged polymer will change its configuration from an extended polymer in fresh water, where charge repulsions are stretching the molecule, to a tightly-coiled structure in a saline solution, where the repulsive forces are lower. This is shown schematically in Figure 3-8. The change in molecular shape will change the physical properties of the polymer in the solution. The coiled up polymer will present a smaller surface for interacting with the water or with other polymer molecules, and thus produce lower viscosity. A non-ionic polymer should be essentially unaltered by salt.

Multivalent ions can act as bridging agents by reacting with more than one charged group on the molecule. Unhydrated cement will feed the drilling fluid with soluble calcium ions and a high alkalinity (pH > 7). Calcium ions (Ca^{++}) react with anionic (-) polymers such as CMC and cause bridging or flocculation. The extent of the reaction is a function of the concentration of the double valent ions and of the pH of the solution.

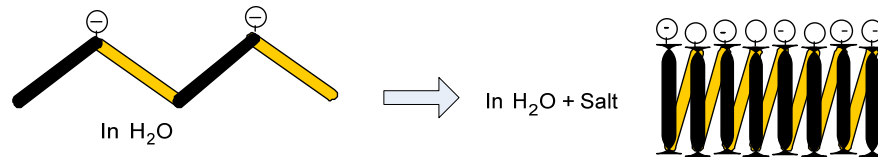


Figure 3-8: Effect of electrolyte concentration on polymer configuration.

3.2.2 Classification of polymers

A rough classification of polymers and some of its associated properties are:

- A. Synthetic polymers
 1. Copolymer, like Vinylacetat-meleic-anhydrid (VAMA).
 2. Polyakrylonitril, like PHPA = partially hydrolyzed polyacrylacetat
- B. Natural polymers (polysaccharides)
 1. Cellulose
 - a) CMC (Sodium Carboxylmetyl cellulose). From wood pulp. Anionic.
 - b) HEC (Hydroxyletyl cellulose). Non-ionic
 - c) PAC (Poly-ionic cellulose)
 2. Starch (of corn). Non-ionic.
 3. Guar. Non-ionic.
 4. Biopolymers, like Sugar + microorganisms. X-C-polymers. Weakly anionic. MW = 2 - 50 mill.

The most common applications of polymers are viscosity building: Polymers are applied as viscosifiers simply by dissolving high-molecular-weight-polymers in water. Natural polymers will start to degrade when exposed to heat. Already at 80 °C biocides are required to slow the decomposition rate down. Above 100 °C, natural polymers are difficult to apply, since the rate of adding polymer to maintain viscosity becomes intolerable. As wells becomes deeper, thermal stability becomes an important performance characteristics of polymers. Synthetic polymer-chemistry has made its most significant contribution to the drilling industry in high-temperature / high-pressure applications. From the early 1990's, numerous synthetic polymers proved technically capable and cost effective at high bottom hole temperatures and pressures. Synthetic polymers specifically formulated for deflocculating, fluid-loss-control, and gel inhibition at high temperature proved to have a wide utility. Using WBM at these hostile conditions would have been impossible without natural, modified, and synthetic polymers.

The application of polymers is described more detailed in Chapter 3.4.

3.3 Rheology of drilling fluids

Rheology models and rheology measurements in the drilling industry has been influenced by the 2-speed rotational viscometer (Fann VG meter), which has been applied in the oil field. The objective behind the use of this viscometer was to simplify rheology control in the field. Today, however, as the petroleum industry has evolved in all aspects, the need for higher quality rheology control has arisen. Now a 6-speed viscometer is the norm. Therefore, three different approaches to determine rheology constants are presented:

- 2 data points oil field approach
- 2 data points SI⁴ approach
- 6 data points regression approach

Flow curve or rheogram is a plot of shear stress reading vs. Shear rate obtained in a rotational viscometer. Table 3-3 presents an example of readings, with the corresponding flow curve in Figure 3-9. Due to the geometry and calibration of the Fann VG viscometer the true shear stress, τ_w , is obtained by multiplying the obtained readings with the correction factor of 1.06. This constant is normally ignored (when applying the readings for other models than the Bingham model) and thus the readings (θ) are incorrectly assumed equal to the shear stress (τ_w).

The test results in Table 3-3 and Figure 3-9 will be used to exemplify different rheology models.

Table 3-3: Shear stress readings (θ) in a 6-speed rotational Fann VG viscometer. The two lower data points represent gel strength build up after 10 seconds and 10 minutes quiescence.

Symbol	RPM	θ		$\dot{\gamma}$	τ_w	τ_w
Unit	rpm	(-)		s ⁻¹	lb/100 ft ²	Pa
Data	600	140		1022	148.4	71.05
	300	98		511	103.9	49.75
	200	78		340	82.7	39.60
	100	54		170	57.2	27.39
	6	16		10.2	17.0	8.14
	3	13		5.1	13.8	6.61
	3 _{10"}	23		5.1	24.4	11.68
	3 _{10'}	48		5.1	50.9	24.37

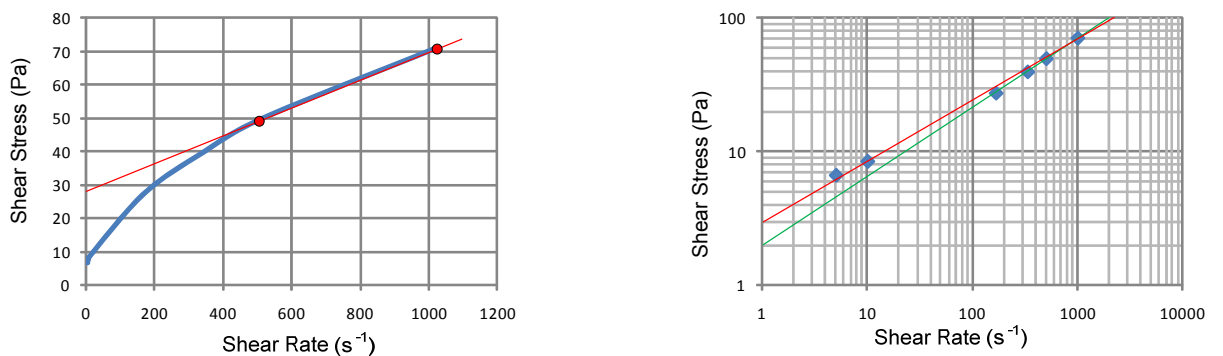


Figure 3-9: Example of flow curve (left). Flow curve in log-log plot (right). Data taken from Table 3-3.

The viscosity of a fluid expresses its resistance to flow. Fluids with a constant viscosity for all shear rates are called Newtonian fluids. Non-Newtonian fluids are those in which the shear stress is not linearly related to the shear rate $\dot{\gamma}$. Shear rate expresses the intensity of shearing action in the pipe, or change of velocity between fluid layers across the flow path:

$$\dot{\gamma} = \frac{dv}{dr} \quad (3.1)$$

Common rheological models are:

Newtonian model: $\tau = \mu\dot{\gamma}$ (3.2)

Bingham plastic model: $\tau = \tau_y + \mu_{pl}\dot{\gamma}$ (3.3)

Power law model: $\tau = K\dot{\gamma}^n$ (3.4)

Herschel & Bulkley model: $\tau = \tau_y + K\dot{\gamma}^n$ (3.5)

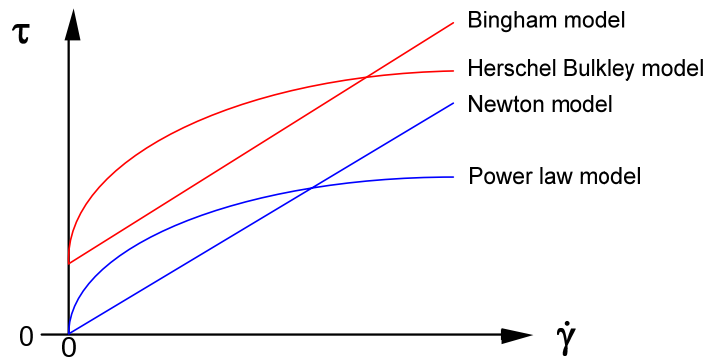


Figure 3-10: The flow curve of four different rheological models (of four different fluid samples).

The principle shape of the four rheological models are shown in Figure 3-10, and their parameters are determined as follows:

Newtonian model; 2 data points SI approach

One constant is sufficient to describe this model. For the Newtonian fluid readings at 300 RPM are selected:

$$\mu_{300} = \frac{\tau_{300}}{\dot{\gamma}_{300}} = \frac{49.75}{511} = 0.09736 \text{ Pas} = 97.36 \text{ cP} \quad (3.6)$$

Bingham model; 2 data points oil field approach:

The Fann VG viscometer is calibrated to suit the Bingham model. The shear rate at 300 is designed to be equal to one shear rate unit, making eqn (3.7) simply a difference between two numbers:

$$\mu_{pl} = \theta_{600} - \theta_{300} = 140 - 98 = 42 \text{ cP} = 0.042 \text{ Pas} \quad (3.7)$$

$$\tau_y = \theta_{300} - \mu_{pl} = 98 - 42 = 56 \text{ lb} / 100 \text{ ft}^2 = 28.8 \text{ Pa} \quad (3.8)$$

Bingham model; 2 data points SI approach

After converting to SI-units and including the conversion factor of 1.06 in Table 3-3, the viscosity is defined by the slope of the curve:

$$\mu_{pl} = \frac{\tau_{600} - \tau_{300}}{\dot{\gamma}_{600} - \dot{\gamma}_{300}} = \frac{71.05 - 49.75}{1022 - 511} = \frac{21.3}{511} = 0.04168 \text{ Pas} \quad (3.9)$$

The yield point is found by solving eqn (3.3) :

$$\tau_y = \tau_{600} - \mu_{pl} \cdot \dot{\gamma}_{600} = 71.05 - 0.04168 \cdot 1022 = 28.45 \text{ Pa} \quad (3.10)$$

Note that oil field and conventional SI procedures give almost identical results; an error of around 1 % for both constants. Without including the 1.06 factor the results would become: $\mu_{pl} = 0.0394$, $\tau_y = 26.8$. This represents an error of 6 % for both constants.

Power law model; 2 data points SI approach

In order to find the two constants, take the logarithm of eqn (3.4) for two different data points. Both resulting equations contain n and K. Solving for n yields:

$$n = \frac{\log \tau_{600} - \log \tau_{300}}{\log \dot{\gamma}_{600} - \log \dot{\gamma}_{300}} = \frac{\log \frac{\tau_{600}}{\tau_{300}}}{\log \frac{\dot{\gamma}_{600}}{\dot{\gamma}_{300}}} = \frac{\log \frac{71.05}{49.75}}{\log 2} = 3.32 \cdot \log \frac{71.05}{49.75} = \underline{0.514} \quad (3.11)$$

With known n, solving eqn (3.4) for K yields:

$$K = \frac{\tau}{\dot{\gamma}^n} = \frac{71.05}{1022^{0.514}} = \underline{2.2} \text{ Pa} \quad (3.12)$$

After a lot checking the Oil Field Approach we note that n is identical in the two approaches, while K is around 6 lower in the in the Oil Field Approach.

Hershel Bulkley model; 3⁵ data points oil field approach

The yield point is found through either reading τ_y from the flow curve plot after extending it to $\dot{\gamma} = 0$, or simply assuming

$$\tau_y = \tau_3 = 3 \text{ Pa} \quad (3.13)$$

The equation can now be solved in a log-log plot with 3 + 1 (ty) data points. The slope of the line is n, and K can be found through:

$$K = (\tau_2 - \tau_y) / (\dot{\gamma}_2 - \dot{\gamma}_2)^n = (71.05 - 3) / 1017^{0.5} = 0.6$$

Herschel & Bulkley model; 3 data points SI approach

Select the three data points and apply standard iteration procedure to solve the three equations.

6 data points regression approach

One reason for using the two upper data points is the remarkable quality of the Bingham model. It turns out that after long periods of still standing, the gel strength of the fluid approaches the yield point, τ_y (obtained through the two upper readings). This is clearly demonstrated through Table 3-3. After 10 minutes the gel strength has climbed to 48 lb/100 ft², whereas the yield point is 56 lbs/100 ft². But the yield point is therefore true only under such conditions; long stationary periods.

Now a day there is no excuse for not applying all six readings to determine the constants through curve fitting (regression analysis). A detailed description of how to do this is presented in Chapter 10.6.

Other known rheological models are:

$$\text{Collins-Graves} \quad \tau = (\tau_y + K\dot{\gamma}) (1 - e^{-\beta\dot{\gamma}}) \quad (3.14)$$

$$\text{Robertson-Stiff} \quad \tau = K(\dot{\gamma}_y + \dot{\gamma})^n \quad (3.15)$$

$$\text{Casson} \quad \tau = \left[\sqrt{\tau_y} + \sqrt{\mu \cdot \dot{\gamma}} \right]^2 \quad (3.16)$$

These models are in little use in conjunction with drilling fluids.

3.4 Additives

In the next sub Chapter the most common additives are presented and later summarized in Chapter 3.4.4.

3.4.1 Viscosity control

Important viscosity control additives are:



Bentonite extender: A simple method to increase the viscosity of Bentonite suspensions is to extend the Bentonite into a partly flocculated state. Anionic polymers mixed into WBM will react with Bentonite as indicated in Figure 3-11 (Flocculant). For the polymer to function as an extender the molecular weight must be medium high and the concentration in the ultra low range (0.05 – 0.10 PPB).

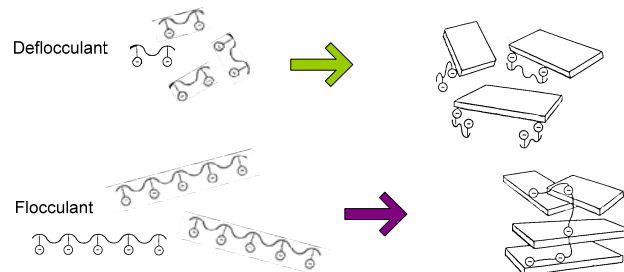


Figure 3-11: Low molecular weight polymers act as deflocculants (upper). High MW polymers act as flocculants. Polymeric flocculants are used in «clear-water» drilling, where the drilled solids are made larger by the flocculants and then removed.

Dispergators: The advantages of maintaining a dispersed mud system are two-fold:

1. Easier to control the viscosity
2. Fluid loss becomes optimal

To maintain a system in a dispersed (deflocculated) state the repulsive forces must be maximised. The negative charges on the clay particles can be maximized in three ways:

a. High pH level:

A pH above 8.0 will increase the number of negative groups on the clay edges. Thus, maintaining an alkaline pH condition with caustic soda will stabilize the clay system. At high pH level, negative charges will predominate.

b. Adding deflocculant or thinner:

There is a wide range of chemicals known as deflocculants or thinners, which have a wide range of chemical structure. However, they can all be described as negatively charged polymers. Figure 3-11 illustrates the mechanism whereby a short chain of negatively charged polymer can neutralise a positive charge on the edge, and thus increase. Then negative groups increase the negative charge density on the clay platelet. Some common chemicals are chrome lingsulphonate, tannin and lignite. Since the deflocculants are reacting with the positive sites on the edges, and the edge surface area is a relatively small proportion of the total, the chemicals can be effective at low concentrations.

c. Fine particles act as dispersants:

Other fine particulate solids, such as calcium carbonate, barites or drilled out fines, are all inert, and will act essentially as physical hinders for clays to flocculate. Such particles are called dispersants.

Flocculants (Clay free/clear water drilling): The process is initiated by creating larger lumps of clay particles as illustrated in Figure 3-11. Then the particles are separated out by means of gravity. Conditions are similar to those mentioned under Bentonite Extension, but polymer concentration must be in the low range (0.1 – 0.3 ppb), added after shale.

3.4.2 Fluid loss control

Fluid loss to permeable formations is reduced through increasing the viscosity of the fluid phase. Non-ionic, low MW polymers are applied, and will therefore become an integrated part of the fluid phase. They do not interact with the solids. The filtrate from filtration tests in the filter press is a surprisingly clear fluid, consisting of water and the fluid loss additives, which are in the size range of molecules.

3.4.3 Friction reducers

Some special polymer suspensions provides much lower friction than the base fluid’s rheology predicts. This is explained by a layer of base fluid being formed along the pipe wall during flowing. When small molecules like polymers are suspended in liquids, they will perform a stochastic movement referred to as Brownian movement. The suspended particles have 6 degrees of freedom, and will normally diffuse equally in all directions. However, close to the wall one freedom of movement is removed, only diffusion away from or along the wall is possible. An additional effect is caused by the shear stress field. The shear stress in the fluid reaches a maximum at the wall, leading to stretching effects of the polymers. The resulting viscosity near the wall will approach the base fluid’s viscosity under certain conditions. Figure 3-12 illustrates the phenomenon, while Table 3-4 summarises the features and friction effects of these special polymer solution.

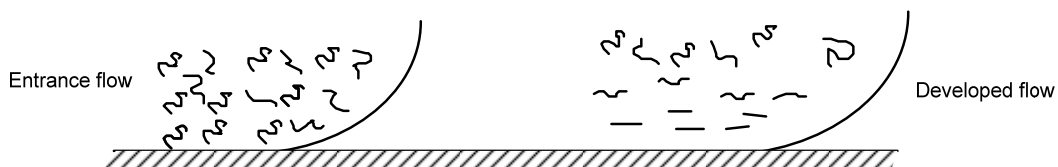


Figure 3-12: Polymers as drag reducers; low viscosity develops at the wall.

Table 3-4: Properties and friction pressure in pipe flow with HEC added to two base fluids.

Mixture No	Composition	Parameter: Unit:	Weight PPG	Pressure drop psi	PV cP	YP lb/100 ft ²
1	Brine of CaCl ₂	Data:	11.0	706	1.5	-
1+	6 ppb HEC		10.8	265	3.5	2.5
2	Base (dispersed Bentonite)	Data:	8.5	548	8.5	8.5
2+	2 ppb HEC		8.4	165	13.0	15.0

3.4.4 Summary of additives

In addition to viscosifiers and to rheology control agents, there are several more groups of additive. We refer to the classification of additives published by World Oil once a year as presented below. They also publish the name and characteristics of more than 3000 additives.

<i>Alkalinity, pH control:</i>	Lime, caustic soda and bicarbonate of soda, control the degree of acidity of a fluid.
<i>Bactericides:</i>	Para formaldehyde, caustic soda, lime and starch preservatives are commonly used to reduce bacteria count.
<i>Calcium removers:</i>	Caustic soda, soda ash, bicarbonate of soda and certain polyphosphates make up the majority of chemicals designed to prevent and overcome the contaminating effects of anhydrite, gypsum and calcium sulphates.
<i>Corrosion inhibitors:</i>	Hydrated lime and amine salts are often added to check corrosion.
<i>Defoamers:</i>	Products designed to reduce foaming action, particularly in brackish and saturated saltwater mud.
<i>Emulsifiers:</i>	Surface active agents create a heterogeneous mixture of two liquids.
<i>Filtrate reducers:</i>	Filtrate, or fluid loss reducers - such as Bentonite clays, CMC (sodium carboxyl methyl cellulose) and pre gelatinized starch – reduces the tendency of the liquid phase of the drilling fluid to pass into the formation.
<i>Flocculants:</i>	Salt, hydrated lime, gypsum and sodium tetra phosphates are used to cause colloidal particles in suspension to group into bunches, or «flocks», causing solids to settle out.
<i>Foaming agents:</i>	Surfactants (foamers) permit air or gas drilling through water-bearing formations.
<i>Lost circulation materials:</i>	Lost circulation additives plug the zone of loss in the formation.
<i>Lubricants:</i>	Oils, graphite, powder and soaps reduce torque and increase horsepower transmitted to the bit by reducing the coefficient of friction.
<i>Pipe-freeing agents:</i>	Detergents, soaps, oils and surfactants are intended to be spotted in an area of suspected pipe sticking to reduce friction, increase lubricity and inhibit formation swelling.
<i>Shale control inhibitors:</i>	Gypsum, sodium silicate and calcium lignosulfonates, as well as lime and salt, are used to control swelling or hydrous disintegration of shale.
<i>Surface active agents:</i>	Reduce the interfacial tension between contacting surfaces (water/oil, water/air, etc.).

4. Hydraulic friction in the circulating system

The objective of estimating hydraulic friction in the circulation system is three-fold:

1. Determine the total frictional loss at its maximum design flow rate, so that the required pump size can be selected
2. Determine pressure loss through the nozzles in the bit to enable determination of optimal nozzle size and thus achieving proper cleaning effect on bottom
3. Establish ECD in the annulus in order to stay inside the pressure window

To reach these goals we rely on three types of knowledge:

- The fluid flow system and drilling engineering operations (Chapter 2)
- Rheology of drilling fluids (Chapter 3)
- The governing equation of fluid mechanics (this Chapter)

We will therefore now go through hydraulic friction losses in pipes and annuli, for laminar and turbulent flow, for three different rheology models;

Newtonian

Bingham plastic

Power law

Not only losses in pipe flow will be covered, but also singularity losses, i.e. losses through sudden expansions or restrictions, like in the rock bit nozzles. Since we are dealing with pipe flow, we apply cylindrical coordinates. The basic equations will initially also be presented in Cartesian coordinates. Cartesian velocity components in the x, y and z direction are denoted v_x , v_y and v_z , while resultant axial flow is simply denoted v , sometimes v_z or v_x . Governing equations of fluid mechanics are summarized in Chapter 10.4, in microscopic and macroscopic views. The microscopic view is characterized by observing the flow behaviour as it develops inside the pipe, and thereby allowing us to observe from one position in the flow profile continuously, referred to as the Lagrangian view. The macroscopic view or the Eulerian view involves a control volume and keeping track of what is entering and what is leaving the control volume.

4.1 Head loss

Before going to friction loss, we introduce an expression from the fluid mechanics course, and some useful definitions. Bernoulli's law can be expressed in terms of fluid head (in meters): Return to pressure by multiplying with ρg :

$$\frac{p_1}{\rho g} + \frac{v_1^2}{2g} + z_1 + h_{pump} = \frac{p_2}{\rho g} + \frac{v_2^2}{2g} + z_2 + h_f \tag{4.1}$$

The different parts of eqn (4.1) represent for left to right; pressure head, velocity head, gravity or potential energy head and pump head. To the far right the friction loss head, referred to as head-loss. Head loss is demonstrated in Figure 4-1.

In a flow systems the total head is composed of energy input, while the hydraulic head is the total head minus the effect of the velocity head.:

$$\begin{aligned} \text{Total head} = h_o &= z + p/\gamma + \bar{v}^2/2g && = \text{energy grade line(EGL)} \\ \text{Hydraulic head} &= z + p/\gamma && = \text{hydraulic grade line(HGL)} \\ &&& = \text{the height in a piezometric tube} \end{aligned}$$

Figure 4-1 demonstrates all expressions.

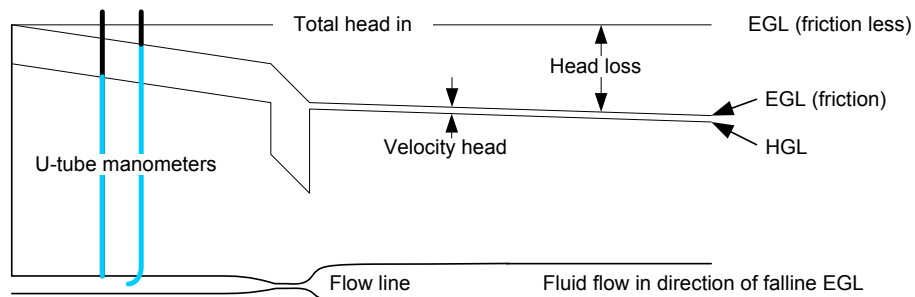


Figure 4-1: Important expressions involved in the evaluation of pipe flow.

4.2 Laminar flow

We start with the simplest case; laminar pipe flow. Since our analysis will assume steady state flow, it will either be laminar or turbulent flow (Figure 4-2 demonstrates the significance of it). Flow regime is determined through the Reynolds number:

$$Re = \rho v d / \mu \quad (4.2)$$

The flow turns from laminar into a transition flow at 1800, and fully turbulent flow is developed at 2100.

Below $Re = 1800$, laminar flow will prevail in slick steel pipes, while above 3000 turbulent flow is fully developed. Figure 4-10 in Chapter 4.3 demonstrates how the flow lines behave in the transition zone. If the pipe wall is not slick, but has a certain roughness, turbulent flow will develop at a much lower Reynolds number.

High mixing energy causes high mechanical energy loss. The mixing length or entrance length, L_e , before flow is fully developed (has obtained a constant flow profile), is given through eqn (4.3) and (4.4):

$$L_e \approx D \cdot 0.06 Re \text{ for laminar flow} \quad (4.3)$$

$$L_e \approx D \cdot 4.4 (Re)^{1/6} \text{ for turbulent flow} \quad (4.4)$$

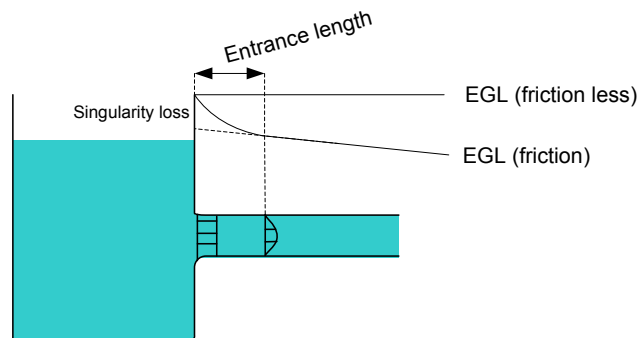


Figure 4-2: After entrance effects flow reaches a stationary flow profile.

4.2.1 Pipe flow

The simplest rheology model is the Newtonian model.

Newtonian model

In this chapter the complete derivation is carried out for the Newtonian rheology model. The complete set of resulting equations for all three type of rheological models are gathered in Chapter 10.5.

Hydraulic flow problems are solved by solving the five basic equations:

1. *Equation of state* relates fluid density to pressure and temperature. For practical purposes liquids are incompressible, we therefore assume that the density is constant.
2. *Constitutive material equation* characterizes fluid behaviour in laminar flow. Fluids subjected to shear rate will resist deformation resulting in shear stress:

$$\tau = -\mu \frac{dv_x}{dr} = \mu \cdot \dot{\gamma} \quad (4.3)$$

The strain rate; $\dot{\gamma} = -\frac{dv_x}{dr}$, across the pipe is the velocity gradient or the rate of shear.

3. *Continuity equation* is the of law of conservation of mass. A general form of the continuity equation states the difference between the input and output of mass to a small volume element:

$$-\frac{\partial \rho}{\partial t} = \nabla(\rho v) = \frac{\partial}{\partial x}(\rho v_x) + \frac{\partial}{\partial y}(\rho v_y) + \frac{\partial}{\partial z}(\rho v_z) \quad (4.4)$$

when expressed in Cartesian coordinates. For incompressible fluids, eqn (4.4) simplifies to: Suio

$$\frac{\partial v_x}{\partial x} + \frac{\partial v_y}{\partial y} + \frac{\partial v_z}{\partial z} = 0 \quad (4.5)$$

4. Momentum equation, or Newton's second law of motion for viscous flow is called the Navier-Stoke equation:

$$\frac{\partial v}{\partial t} + \frac{\mu \nabla^2 v}{\rho} = -\frac{\nabla p}{\rho} + g \quad (4.6)$$

Expressed in cylindrical coordinates the eqn. of motion (only the axial component (x-direction) is of interest) for steady state, constant density and constant viscosity yields:

$$0 = -\frac{\partial p}{\partial x} + \mu \left[\frac{1}{r} \frac{\partial}{\partial r} r \left(-\frac{\partial}{\partial r} v_x + \frac{\partial^2}{\partial x^2} v_x \right) + \frac{1}{r^2} \frac{\partial^2 v_x}{\partial \theta^2} \right] + \rho g_x \quad (4.7)$$

Both $\frac{\partial p}{\partial x}$ and $\frac{\partial v_x}{\partial r}$ are negative since ∂p and ∂v_x decreases for increasing x and r values respectively.

5. Energy equation, or law of conservation of energy is interesting only for problems involving temperature change.

Except for the energy equation, all the other four equations are needed. By assuming that an incompressible, Newtonian fluid is flowing at steady-state in a horizontal pipe, the term $\partial^2 v_x / \partial \theta^2$ becomes 0 in the momentum equation since the flow is symmetrical about the pipe axis. Under these circumstances the state, continuity and momentum equations simplify to:

$$\text{state:} \quad \frac{\partial \rho}{\partial t} = 0 \quad \text{since } \rho = \text{constant} \quad (4.8)$$

$$\text{continuity:} \quad \frac{\partial v}{\partial x} = 0 \quad \text{since } v_y = v_z = 0 \quad (v_x = v) \quad (4.9)$$

$$\text{momentum:} \quad \frac{dp}{dx} = \mu \left[\frac{1}{r} \frac{\partial}{\partial r} \left(r \frac{\partial v}{\partial r} \right) + \frac{\partial^2 v}{\partial x^2} \right] + \rho g_x \quad (4.10)$$

Leaving ρg_x out (for horizontal flow) and substituting eqn (4.9) into eqn (4.10) yields:

$$\frac{dp}{dx} = -\frac{1}{r} \frac{\partial}{\partial r} \left(r \cdot \mu \frac{\partial v}{\partial r} \right) \quad (4.11)$$

Separating and integrating eqn (4.11) from $r = 0$ to $r = r$:

$$\int_0^r \frac{r}{\mu} \cdot \frac{dp}{dx} \partial r = \int_0^r r \partial \left(\frac{\partial v}{\partial r} \right) \quad (4.12)$$

At $r = 0$, $\frac{\partial v}{\partial r} = 0$, resulting in the following expression:

$$\frac{1}{2} \cdot \frac{r^2}{\mu} \frac{dp}{dx} = -r \left(\frac{\partial v}{\partial r} \right) \quad (4.13)$$

Separating

$$\frac{\partial v}{\partial r} = -\frac{r}{2\mu} \cdot \frac{dp}{dx} \quad (4.14)$$

Combining eqn (4.3) and (4.14) gives this expression:

$$\tau_r = \frac{r}{2} \cdot \frac{dp}{dx} \quad (4.15)$$

Integrating eqn (4.14) from r to R , where $v = 0$ (no slip):

$$\int_{v_x(r)}^0 \partial v_x = -\frac{dp}{dx} \cdot \frac{1}{2\mu} \cdot \int_r^R r \partial r \quad (4.16)$$

and solving for v yields the parabolic eqn (4.17) as shown in Figure 4-3:

$$v_x(r) = \frac{dp/dx}{4\mu} (R^2 - r^2) \quad (4.17)$$

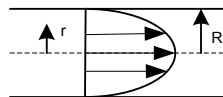


Figure 4-3: Eqn (4.17) presented graphically.

A third integration along r to include total flow over the cross sectional area;

$$q = \bar{v} \cdot A = \bar{v} \cdot \pi r^2 \quad (4.18)$$

Eqn (4.18) on a differential form yields:

$$dq = v \cdot 2\pi r dr \quad (4.19)$$

Integrating from $r = 0$ to R yields:

$$q = \frac{\pi R^4 \cdot dp / dx}{8\mu} \tag{4.20}$$

Integrating along the x-direction and letting $q = \bar{v} A = \bar{v} \cdot \pi/4 \cdot d^2$, gives the pressure change along L ;

$$\Delta p = \frac{32\mu\bar{v}L}{d^2} \tag{4.21}$$

Eqn (4.21) is known as the Hagen-Poiseuille equation for laminar pipe flow. The pressure loss Δp is due to viscous stress only, and is linearly proportional to flow rate or average velocity and to length of pipe.

For the Bingham model (and Power law model) the procedure is identical, only boundary conditions are different as indicated in Figure 4-4.

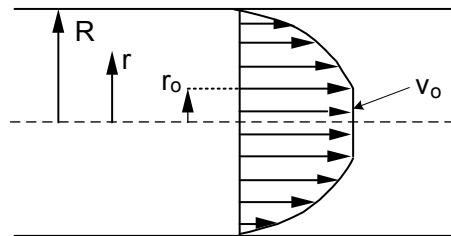


Figure 4-4: Flow profile for laminar flow of a fluid obeying the Bingham rheology model.

Radius r_0 is calculated from eqn (4.6) by using $\tau = \tau_y$ at $r = r_0$.

$$r_0 = \frac{2 \cdot \Delta x \cdot \tau_y}{\Delta p} \tag{4.23}$$

Derivation of pressure loss for laminar pipe flow, through macroscopic view:

The same results as achieved above in the previous paragraph can be achieved through a macroscopic view.

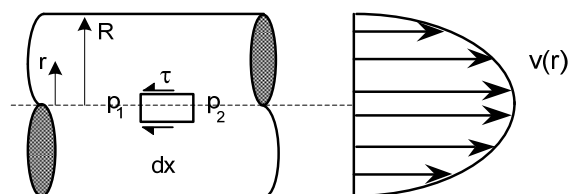


Figure 4-5: A fluid element in pipe flow.

Conservation of momentum of the flow element in Figure 4-5 shows that for steady state flow, shear and pressure forces are the only forces acting and must be equal to each others:

$$(p_1 - p_2) \cdot A = \int \tau(r) \cdot dA = \int \tau(r) \cdot 2\pi r dr \quad (4.24)$$

Taking $\tau(r)$ as a constant for a given r , integration leads to:

$$\Delta p \cdot \pi r^2 = \tau(r) \cdot 2\pi r \cdot \Delta x \quad (4.25)$$

Solving for $\tau(r)$:

$$\tau(r) = \frac{r}{2} \cdot \frac{\Delta p}{\Delta x} \quad (4.26)$$

For $r = R$ (at the wall (w)):

$$\tau_w = \frac{R}{2} \cdot \frac{\Delta p}{\Delta x} \quad (4.27)$$

Eqn (4.27) is graphically shown in Figure 4-6:

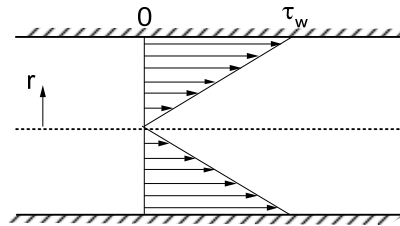


Figure 4-6: Shear stress distribution in a liquid flowing laminarly through a pipe.

Similarly for slot flow;

$$\tau_w = \frac{d_o - d_i}{4} \cdot \frac{dp}{dx} \tag{4.28}$$

These two equations are referred to as the universal pressure loss equations since they are valid for all rheologies. And the macroscopic view give the same result as the microscopic (see eqn (4.15)).

4.2.2 Annular flow

Newtonian fluids

Flow in between two concentric pipes can be treated either as flow in true concentric pipes, or in a simplified manner, as flow between two parallel plates. For narrow annuli the deviation between true and parallel flow is highest, and where the losses may become a large portion of total loss, significant errors are introduced. By presenting both solutions we can pursue this difference.

The simplified annular flow between two parallel plates is shown in Figure 4-7:

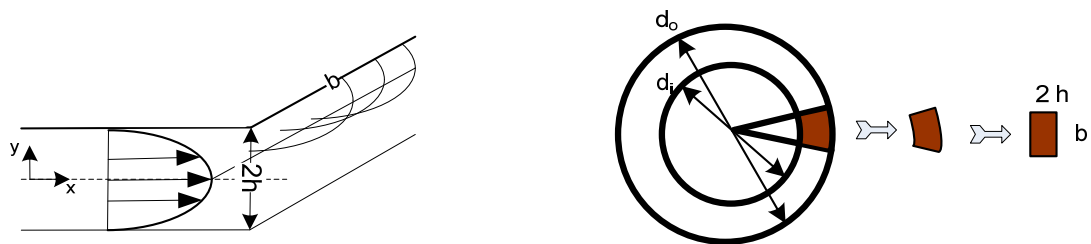


Figure 4-7: Geometry and velocity profile for flow between two parallel plates

Navier Stoke form of the momentum equation:

$$\rho \left(u \frac{\partial v_x}{\partial x} - v \frac{\partial v_y}{\partial y} \right) = -\frac{\partial p}{\partial x} + \rho g_x + \mu \left(\frac{\partial^2 v_x}{\partial x^2} + \frac{\partial^2 v_x}{\partial y^2} \right) \quad (4.29)$$

For steady state flow the continuity equation shows that in the x-y dimension $\frac{\partial v_x}{\partial x} = \frac{\partial v_y}{\partial y} = 0$ and $\frac{\partial v_x}{\partial y} \neq 0$, then eqn (4.29) reduces to:

$$\rho(0+0) = -\frac{\partial p}{\partial x} + \mu \left(0 + \frac{\partial^2 v_x}{\partial y^2} \right)$$

Separating and integrating from 0 to y:

$$\int \partial^2 v_x = \frac{1}{\mu} \frac{dp}{dx} \int dy^2 \quad (4.30)$$

Integration yields:

$$v_x = \frac{1}{\mu} \frac{dp}{dx} \frac{y^2}{2} + C_1 y + C_2 \quad (4.31)$$

By referring to Figure 4-7, $y=h$ for $v_x = 0$, eqn (4.31) gives $C_1 = 0$, $C_2 = -\frac{dp}{dx} \cdot \frac{h^2}{2\mu}$, and eqn (4.31) takes the form:

$$v_x = -\frac{dp}{dx} \frac{h^2}{2\mu} \left(1 - \frac{y^2}{h^2} \right) \quad (4.32)$$

If the channel has width b, the volume flow becomes:

$$q = \int_{-h}^{+h} v(y) b dy = \frac{bh^3}{3\mu} \left[-\frac{d}{dx} (p + \rho g z) \right] \quad (4.33)$$

Solving for average pipe velocity:

$$v_{Av} = \frac{q}{bh} = \frac{h^2}{3\mu} \left[-\frac{d}{dx} (p + \rho g z) \right] \quad (4.34)$$

The wall shear stress in developed channel flow is a constant (at $y = h$):

$$\tau_w = \mu \left. \frac{dv_x}{dy} \right| = h \left[-\frac{d}{dx} (p + \rho g z) \right] \quad (4.35)$$

This may be made non dimensional as a friction factor:

$$f_M = 4 \cdot \frac{8\tau_w}{\frac{1}{2} \cdot \rho \bar{v}^2} = \frac{24\mu}{\rho \bar{v} h} = \frac{24}{N_{Re}} \quad (4.36)$$

Finally we convert slot flow to annular flow by converting width (breadth) to radius. If we follow the center line of the gap, the average breadth can be expressed as the periphery:

$$b = 3.14 (d_o + d_i) / 2 \quad (4.37)$$

The hydraulic diameter is defined as:

$$d_{hydr} = \frac{4A}{perimeter} = \frac{4 \cdot 2hb}{2b + 4h} \quad (4.38)$$

For infinite breadth eqn (4.38) approaches $4h$. Inserting $h = \frac{1}{4} * d_{\text{hyd}}$ in eqn (4.36), combining with eqn (4.34) and solving for dp/dx yields;

$$\frac{dp}{dx} = 48 \frac{\bar{v}\mu}{d_{\text{hydr}}^2} \quad (4.39)$$

The exact solution of annular flow results from the true flow profile in the annular space between two concentric cylinders, shown in Figure 4-8.

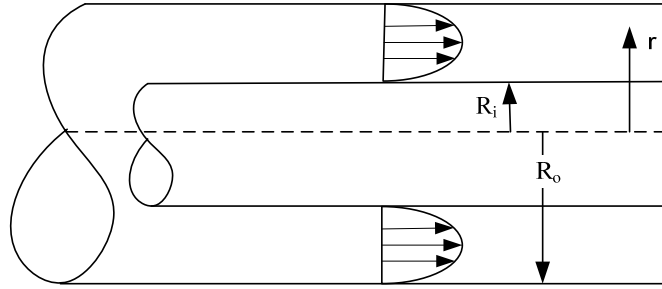


Figure 4-8: Geometry and flow profile for flow through a concentric annulus.

Since we do not know where the velocity has its maximum (where $\partial v_x / \partial r = 0$) we make an unbound integration of eqn. (4.16) and obtain

$$v_x(r) = -\frac{r^2}{4\mu} \frac{dp}{dx} - \frac{C_1}{\mu} \ln r + C_2 \quad (4.40)$$

At $r = R_0$ and $r = R_i \rightarrow v(r) = 0$ (no slip), and eqn. (4.40) becomes;

$$v_x(r) = \frac{1}{4\mu} \left[(R_0^2 - r^2) - (R_0^2 - R_i^2) \frac{\ln \frac{R_0}{r}}{\ln \frac{R_0}{R_i}} \right] \frac{dp}{dx} \quad (4.41)$$

Hence, the flow rate is:

$$q = \int_{R_i}^{R_0} v_x 2\pi r \cdot dr = \frac{\pi}{8\mu} \frac{dp}{dx} \left[R_0^4 - R_i^4 - \frac{(R_0^2 - R_i^2)^2}{\ln \frac{R_0}{R_i}} \right] \quad (4.42)$$

It is seen that for $R_i \rightarrow 0$ (pipe flow), eqn. (4.42) reduces to eqn. (4.20). Expressing the flow rate in terms of average flow velocity and solving eqn. (4.41) for dp/dx gives:

$$\frac{\Delta p}{\Delta x} = \frac{32 \mu \bar{v}}{d_L^2} \quad (4.43)$$

where

$$d_L^2 = d_0^2 + d_i^2 - \frac{d_0^2 - d_i^2}{\ln \frac{d_0}{d_i}} \quad (4.44)$$

Note that eqn (4.43) reduces to the corresponding pipe flow equation eqn (4.21) as $d_i \rightarrow 0$.

4.2.3 Shear rate and effective viscosity

In some situations it may be useful to find the shear rate at the pipe wall, to compare with a rheometer shear stress. Eqn (4.27) is valid for all rheologies. Combining Eqn. (4.27) and (4.21) yields:

$$\dot{\gamma}_w = \frac{8\bar{v}}{d} \quad (4.45)$$

In similar manner it may be shown that for the Power law model:

$$\dot{\gamma}_w = \frac{8\bar{v}}{d} \cdot \frac{3n+1}{4n} \quad (4.46)$$

and for Bingham fluids

$$\dot{\gamma}_w = \frac{8\bar{v}}{d} + \frac{d \cdot \tau_0}{3} \quad (4.47)$$

It is also possible to apply the Newtonian pressure loss equations for other rheological models when expressing them through the equivalent Newtonian viscosity. The equivalent viscosity is often referred to as effective or apparent viscosity. For Bingham plastic, the equivalent viscosity for circular pipes is found by comparing eqn. (4.21) with the Bingham fluid loss equation (see Chapter 10.5):

$$\frac{32 \cdot \mu_{eff} \cdot L \cdot \bar{v}}{d^2} = \frac{32 \cdot \mu_p \cdot L \cdot \bar{v}}{d^2} + \frac{16 \cdot \tau_y \cdot L}{3d} \quad (4.48)$$

Solving for μ_{eff} yields:

$$\mu_{eff} = \mu_{pl} + \frac{\tau_y \cdot d}{6 \cdot \bar{v}} \quad (4.49)$$

Chapter 10.5 summarises hydraulic friction equations for all rheologies.

4.2.4 Laminar pressure loss example

The following example will summarize much of what has been presented so far in Chapter 4. Starting with viscometer data in Table 3-5 and operational data in Figure 4-9:

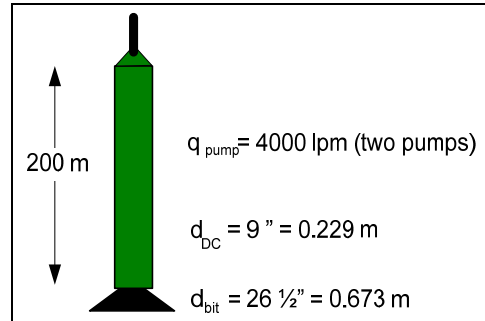


Figure 4-9: Example data; flow around DC. Rheology as in Figure 3-4.

The task in this example is to find Δp along the DC annulus, for two models: Bingham and Universal.

$$v = q/A = \frac{0.0667}{0.3145} = 0.212 \text{ m/s}$$

$$A_{\text{DC-OH}} = \frac{\pi}{4} (0.673^2 - 0.229^2) = 0.3145 \text{ m}^2$$

$$q = 4000 \cdot \frac{1}{1000 \cdot 60} = 0.0667 \text{ m}^3/\text{s}$$

Bingham (2 data points, SI approach):

$$\mu_{pl} = 0.0417 \text{ Pas}$$

$$\tau_o = 28.5 \text{ Pa}$$

$$\mu_{eff} = \mu_{pl} + \frac{\tau_o(d_o - d_i)}{8v} = 0.0417 + \frac{28.5(0.673 - 0.229)}{8 \cdot 0.212} = 7.50 \text{ Pas}$$

At low shear rates the yield point plays a major role. And it leads to extremely low Reynolds numbers:

$$\text{Re} = \frac{\rho v d_{hydraulic}}{\mu_{eff}} = \frac{1000 \cdot 0.212 \cdot 0.444}{7.5} = 12.5$$

$$\Delta p_{ann} = \frac{48 \cdot 0.0417 \cdot 200 \cdot 0.212}{(0.444)^2} + \frac{6 \cdot 200 \cdot 28.5}{0.444} = 430 + 77\,027 = 77\,457 \text{ Pa} = \underline{0.8 \text{ bar}}$$

Universal:

$$\dot{\gamma} = \frac{12 \bar{v}}{d_{hydraulic}} = \frac{12 \cdot 0.212}{0.444} = 5.7 \text{ s}^{-1}$$

τ_w from graph in Figure 39 can be reads to 7 Pa.

$$\Delta p_{ann} = \frac{4}{d_{hydraulic}} \cdot \tau_w \cdot dx = \frac{4}{0.444} \cdot 7 \cdot 200 = 12\,612 \text{ Pa} = \underline{0.12 \text{ bar}}$$

A large difference in result is observed in the two models. This is due to the fact that the Bingham model aims too high for the τ_y . It is clearly seen in Figure 3-9 that at these low shear rates the Bingham model gives 3 times higher shear stress than the true readings. From the logarithmic plot of measured rheology data in Figure 3-9 it is seen that the 4 upper readings fall into a straight line, while the two lower ones do not. It is fair to conclude that the upper 4 points describe the Power law behavior of the mud, while the two lower ones point out the Binghamian nature of the fluid.

4.3 Turbulent pipe flow

When kinetic energy dominates over shear stress, the flow turns into turbulent flow. A dimensionless number called the Reynolds number, Re, is used for determining the flow regime;

$$\text{Re} = \rho \bar{v} d / \mu \tag{4.2}$$

Turbulent flow is chaotic flow and the velocity varies continuously both in the x and y direction, resulting in high energy consumption, and correspondingly high loss due to friction (head loss). Figure 4-10 demonstrates the higher loss rate at turbulent flow regime.

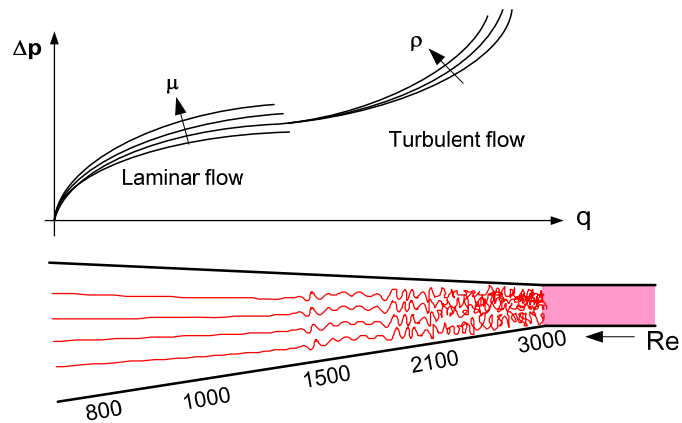


Figure 4-10: The Reynolds number is a function of flow rate, and friction increases exponentially with flow rate in the turbulent regime (upper Figure). Transition from laminar (parallel flow lines) to turbulent flow regime vs. pipe diameter decrease (lower).

Turbulent pressure loss relationships are based on experimentally determined friction factors (Fanning (f_F) or Moody (f_M)):

$$f_M = 4\tau_w / \frac{1}{2}\rho\bar{v}^2 = 4f_F \tag{4.50}$$

Example of data from such experiments are shown in Figure 4-11.

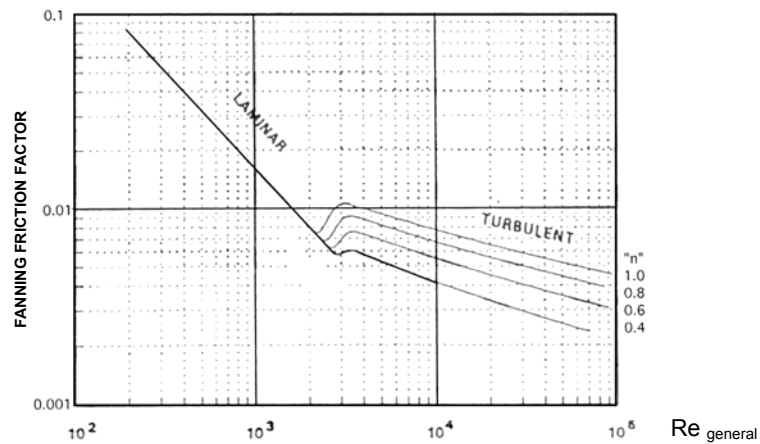


Figure 4-11: Fiction factors for power-law fluids in smooth pipes.

Substituting the general (eqn (4.27)) pressure loss equation and the Power law fluids model into eqn (4.50) yields:

$$f_F = \frac{16 \cdot 8^{n-1} K \left(\frac{3n+1}{4n} \right)}{d^n \bar{v}^{2-n} \rho} = \frac{16}{Re_{general}} \tag{4.51}$$

The general Reynolds number can now be defined as:

$$\text{Re}_{\text{general}} = \left(\frac{4n}{3n+1} \right)^n \frac{d^n \bar{v}^{2-n} \rho}{8^{n-1} K} \quad (4.52)$$

For $n = 1$ and $K = \mu$, eqn (4.52) reduces to eqn (4.2), which is valid for Newtonian fluids. By curve fitting the experimental data in the turbulent region of Figure 4-10, several mathematical relationships have been suggested, and named after its author:

1. Blasius: Eqn (4.53) is valid for smooth pipes and for $10^3 < \text{Re} < 10^5$, and Newtonian fluids:

$$f_F = 0.0791 * \text{Re}^{-0.25} \quad (4.53)$$

2. Moore: His equation is valid for drill pipes (smooth steel pipes) and for drilling fluids where the turbulent viscosity is equal to $\mu_{pl} / 3.2$

$$f_F = 0.046 * \text{Re}^{-0.2} \quad (4.54)$$

3. Metzner & Reed: This model is valid for power law fluids in smooth steel pipes:

$$f_F = a * Re_{general}^{-b} \tag{4.55}$$

where $a = [\log(n) + 3.93]/50$ and $b = [1.75 - \log(n)]/7$

4. Prandtl: Eqn (4.56) is derived from the logarithmic law of the turbulent velocity profile.

$$\frac{1}{\sqrt{f_M}} = 2 \log \left(Re \sqrt{f_M} \right) - 0.8 \tag{4.56}$$

5. Nikuardse/Colebrook/Wood: Eqn (4.57) is developed for naturally rough pipes and for $10^4 < N_{re} < 10^5$

$$f_F = a + b * N_{Re}^{-c} \tag{4.57}$$

where $a = 0.026 (\epsilon/d)^{0.25} + 0.133 (\epsilon/d)$, $b = 22 (\epsilon/d)^{0.44}$ and $c = 1.62 (\epsilon/d)^{0.34}$.

Figure 4-12 is applied in conjunction with eqn (4.57). Absolute roughness, ϵ , in a pipe in service will increase with time due to corrosion and scale build up.

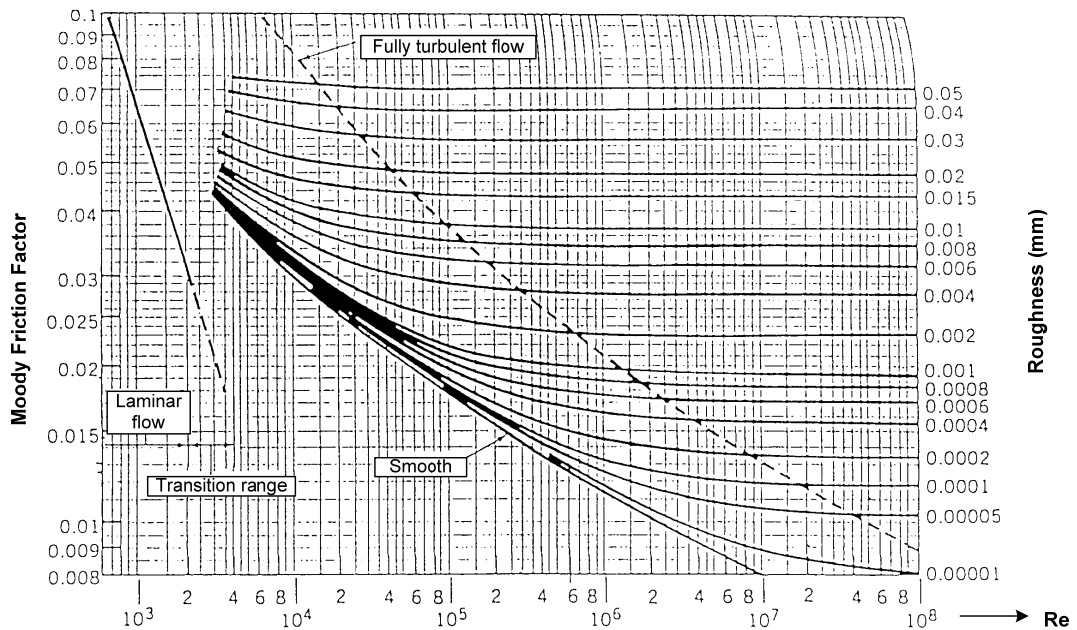


Figure 4-12: Moody friction factors vs. roughness.

Roughness for new pipe materials is shown in Table 4-2.

Table 4-2: Equivalent roughness calculated on basis of experimental data. The uncertainty is +/- 50 %.

Material	Roughness ϵ (mm)
Concrete	0.3 – 3.0
Wood	0.2 – 0.9
Cast Iron	0.26
Galvanized iron	0.15
Commercial steel	0.046
Drawn steel tubing	0.0015
Glass	0.00 (smooth)

For non-Newtonian fluids the effective viscosity should be applied. It has been found that for Bingham fluids the transition to turbulent flow is insufficiently determined by the Reynolds number. The Hedstrom number is related to the critical Reynolds number, below which the flow pattern is laminar, as shown in Figure 4-13.

The Hedstrom number is:

$$\text{Hedstrom Number} = \rho \tau_y d^2 / \mu_{pl} \tag{4.58}$$

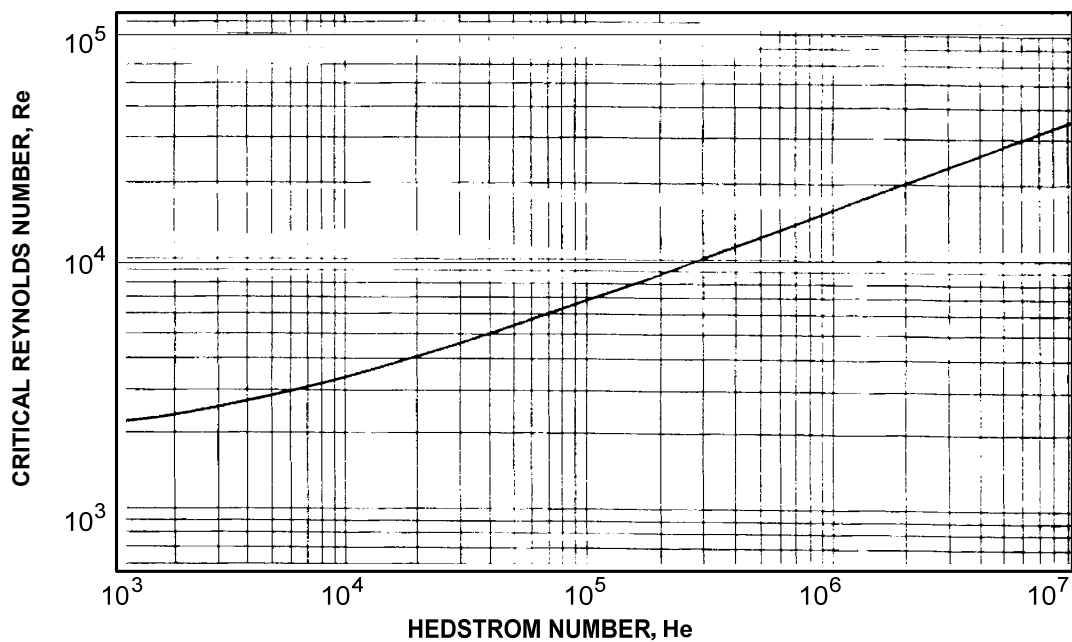


Figure 4-13: Critical Reynolds number for Bingham plastic fluids.

4.4 Singularity losses

Valves, bends, tees, pipe entrances, sudden expansions etc. have no length dimension, and pressure loss through such restrictions are called singularity losses or minor losses. The losses are determined experimentally. The flow is always turbulent, and inertia effects will dominate over viscous effects. The loss coefficient, K_L , is therefore a comparison of how large a part of the dynamic pressure is lost:

$$K_L = \Delta p / \left(\frac{1}{2} \rho \bar{v}^2 \right) \quad (4.59)$$

The loss coefficient is a function of geometry. At the entrances or contractions the head loss is largely dependent on how well the entrance is rounded.

Table 4-3 presents loss coefficients for typical singularity loss geometries. In sudden contractions up to 50 % of the kinetic energy can be lost, while for sudden enlargements 100 % can be lost. K_L for pipes leading to a submerged tank is always equal to 1.0, independent of geometry. In a submerged exit all velocity head is lost due to viscous dissipation. This is in accordance with the second law of thermodynamics. Submerged exit losses are independent of geometry.

In sudden expansions, the loss coefficient can be determined by simple analysis. Conservation of mass, momentum and energy are summarized here:

$$\begin{aligned} \text{mass :} & \quad A_1 \bar{v}_1 = A_2 \bar{v}_2 \\ \text{momentum :} & \quad p_1 A_2 - p_2 A_1 = \rho A_2 \bar{v}_2 (\bar{v}_2 - \bar{v}_1) \\ \text{Bernoullis :} & \quad \frac{p_1}{\rho g} + \frac{\bar{v}_1^2}{2g} = \frac{p_2}{\rho g} + \frac{\bar{v}_2^2}{2g} + \frac{\Delta p_{loss}}{\rho g} \end{aligned}$$

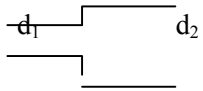
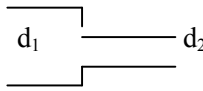
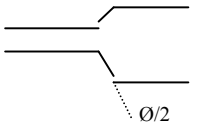

A control volume analysis shows that the loss coefficient for sudden expansions becomes:

$$K_{L,expansion} = \left(1 - \frac{A_1}{A_2}\right)^2 \tag{4.60}$$

And for sudden contractions:

$$K_{L,contraction} = 0.5 \cdot K_{L,expansion} \tag{4.61}$$

Table 4-3: Typical loss coefficients for restrictions vs. its geometry.

Sudden area enlargements		d_2/d_1	1.5	2	2.5	10
		K_L	0.3	0.6	0.7	1
Sudden area contraction		d_2/d_1	1	0.8	0.6	0.4
		K_L	0	0.2	0.3	0.4
Diffusor		$\text{Ø}(\text{°})$	0	15	30	45
		K_L	0	0.2	0.7	1
Bend		r	d	$4d$		
		K_L	0.4	0.2		

The most known singularity losses in the drilling fluid circulation system are summarized below.

Bit nozzle

Drilling mud is discharged at the bottom of the hole through the bit nozzles. In order to aid cuttings removal from the bottom, the nozzles have a relatively small cross-sectional area so that the mud is discharged at high velocities.

By applying the Bernoulli equation, flow of incompressible fluids through a nozzle is written:

$$p_1 + \frac{1}{2} \rho \bar{v}_1^2 = p_2 + \frac{1}{2} \cdot \rho \bar{v}_2^2 + \Delta p_{loss} \tag{4.62}$$

Eqn (4.62) is simplified in several ways. The loss of pressure head through the nozzles is composed of three parts: loss of kinetic pressure at the entrance of the nozzles, loss of kinetic pressure at the outlet of the nozzles to the annulus, and frictional pipe pressure loss through the 0.1 – 0.2 m long pipe leading to the nozzles. Since the nozzle velocity is much larger than the velocity at the entrance and at the outlet, the effect of ignoring entrance and end effect plus friction through the nozzle-pipe are compensated by including them in the loss coefficient, K_{bit} . The discharge coefficient K_{bit} for high-velocity jet bit nozzles is equal to 1.0 (the losses at the entrance are small due to the ellipsoidal shape of the entrance). By including the other loss effects, the coefficient becomes larger than 1.0. A typical value listed in the literature is 1.11. However, the uncertainty of estimating pressure loss through bit nozzles is high. When the coefficient is 1.11, the bit pressure loss becomes:

$$\Delta p_{bit} = 1.11 \cdot \frac{1}{2} \rho \bar{v}^2 \quad (4.63)$$

Tool joint

Pressure loss across a tool joint restriction can be expressed in terms of the loss of dynamic energy when the mud is passing the tool joint;

$$p_1 - p_2 = K_L \cdot \frac{1}{2} \rho (\bar{v}^2) \quad (4.64)$$

Here \bar{v} is the velocity across the tool joint and K_L is given by the sum of eqn (4.60) and (4.61).

PDM

Positive Displacement Motors (PDM) are characterized by a tortuous internal flow path, comprising by-pass valves, stator/rotor, transmission and shaft bearing. In addition an unknown percentage of the fluid flow (2-15 %) is used for lubrication and passing through the axial bearing. The losses are a function of flow rates, WOB and resulting downhole torque. A general model is proposed:

$$\Delta p_{PDM} = \Delta p_{NL} + (\Delta p_{max} - \Delta p_{NL}) \cdot \frac{WOB}{WOB_{max}} \cdot (tool\ factor) \tag{4.65}$$

Δp_{NL} = pressure loss measure at no load (NL) (WOB = 0), and Δp_{max} = pressure at maximum recommended WOB. The vendor specifies these numbers.

MWD

Pressure losses through MWD tools are simpler to model than losses through PDMs. Pressure loss data obtained from the vendor are used to construct a data base of tool-specific pressure loss polynomial coefficients. Pressure loss curves can be constructed as a function of flow rate for different mud weights and for different additional influencing parameters.

$$\Delta p_{MWD} = a + bq + cq^2 + dq^3 \tag{4.66}$$

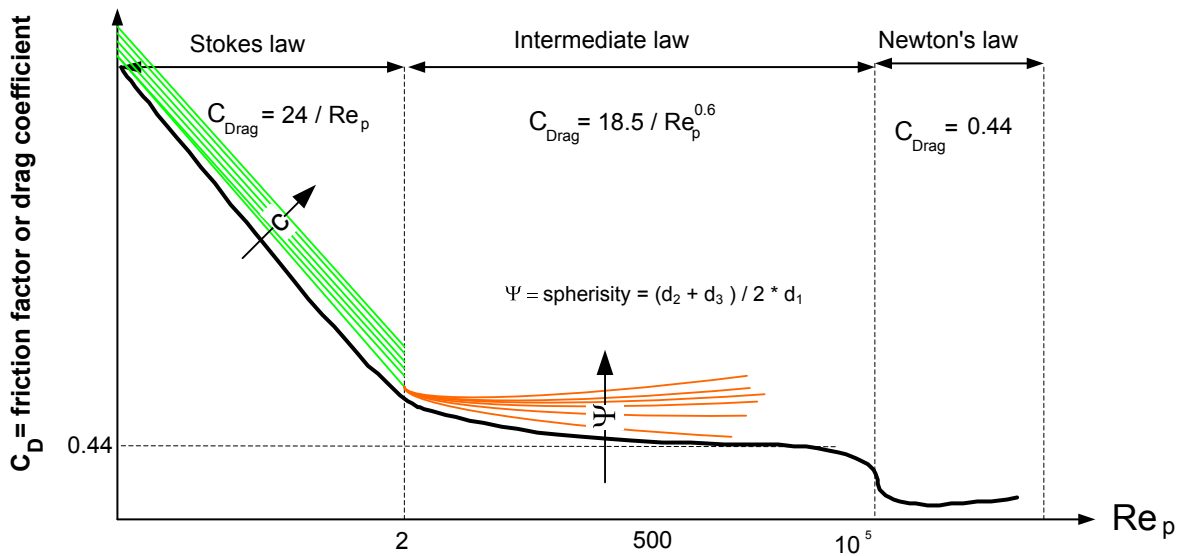


Figure 5-1

5. Removal of cuttings from under the bit

5.1 Cuttings removal process

In the rotary drilling process the rock surface is crushed by the drilling bit. In order to provide further crushing and progress, the cuttings must be removed instantly and efficiently from the rock surface. For this purposes, two forms of energy are brought from the surface to the rock surface, illustrated in Figure 5.1 (left).

- Mechanic energy
- Hydraulic energy

Once at the rock surface, the energy should be applied in an optimal manner: Mechanical energy is responsible for the rock crushing process, while hydraulic energy is applied for the purpose of cuttings removal. While drilling in soft and medium hard formations, both types of energy play an important part in rock crushing and rock removal. Several investigations have shown that drilling rate is increased significantly with increased hydraulic energy, expressed either as hydraulic horse-power, jet impact force or jet velocity through the bit nozzles. Opinions vary to which hydraulic quantity has the greatest effect on drilling rate.

The methods of hydraulic program design can be divided into two groups:

1. Determining the level of bottom hole cleaning energy required in order to balance the mechanical energy level.
2. Maximise criterion of estimation, e.g. jet impact force.

Methods in group 1 require field tests. These tests are based on the theory that the drilling rate is proportional to bit weight if bottom hole cleaning is adequate. When this proportionality curve, shown in Figure 5-1, at some point starts deviating from its increasing trend, the minimum required bottom hole cleaning energy to avoid bit balling at that level of WOB is determined.

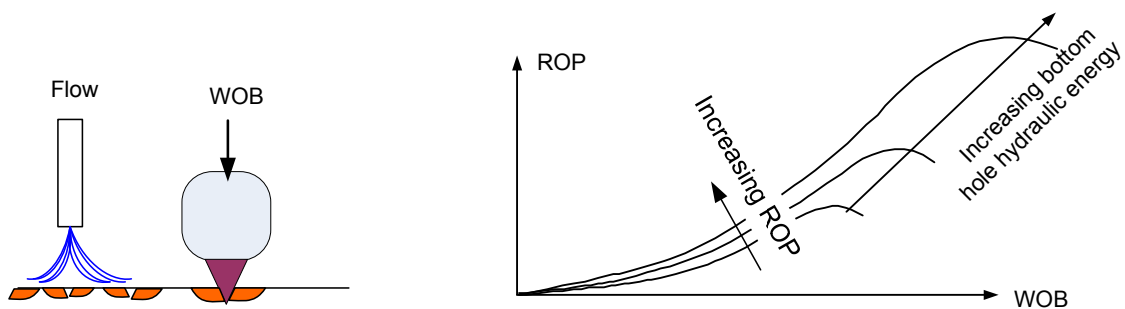


Figure 5-1: ROP vs. WOB for different bit hydraulic energy levels. The points where the curves are turning and pointing downwards are called the bit balling point.

For methods in group 2, optimum hydraulics is the proper balance of the hydraulic elements (flow rate, bit nozzles diameter) which satisfy some criterion of estimation (the objective function) e.g. maximizing the jet impact force. In this book we select the hydraulic quantity q/d_{nozzle} as a common quantity representing the above mentioned bit hydraulic objective function. From experiments and observations demonstrated through Figure 5-1, we suggest a mathematical model that relates ROP and the hydraulic objective function:

$$ROP = A \cdot (q / d_{\text{nozzle}})^{a_8} \quad (5.1)$$

Figure 5-1 demonstrates rather clearly, that there is a general increasing trend of ROP when hydraulic energy is increased. Constant A in eqn (5.1) includes the effect of all other parameters (others than q , d_{nozzle} , and a_8) having an influence on ROP. All these parameters are assumed to be kept constant during the experimental phase and assumed to have little influence on the hydraulic parameters. Our task is to utilize the hydraulic energy of the drilling fluid to achieve the best possible cleaning below the bit so that ROP is maximized.

The performance of the pump and the flow system has several limitations or boundaries. These limitations are discussed next.

5.2 Boundary conditions of the drilling process

First, we have the limitations of the pump itself. Each pump is defined with a maximum recommended pressure, p_{\max} , and a maximum flow rate. The characteristics of the pump is presented in Chapter 2, and repeated in Figure 5-2 below.

5.2.1 Friction loss increases with depth

Due to friction in the ever extending wellbore, the pump would at some stage reach its maximum available pressure during transmission of hydraulic effect through the circulation system. Previously it has been shown that the pump pressure is a mirror image of the pressure losses in the circulating system. For hydraulic optimization purposes, we now split the friction losses in two parts; bit pressure losses, Δp_{bit} , and remaining pressure losses in the circulation system, Δp_{loss} , also called parasitic pressure losses. This is expressed through eqn (5.2):

$$p_{\text{pump}} = \Delta p_{\text{bit}} + \Delta p_{\text{loss}} \quad (5.2)$$

Figure 5-2 displays both mentioned pressure losses, when they are embedded on to the pump characteristics. When the flow rate increases, for a given well length, the pump pressure will be more and more consumed as friction, Δp_{loss} , and less and less is left for the bit.

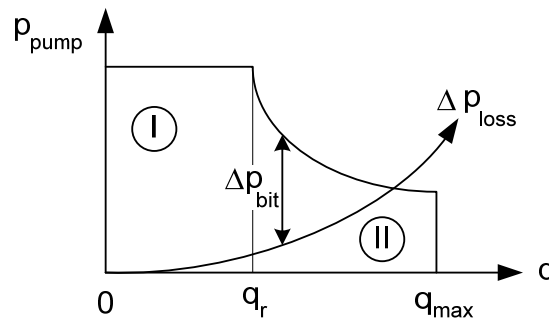


Figure 5-2: Hydraulic friction as a function of flow rate, superimposed on the pump characteristics.

The parasitic pressure loss can be estimated according to formulas presented in Chapter 3. For hydraulic optimization purposes, we apply a simpler expression, reduced to variables important for hydraulic optimization:

$$\Delta p_{\text{loss}} = K_1 \cdot D \cdot q^m \quad (5.3)$$

Parasitic pressure loss varies linearly with depth and is an exponential function of pump rate. The constants K_1 and m can be found by solving eqn (5.3). Since there are two unknowns, two data sets are needed, at two different pump rates, rate 1 and rate 2. Taking the logarithm of eqn (5.3) for two rates, we obtain:

$$m = \frac{\log \Delta p_{\text{loss}2} - \log \Delta p_{\text{loss}1}}{\log q_2 - \log q_1} \quad (5.4)$$

When m is known, K_1 is found through:

$$K_1 = \frac{p_{loss2}}{D \cdot q_2^m} \quad (5.5)$$

Now a practical example of finding m and K_1 from simple rig experiments is summarized in Table 5.1:

Table 5-1: Rig test for determining hydraulic parameters.

Pump rate	Pump pressure	Estimated bit pressure loss
$q_1 = 0.0135 \text{ m}^3/\text{s}$	$p_1 = 100 \cdot 10^5 \text{ Pa}$	$\Delta p_{bit_1} = 11 \cdot 10^5 \text{ Pa}$
$q_2 = 0.027 \text{ m}^3/\text{s}$	$p_2 = 320 \cdot 10^5 \text{ Pa}$	$\Delta p_{bit_2} = 44 \cdot 10^5 \text{ Pa}$

Observe that in Table 5-1 the bit pressure loss is estimated. For that purpose eqn. (4.63), was applied. Now Δp_{loss} can be found from eqn (5.2):

$$\Delta p_{loss1} = p_1 - \Delta p_{bit_1} = 89 \cdot 10^5$$

$$\Delta p_{loss2} = p_2 - \Delta p_{bit_2} = 136 \cdot 10^5$$

m and K_1 are found from eqn (5.4) and (5.7) to be:

$$m = \frac{\log(\Delta p_{loss2} / \Delta p_{loss1})}{\log(q_2 / q_1)} = 1.63, \quad K_1 = \frac{P_{loss1}}{D \cdot q_1^m} = 1.99 * 10^6$$

Table 5-2 presents some typical calculated values for m and K_1 , based on the same field tests as described through Table 5-1.

Table 5-2: Pressure loss constants in two well sections.
Recorded data in left section, estimated to the right.

Bit no.	d_b in	Drilling depth m	Nozzle dia.(3) 32.in	ρ_m kg/m ³	μ_{pl}/Y_p cP/lb/100ft ²	n	K Pas ⁻ⁿ	Δp_{bit} bar	Δp_{loss} bar	m	K_1 10 ⁶
9	12 1/4	950	14	1100	13 / 13	.58	.40	151.7	55.8	1.79	1.46
11	12 1/4	1700	16	1200	13 / 11	.62	.38	100.4	105.3	1.78	1.45
14	12 1/4	1840	14	1210	12 / 12	.58	.32	122.2	76.7	1.77	1.28
16	12 1/4	2100	13	1210	12 / 12	.58	.30	139.8	61.4	1.76	1.01
24	8 1/2	2560	11	1200	16 / 14	.62	.27	168.1	43.6	1.72	.78
28	8 1/2	2663	13	1320	15 / 10	.68	.18	132.1	73.2	1.76	1.08
44	8 1/2	2800	11	1290	18 / 9	.74	.13	150.7	55.6	1.68	.92
47	8 1/2	2916	12	1280	16 / 9	.71	.13	137.4	73.5	1.72	1.09
51	8 1/2	3014	12	1280	15 / 8	.72	.13	125.6	81.9	1.71	1.24
53	8 1/2	3060	12	1280	13 / 10	.65	.15	144.9	75.3	1.74	1.11

From Table 5-2 we see that this well consumed extremely many bits. The year was 1985, which was before the major improvement of bit bearings; in the 1990's they turned to frictional bearings. We also observe from Table 5-2 that bit nozzles were changed equally frequent.

If flow is mainly turbulent in the drill string and the annulus, the exponent m will approach 2.0. When the flow is completely laminar in the complete flow system, m will approach the rheological power law exponent n. Previously presented Figure 3-9 demonstrates this fact. Usually m is somewhere in between, although closer to 2.0 since turbulent pressure drop (in drill string), dominates over laminar (in annulus).

5.2.2 Annular flow velocity limitations

Flow velocity in the annulus of vertical wells must be held within two boundaries. The upper one is normally designed so that turbulence is not developed around the drill collars. In horizontal wells, turbulent flow in the BHA-annulus is normally accepted; it helps largely in removing cuttings from this part of the annulus. ECD dictates if this can be accepted.

Cuttings concentration determines the lower boundary. It must be lower than 0.04, or 4 volume percent. If it gets higher, problems related to accumulation of cuttings, like struck pipe, show an increasing trend. The lowest recommended flow rate is referred to as the required flow rate, and denoted q_r . In inclined wells the criteria concerning annular flow velocities are different and will result in a different hydraulic program compared to vertical wells. Optimal hydraulic parameter estimated for vertical wells can probably be used as a first approach for inclined wells. Summarized annular flow velocity limitations in vertical wells:

$$\begin{aligned} v_{\max} &< v_{\text{turb}} && \text{(around drill collars)} \\ v_{\min} &> q_r && \text{(cuttings concentration in largest annulus < 0.04)} \end{aligned}$$

5.3 Optimizing ROP, liner by liner

As indicated by the heading, the hydraulic program is dependent on first selecting the most suitable liner of the piston pump, before optimizing. It is the annular flow rate limitation, q_r , which determines the selection of liners, as indicated in Figure 5-2. The smallest possible liner should be selected since this will result in the highest possible pressure available. The hydraulic variables are given by eqn (5.1). By requiring pump pressure in eqn (5.2) to be maximum and combining it and (4.63) with eqn (5.3) and multiplying by q^2 we obtain:

$$p_{\max} \cdot q^2 = K_1 \cdot D \cdot q^{m+2} + 1.11 \frac{1}{2} \rho \cdot \frac{q^2 \cdot q^2}{\left(\frac{\pi}{4} d_e^2\right)^2} \quad (5.6)$$

Here the equivalent single nozzle diameter d_e is defined through total nozzle area. Assuming there are three nozzles in the bit, the equivalent bit nozzle becomes:

$$d_e^2 = (d_1^2 + d_2^2 + d_3^2) \quad (5.7)$$

If the three diameters are of identical size:

$$d_e = d_1 \sqrt{3} \quad (5.8)$$

Rearranging eqn (5.6) we obtain:

$$K_{bit} \left(\frac{q}{d_e}\right)^4 = p_{\max} \cdot q^2 - K_1 \cdot D q^{m+2} \quad (5.9)$$

The constant $K_{bit} = 1.11 \cdot \frac{1}{2} \rho / \left(\frac{\pi}{4}\right)^2$. Solving eqn (5.9) with respect to q/d_e yields:

$$\frac{q}{d_e} = \left[\frac{1}{K_{bit}} (p_{\max} \cdot q^2 - K_1 \cdot D q^{m+2}) \right]^{1/4} \quad (5.10)$$

Combining eqn (5.10) and eqn. (5.1) and deriving with respect to the two variables, flow rate and nozzle diameter, and equating it to zero, eqn (5.11) defines the optimum of variable q:

$$\frac{\partial R_p}{\partial q} = \frac{\partial}{\partial q} A \left[\frac{1}{K_{bit}} (p_{max} \cdot q^2 - K_1 D q^{m+2}) \right]^{\frac{a_s}{4}} = 0 \quad (5.11)$$

Deriving with respect to the variables d_e gives the following answer; minimize d_e . Moreover, since minimizing d_e is not feasible, only the q-derivation represents an applicable solution of eqn (5.11). In eqn (5.11) the constant p_{max} is the maximum recommended pressure for the selected liner. The meaningful solution yields:

$$2 p_{max} \cdot q - (m+2) K_1 D \cdot q^{m+1} = 0 \quad (5.12)$$

which, when solved for q results in the optimal solution:

$$\underline{\underline{q_{opt} = \left(\frac{2 p_{max}}{(m+2) K_1 D} \right)^{\frac{1}{m}}}} \quad (5.13)$$

Combining eqn. (5.12) and eqn. (5.2), and solving for Δp_{bit} we obtain an additional optimal expression:

$$\Delta p_{bit,opt} = \frac{m}{m + 2} p_{max} \tag{5.14}$$

The equivalent nozzle diameter d_e is sought, and can be found from eqn (4.63)):

$$d_e = \left[K_{bit} \cdot \frac{q^2}{(\Delta p_b)} \right]^{1/4} \tag{5.15}$$

Now the job is done, we have determined optimal parameters for a selected liner. The above procedure and solutions can also be solved graphically, as shown in Figure 5-3. Δp_{loss} from eqn (5.3) becomes a straight line in a log-log plot. Δp_{loss} represents the losses of the available pump pressure. When $\Delta p_{bit,opt}$ is secured, through the horizontal line, the sum of the two, $\Delta p_{loss} + \Delta p_{bit} = p_{pump}$, is given by the point where the two lines meet.

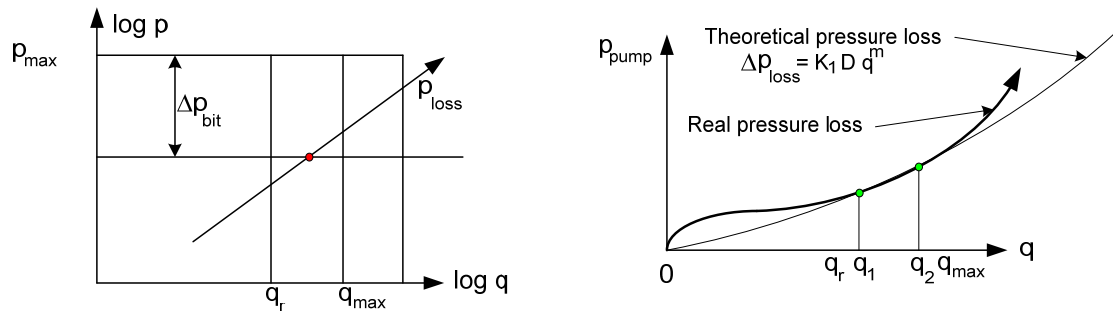


Figure 5-3: Graphical determination of optimal flow rate.

The technique presented in Chapter 5.3 represents the standard method of hydraulic optimization for vertical wells. A flow sheet of how to routinely determine the optimal bit nozzle and optimal flow rate is presented in Figure 5-4. Within a selected liner, the optimal flow rate will be a function of depth in accordance with eqn (5.13), while nozzle size will stay constant in accordance with eqn (5.14). With high quality drilling bits and pumps, it is probably sufficient to change liner and bit every time a new section is started. This program would suggest which liner, which nozzles and which flow rate is optimal at the selected depth.

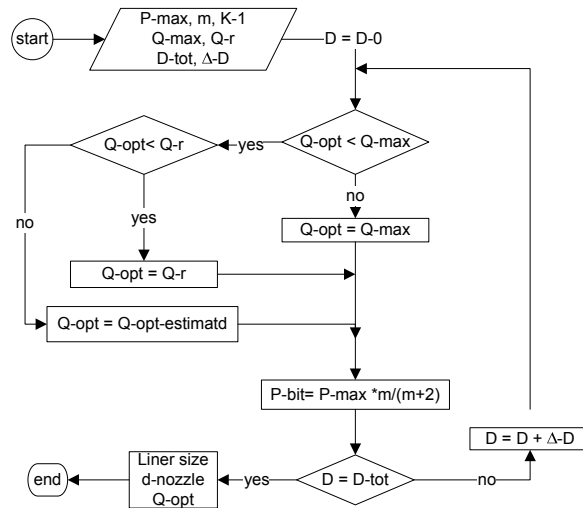


Figure 5-4: Flow diagram of how to compute optimal flow rates and nozzle diameter in a vertical well when pump liner has been selected.

5.4 Optimizing the complete well

To plan the complete well for all sections in one complete hydraulic program requires that the standard hydraulic program must be expanded. All the constants must be known before the well is drilled. One positive side effect obtained through this technique, is that it will be possible to suggest at what depth the pump liners can be changed. a day, with high quality bits and pumps, it is probably sufficient to change liner and bit every time a new section is started. A complete hydraulic program would suggest which liner, which nozzles and which optimal flow rate should be chosen for every section.

First we need to define two pump operating ranges, as already suggested in Figure 5-2. In operating range I, defined by the smallest liner, the pump pressure can be held constant. In order to utilize the pumps full capability, and thereby optimizing ROP, the pump pressure is kept at its maximum pressure. In range II, defined by the remaining liners, the pump power, E_{pump} , can be held constant as seen in previous Figure 2-2 and from Table 2-3. Summarized we have:

- Range I : $p_{max} = const$
- Range II: $E_{max} = const$

The optimal solution in range II is found by combining eqn (5.1) and (5.10):

$$ROP = A \left(\frac{q}{d_e} \right)^{a_8} = \frac{1}{K_{bit}} \left(p_{max} q^2 - K_1 \cdot D \cdot q^{m+2} \right)^{a_8/4} \tag{5.16}$$

By substituting $p_{max} \cdot q$ by E_{max} (which is constant over pump range II) in eqn (5.16) we obtain:

$$A \left(\frac{q}{d_e} \right)^{a_8} = \frac{1}{K_{bit}} \left(E_{\max} \cdot q - K_1 D q^{m+2} \right)^{a_8/4} \quad (5.17)$$

By deriving eqn (5.17) with respect to q , we obtain one meaningful solution:

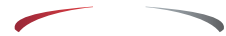
$$\frac{\partial ROP}{\partial q} = E_{\max} - (m+2)K_1 \cdot D \cdot q^{m+1} = 0 \quad (5.18)$$

which, when solved for q yields:

$$q_{opt_{it}} = \left[\frac{E_{\max}}{K_1 \cdot D (m+2)} \right]^{\frac{1}{m+1}} \quad (5.19)$$

Combining the optimal solution in eqn (5.18) with eqn (5.2) and solving for Δp_{bit} we obtain

$$(\Delta p_{bit})_{opt_{it}} = \frac{m+1}{m+2} \cdot p_{\max} \quad (5.20)$$



ROP, which is proportional to the cleaning function, can be plotted as a function of pump rate, as shown in Figure 5-6.

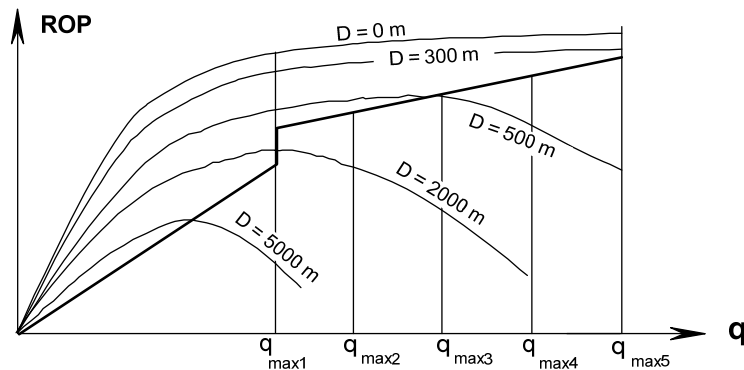


Figure 5-6: ROP (eqn (5.10) in range I and eqn (5.17) in range II) vs. pump rate and depth.

We are now able to decide when to change liner in order to fully utilize the mud pump. By studying Figure 5-6 we can find graphically at which depth the pump liner has to be changed. A pc-program to monitor pump range and respective optimal solution is suggested in Figure 5-7.

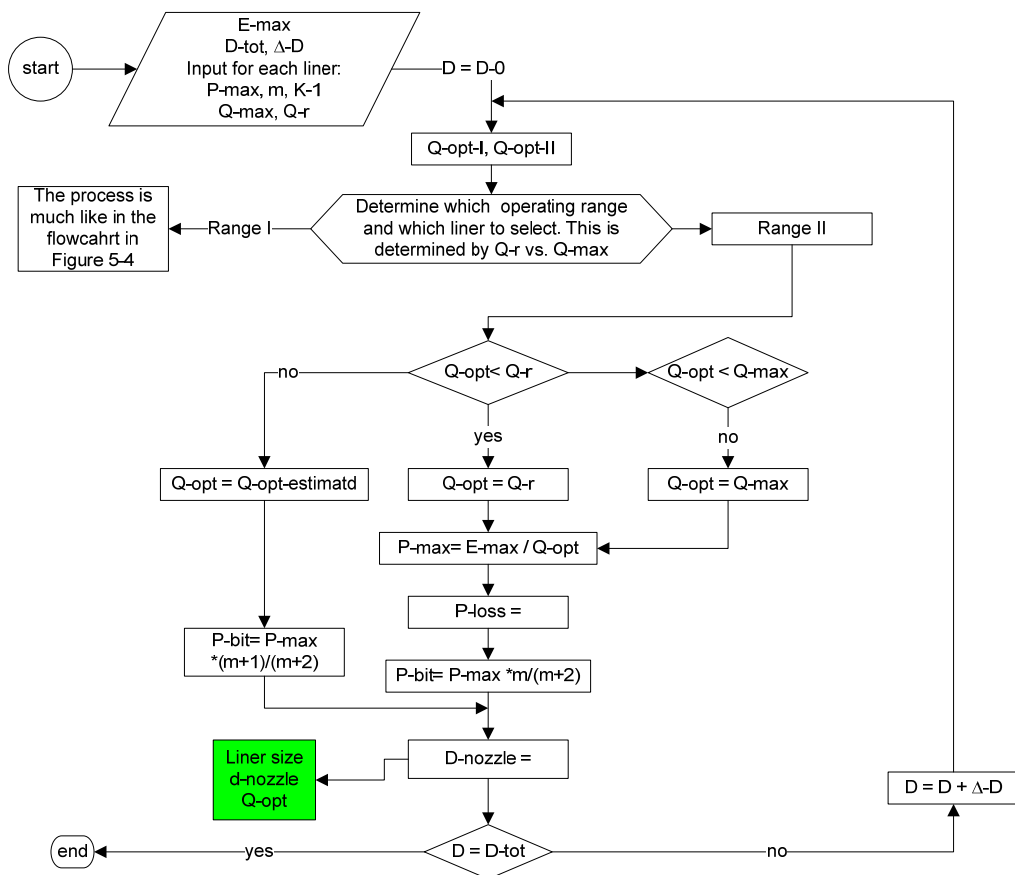


Figure 5-7: A simplified flow sheet to compute optimum hydraulic parameters in pump operating range II.

To optimize the complete well in one operation, the two programs indicated in Figure 5-4 and 5-7 have to be combined and expanded. Now let us exemplify the routine to prove its applicability:

Example :

Use mud pump specified in Table 2-3.

$$\text{Effect} = 1441.7 \text{ Hp} \cdot 745.7 = 1.075 \cdot 10^6 \text{ (W)} = 322 \cdot 10^5 \cdot 0.0334 \text{ m}^3/\text{s} = 4670 \text{ psi} \cdot 529 \text{ GPM} / 1714$$

Well and hydraulic data

$$D = 2500 \text{ m} \quad m = 1.7$$

$$\rho = 1200 \text{ kg/m}^3 \quad q_{\text{required}} = 0.018 \text{ m}^3/\text{s} \text{ (} d_{\text{bit}} = 12 \text{ 1/4"}$$

$$K_1 = 1.1 \cdot 10^6 \quad q_{\text{max}} = 0.04 \text{ m}^3/\text{s}$$

- Which liner should be used, and what is the optimal flow rate?
- When should it be changed to a smaller liner dimension?
- What is optimal nozzle size in 2500 meters depth?

a) Liner: from Table 5.1, the necessary liner is 6 1/4" $\Rightarrow p_{6.25, \max} = 296.8 \cdot 10^5 P$

$$q_{opt, II} = \left[\frac{E_{\max}}{K_1 \cdot D(m+2)} \right]^{\frac{1}{m+1}} = \left[\frac{1.075 \cdot 10^6}{1.1 \cdot 10^6 \cdot 2500(1.7+2)} \right]^{\frac{1}{1.7+1}} = 0.0337 \text{ m}^3/s$$

b) When $q_{opt, II}$ reaches 0.0334 then change to the next liner, which is 6". At which depth to change, we can determine by solving the $q_{opt, II}$ eqn with respect to Depth:

$$D = \frac{E_{\max}}{K_1 \cdot (m+2) \cdot (0.0334)^{m+1}} = \frac{1441.7 \cdot 745.7}{1.1 \cdot 10^6 \cdot (3.7) \cdot (0.0334)^{2.7}} = \underline{2557.5 \text{ m}}$$

c) Solve the $\Delta p_{bit, opt}$ with respect to nozzle size:

$$d_e = \left[K_{bit} \cdot \frac{q_{opt, II}^2}{(\Delta p_{bit})_{opt, II}} \right]^{1/4} = \left[1.11 \cdot \frac{1200}{2 \left(\frac{\pi}{4} \right)^2} \cdot \frac{.0337^2}{\frac{1.7+1}{1.7+2} \cdot 296.840^5} \right]^{1/4} = \underline{0.0154 \text{ m}}$$

$d_e = \sqrt{3}d_1$, assuming they are all identical sized.

$$d_1 = \frac{d_e}{\sqrt{3}} = \frac{0.0154}{\sqrt{3}} [m] = 0.0154/\sqrt{3} = 0.0111$$

Now meters must be translated into 32nds of inches:

$$\frac{0.01111}{\frac{2.54 \cdot 10^{-2}}{32} [m / 32in]} = 11.2 \Rightarrow \frac{11}{32} + \frac{11}{32} + \frac{12}{32}$$

If $d_e > 11.3333$ we would have to increase nozzles size two 12/32 nds in order on to take out less pressure across the nozzles than optimal (conservative).

6. Transport of cuttings to the surface

6.1 Hole cleaning in vertical wells

In vertical wells, hole cleaning is a question of pumping fast enough to counteract the vertical slipping of cuttings, thus causing its concentration to decrease. In horizontal wells it is different, the settling distance is short, the cuttings will fall to the bottom side of the well, and the particles will form beds and dunes.

The rate at which cuttings are generated by the drilling process is:

$$q_{cuttings} = \pi/4 \times d_{bit}^2 \times ROP \quad (6.1)$$

During simultaneous pumping while drilling, the initial cuttings concentration at the bottom of the annulus becomes:

$$c_{cuttings,0} = q_{cuttings} / (q_{pump} + q_{cuttings}) \cong q_{cuttings} / q_{pump} \quad (6.2)$$

In the next chapter, we will study which parameters are of importance for the vertical slip velocity.

6.1.1 Slip velocity of perfect spheres

As a first approach we will simplify the cuttings geometry to spheres. The slip velocity, v_{slip} , will be calculated for a single sphere with particle diameter d_p and density ρ_p , settling in a Newtonian fluid with viscosity μ and density ρ_{mud} . The settling of spheres in laminar conditions is shown and modelled in Figure 6-1:

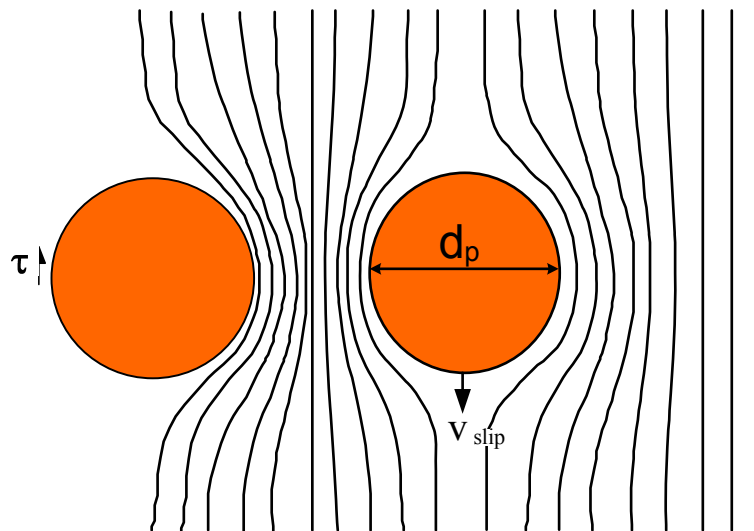


Figure 6-1: Two spheres settling in a fluid.

Only two forces are active; gravity and shear force. At stationary, laminar flow they oppose each other:

$$(\rho_p - \rho_{mud}) V_{sphere} = \tau A_{sphere} \quad (6.3)$$

where:

$$V_{sphere} = \frac{4}{3} \pi r^3 = \frac{\pi}{6} d_p^3 \quad (6.4)$$

$$A_{sphere} = 4\pi r^2 = \pi d_p^2 \quad (6.5)$$

The shear stress of a Newtonian fluid flowing in a pipe is given by:

$$\tau = \mu \cdot \frac{dv_x}{dr} \quad (6.6)$$

The axial velocity of the fluid, v_x , relative to the moving sphere is proportional to the length the fluid must travel along the periphery of the sphere (see Figure 6-1):

$$\frac{v_x}{v_s} = \frac{v_{periphery}}{v_{center\ of\ sphere}} = \frac{l_{periphery}}{2r} = \frac{2\pi r / 2}{2r} = \frac{\pi}{2} \quad (6.7)$$

resulting in $v_x = \pi / 2 \cdot v_{slip}$. The shear rate in the fluid is the relative velocity change across the half sphere; the sphere and the fluid: $\frac{\pi}{2} \cdot v_{slip} - 0$, which results in:

$$\frac{dv_x}{dr} = \frac{\frac{\pi}{2} v_{slip}}{r} = \frac{\pi}{d_p} v_{slip} \tag{6.8}$$

Combining eqn (6.3), (6.4), (6.5), (6.6) and (6.8) we obtain:

$$(\rho_p - \rho_{mud}) g \cdot \frac{\pi}{6} d_p^3 = \mu \cdot \frac{\pi v_{slip}}{d_p} 4\pi \left(\frac{d_p}{2}\right)^2 \tag{6.9}$$

which reduces to Stokes law of a falling sphere:

$$v_{slip} = \frac{d_p^2 \cdot g (\rho_p - \rho_{mud})}{6\pi\mu} \tag{6.10}$$

Stokes law is only valid for infinite dilution (one sphere alone), small spheres ($r < 0.1$ mm) and laminar flow around the particle: $\frac{\rho v}{\mu} \approx 1$.

When particle concentration, c , increases, the interaction between the particles and hence the shear rate will also increase, as illustrated in Figure 6.1. When two particles are present (left), the flow lines are closer (higher shear) compared to when only one is present (to the right of the right most particle). The flow resisting-function $f(c)$ is related to the concentration as shown in Figure 6-2, resulting in a reduced settling velocity, $v_{slip, reduced}$:

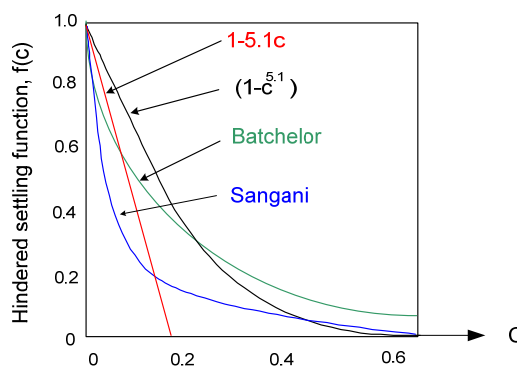


Figure 6-2: The hindered settling function $f(c)$ vs. concentration .

$$v_{slip, reduced} = v_{slip} \cdot f(c) \tag{6.11}$$

Cuttings volume concentration can be estimated through eqn (6.2) and exemplified through:

$$q_{\text{cuttings}} = \text{ROP} \cdot A_{\text{bit}} = 20 \text{ m/h} \cdot 12 \frac{1}{4}'' = 0.155 \text{ m}^3/\text{s}$$

$$q = 1000 \text{ l/min} = 0.667 \text{ m}^3/\text{s}$$

Under these conditions $c_{\text{cuttings},0} = 0.052$. A concentration of 5 %, produces an $f(c) = 1 - 5.1 \cdot 0.052 = 0.74$, reducing the settling velocity of a single particle by 30 %. Other hindered settling functions in Figure 6-2 will give higher or lower results.

6.1.2 Slip velocity of imperfect spheres

Cuttings are non spherical and perform strange settling motions. A more true slip velocity can therefore be found through an empirical drag force, C_{Drag} :

The two forces acting on slipping cuttings are gravity, F_g , and shear, F_{Drag} :

$$F_g = V_p (\rho_p - \rho_{\text{mud}})g \quad (6.12)$$

$$F_{\text{Drag}} = C_{\text{Drag}} A_p \cdot 0.5 \rho_{\text{mud}} v_{\text{slip}}^2 \quad (6.13)$$

At terminal (stationary) settling velocity the gravity and shear force will be equal, and the resulting particle slip velocity is found by combining eqn (6.12) and (6.13):

$$v_{\text{slip}} = \sqrt{4g(\rho_p - \rho_{\text{mud}})d_p / (3gC_{\text{Drag}}\rho_{\text{mud}})} \quad (6.14)$$

C_{Drag} is a function of Reynolds number of the slipping particle;

$$Re_p = v_{\text{slip}} d_p \rho_{\text{mud}} / \mu_{\text{eff}} \quad (6.15)$$

Figure 6-3 shows that these inter relationship are subdivided into three ranges:

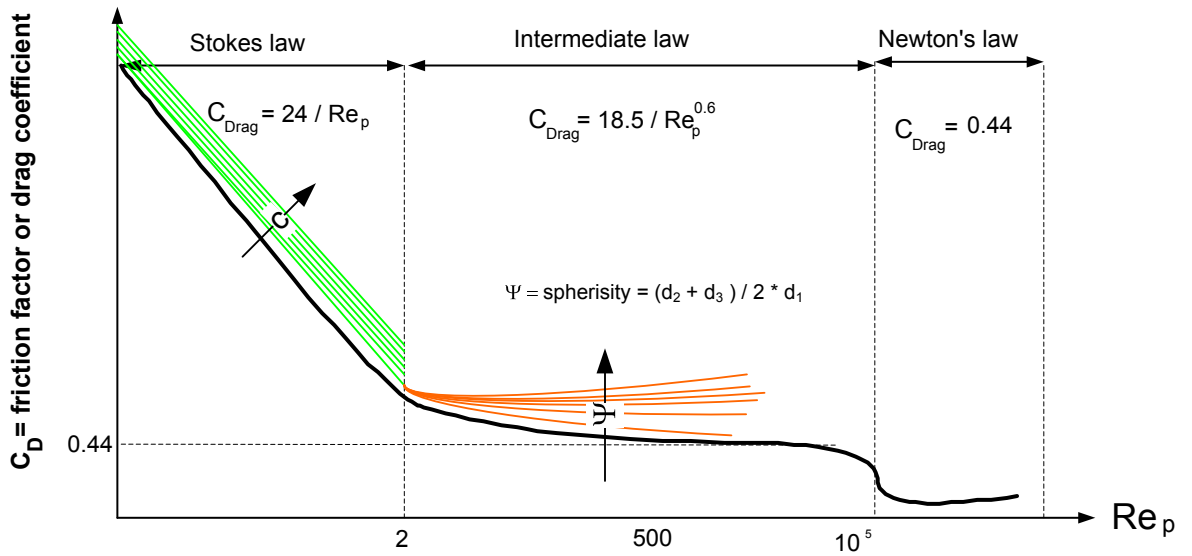


Figure 6-3: Relationship between C_{Drag} and Reynolds Number for particle settling of real particles in Newtonian fluids.



When the average mud velocity exceeds the resulting slip velocity, the particles will be transported out of the well at the resulting transport velocity;

$$v_{transport} = v_{ann} - v_{slip} \quad (6.16)$$

The differential speed can also be presented through a transport ratio:

$$R_{transport} = v_{transport} / v_{ann} = 1 - v_{slip} / v_{ann} \quad (6.17)$$

The interdependency between the transport ratio and annular flow rate is determined through experiments as shown in Figure 6-4.

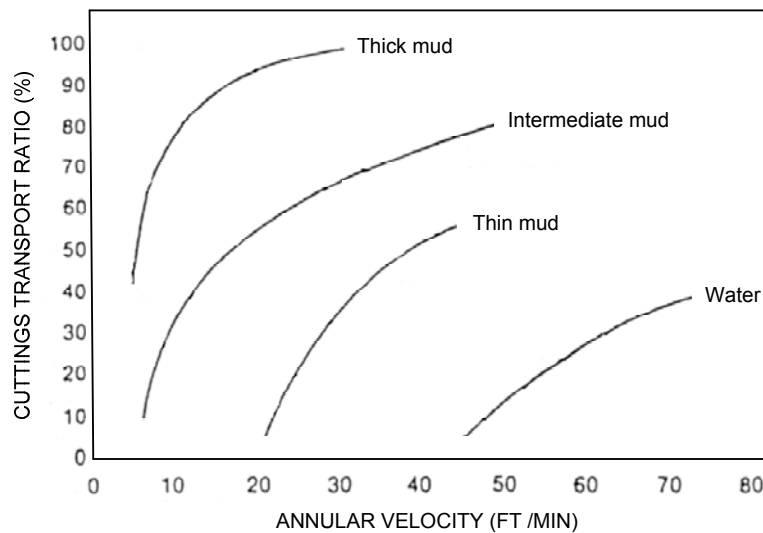


Figure 6-4: Annular velocity vs. transport ratio.

It is of interest to determine the minimum required annular velocity, below which problems related to accumulated cuttings become too serious. Practice has proven that this boundary velocity coincides with a cuttings concentration of 4 volume %. This realization is expressed through solving $R_{transport}$ with respect to $c_{cuttings}$ and set it to 0.04. The result is shown in Figure 6-5. The required annular velocity is a function of rheology, and is typically 30 – 60 ft/min.

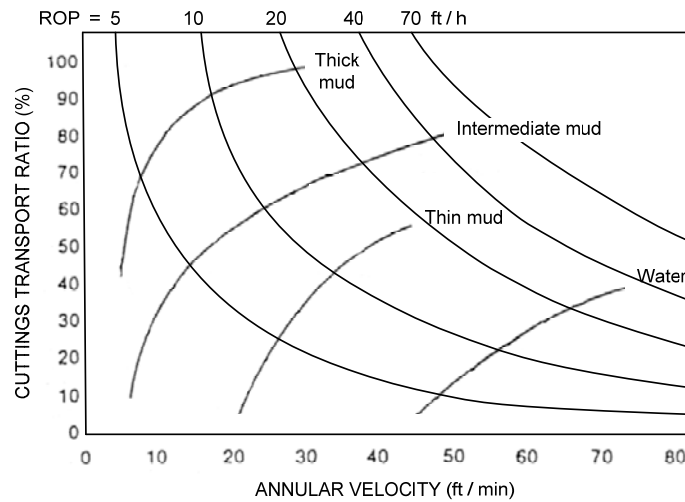


Figure 6-5: Annular velocity in a 5 * 12 ¼ “ annulus to keep cuttings concentration above 4 vol %.

At stationary settling conditions the cuttings concentration in the annulus becomes:

$$C_{\text{cuttings}} = C_{\text{cuttings},0} / R_{\text{transport}} \tag{6.18}$$

Cuttings size must be determined from samples taken at the shale shaker or from historical default values, related to lithology. As a first approach assume a cuttings diameter from the upper quarter of the size distribution profile.

6.2 Hole cleaning in inclined wells

The economical advantage of drilling directional wells is now firmly established and for offshore operations only exploratory wells are vertical. The direction of cuttings settling is still vertical, but for inclined wells the fluid velocity has a reduced vertical component. This decreases the mud's capability of suspending drilled cuttings, and it results in an increased tendency for particles to settle out of suspension, more so with increasing hole inclination. Once reached the borehole floor, the particle has little chance of re-entering the fluid, because local fluid velocities near the wall are small and insufficient (no slip effect). Consequently, particle resident time in the annular space increases significantly resulting in higher concentration of cuttings in the well bore, and, alas, cuttings bed are created.

The most common drilling problems related to insufficient hole cleaning occurs during tripping and reaming operation. Such problems manifest themselves as small and large restriction. However, when not cleared, the situation may worsen and end up in creating stuck pipe, lost circulation and serious hindrances during casing running.

The main objective of cuttings transport predictions is to avoid such operational problems and to operate with the most optimum; safe and economical cuttings transport option.

6.2.1 Mechanistic model

Mechanisms of particle transport in inclined wells are complex, and there are many mechanisms involved in transportation of cuttings. There are two main schools of modelling the complex system of cuttings transport:

1. Mechanistic models
2. Empirical models

The mechanistic model explains the physics and defines all forces involved basing the analysis of the balance between hydraulic and mechanical forces for a given particle in the bed made up of solids. According to this model, two mechanisms are considered responsible for removing protruding cuttings; rolling and lifting. The forces required to activate a single cuttings particle determines the mechanisms that dominate the process of removal. Figure 6-6 shows the forces involved in cutting transportation.

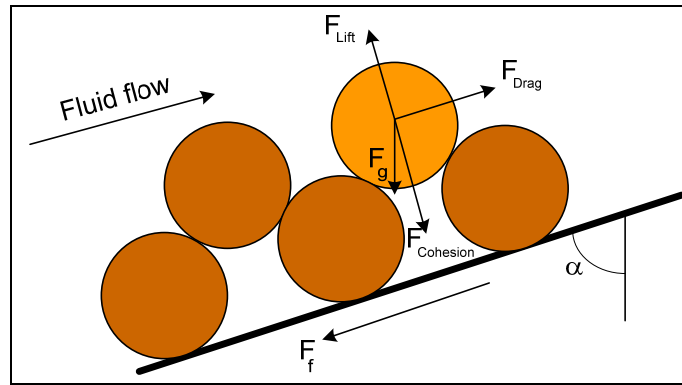


Figure 6-6: Forces acting on particle at an active erosion site of a cuttings bed.

Of the five forces defined in Figure 6-6, friction forces are not included in cuttings transport. Friction is involved only during avalanching of cuttings bed, and then known as the angle of repose.

Drag force

In physical terms, drag force is the sum of the pressure and shear force over the surface area. Drag can be estimated using the drag coefficient C_{Drag} as follows:

$$F_{Drag} = C_{Drag} \frac{\pi d_p^2}{8} \rho v_x^2 \tag{6.19}$$

where v_x is assumed local flow velocity at the center of the particle.

Lift force

Drag force is present in all types of flow around a solid particle. However, lift on a spherical particle is present only if there is asymmetry in the flow field, which is the case for the velocity profile in pipe flow. Eqn (6.20) represents the classical form, using the lift coefficient:

$$F_{Lift} = C_{Lift} \frac{\pi d_p^2}{8} \rho v_x^2 \tag{6.20}$$

In eqns (6.19) and (6.20), we are relying on experimentally determined drag and lift coefficients. Moreover, the viscosity and velocity distribution across the flow path must be calculated. Drag coefficient for non-spherical objects has not been established yet. In the meantime the experimental determined C_{Drag} for spherical objects presented in Figure 6-3 can be applied, until better correlations are found. The lift coefficient can be expressed at uneven horizontal surfaces through:

$$C_{Lift} = 5.82 \left[\frac{d_p}{2v_x Re_p} \frac{dv_x}{dr} \right]^{0.5} \tag{6.21}$$

$$C_{Lift} = 0.09 \tag{6.22}$$

The largest coefficient of the two applies.

Cohesive force

Cohesive force is a force of attraction between particles in the mud and the bed and is classified as:

- Attraction forces without contact consist of van der Waals forces and electrostatic forces
- Attraction forces with contact consist of viscous bridges or solid bridges

One way of estimating cohesive forces is based on the slip-line theory, the start of avalanche, and is given by eqn (6.23):

$$F_{cohesive} = \frac{\pi d_p^2 \tau_y}{2} (\phi + (\pi/2 - \phi) \sin^2 \phi - \cos \phi \sin \phi) \quad (6.23)$$

ϕ is the angle of repose, and τ_y is the yield strength of the drilling fluid.

Force of gravity

The weight of the particle in the fluid minus buoyancy force is given by:

$$F_g = g \frac{\pi d_p^3}{6} (\rho_s - \rho_{fluid}) \quad (6.24)$$

These forces come into action as soon as one of the critical velocities are reached. Then lift force will bring the particle into the flow stream, and gravity will bring it back to the bed.

Critical velocity of lifting and rolling.

According to this model, when the annular mud velocity is high enough, cuttings in the wellbore will lift up to join the flowing mud. Generally, the annular mud flow velocity needs only to exceed a given critical value, known as the critical mud velocity, to reach the condition sufficient to initiate lifting / rolling of cuttings. Therefore, for a given flow rate, the concept of critical velocity lead to the existence of an equilibrium bed height that correspond to the incipient condition of cuttings transportation.

If we now consider a drilling fluid with some amount of cuttings at a given flow rate at sub-critical velocity, a cuttings bed will start to build. As it builds up, the mud velocity over the bed increases accordingly (assuming constant pump rate), until the mud velocity eventually reaches the critical value. At this condition, the bed height remains unchanged. If additional cuttings are deposited on the bed, the mud velocity in the neighbourhood of that region exceeds the critical velocity. Consequently, the flow will dislodge the cuttings from the surface of the bed. After these extra cuttings are moved downstream, the local equilibrium bed height is maintained.

A force balance for a single bed particle in the direction normal to the bed, will increase the local critical velocity sufficiently to lift the particles from the surface of the bed. After simplifications the formula reads:

$$v_x = \left[\frac{4 \left[3 \tau_y (\varphi + (\pi/2 - \varphi) \sin^2 \varphi - \cos \varphi \sin \varphi) \tan \varphi + d_p (\rho_p - \rho) \cdot (\cos \alpha + \sin \alpha \tan \varphi) \right]}{3 \rho (C_{Drag} + C_{Lift} \tan \varphi)} \right]^{0.5} \quad (6.25)$$

The local critical velocity is the undisturbed velocity, i.e. the axial velocity acting above the cuttings bed at a point that corresponds to the protruding cuttings centre at the start of lifting, as shown in Figure 6-6.

The other mechanism involved in cuttings transportation is rolling. Rolling of the particles commence when the rolling torque resulting from the drag and lift force is able to overcome the counteracting torque from gravity and cohesion forces. The local critical velocity during rolling can be obtained by equating these two torques:

$$v_x = \left[\frac{4 \left[3 \tau_y (\phi + (\pi/2 - \phi) \sin^2 \phi - \cos \phi \sin \phi) + d_p (\rho_p - \rho) \sin \alpha \right]}{3 \rho (C_{Drag} - C_{Lift} \cdot \tan \phi)} \right]^{0.5} \quad (6.26)$$

Usually, these two calculated values of local velocities are different. In such cases, the lower has to be taken to estimate the bed shear stress and the critical velocity. Finally, the mean velocity required to initiate the movement of a particle from the surface of the bed can be estimated from the lowest local critical velocity.

When the rolling torque exceeds the static torque of cohesive and gravity forces, the cuttings tend to roll along the bed. This is the most dominant and important transport mechanism in stratified solid liquid flow. The rolling torque increases with mud velocity. Rolling is somehow related to the formation of ripples. Ripples are formed when particles at a given point are rolled over the stationary part of the bed. The formation of ripple changes the drag and lift forces acting on the particles. Here we have to note that the random nature of lifting and rolling mechanisms originate from the stochastic behaviour of particle size, shape, density, rearrangement and the hydrodynamic forces of lift and drag. Therefore, it is ideal to assume a uniform process of cutting transportation over the bed and the formation of ripple has to be understood in this sense. Hence, we can say that during cutting transportation both erosion and deposition are simultaneously involved. Since only rolling and lifting are involved in this mechanistic model, no friction is involved. Dragging of a particle is less likely than rolling.

6.2.2 Empirical model

When it comes to empirical transport models, particle transport can be classified with respect to cuttings bed behaviour as illustrated in Figure 6-9. The models are classified into two layer models or, three layer models as shown in Figure 6-9. In the two and three layer models the modelling approach is based on mass, momentum and energy balance of each layer. And bed behaviour is to a large part determined by particle size:

1. Particles less than $40\ \mu$: Homogeneous suspension
2. Particles from $40\ \mu$ to $150\ \mu$: Heterogeneous suspension maintained by turbulence
3. Particles between $150\ \mu$ and $1500\ \mu$ ($1.5\ \text{mm}$): Increased rheology will lead to an increase of which sizes can be transported in a heterogeneous suspension
4. Particles larger than $2\ 500\ \mu$ transported by saltation. Otherwise stationary bed.

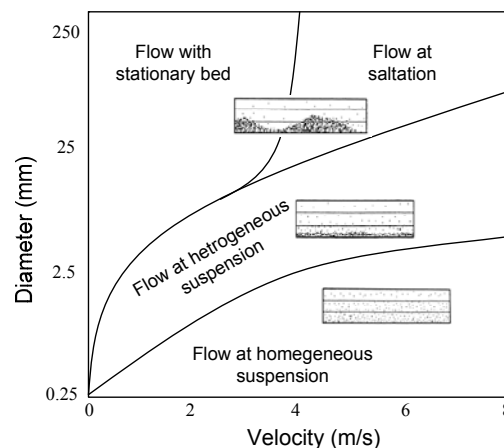


Figure 6-7: Three flow patterns for cuttings transport in deviated wells

According to Figure 6-7, decreased cutting size leads to increased shear area available to move the cutting along the wellbore. And increasing flow rate increases available energy for saltation and maintains turbulent cross flow. Higher viscosity reduces the slip velocity and increases the distance traversed during one cycle of saltation. Pipe rotation serves a dual purpose in horizontal hole cleaning. The pipe can mechanically crush cuttings to reduce cutting size; rig experience has shown that cutting size on the shale shaker is often smaller with pipe rotation. Pipe rotation tends to induce cross flow in laminar flow profiles. Tools, such as stabilizers, act to break up cutting beds.

6.2.3 Effect of barite segregation

A sub problem of directional drilling at depths where mud density is relatively high is barite segregation.

When $\rho_{\text{mud}} > \sim 1.5 \text{ kg/l}$, the barite concentration is high. At still stand, most mud types quickly develop a yield point, and barite is suspended in the gelled mud. During pumping, at flow rates in laminar mode, any existing gel is broken, and barite will not be held in suspension as during stillstand with gelled mud. However, the mud will under these conditions exhibit a high effective viscosity. Agglomeration may also effect the settling rate. Barite has a specific density of 4.2, and an average particle size of approximately $20 \mu\text{m}$. In accordance with Stokes's law of settling, barite particles will settle, but as indicated above, very slowly. However, inclination will shorten the settling distance to only a few centimetres, and a stratified bed of barite and cuttings are formed. The stratified layers of solids of different densities will, when angle of repose is surpassed, slide downwards. Angle of repose is found mainly in the build up section of the well, and here sliding takes place.

The phenomena described above are called sagging. Sagging takes place even at periods when mud is at rest, e.g. during tripping operations. Sliding may occur at any time, independent of stirring movements of the mud. But the avalanching barite will create eddies and stir the stillstanding mud and hence break the yield point, and initiate settling of barite and cuttings. There may be other effects also which maintain the disturbance of the settling; agglomerating of solids will enhance settling. A continuous, dynamic effect of sustainable settling and sliding has a dramatic effect on the operation. When the mud pump is started after a round trip, to drill further, and after barite sagging has taken place in the critical inclined part of the well, the mud density of this mud, when circulated to surface, can vary as much as 0.5 kg/l . This effect is shown in Figure 6-8, and can lead to kick, lost circulation and stuck drill string.

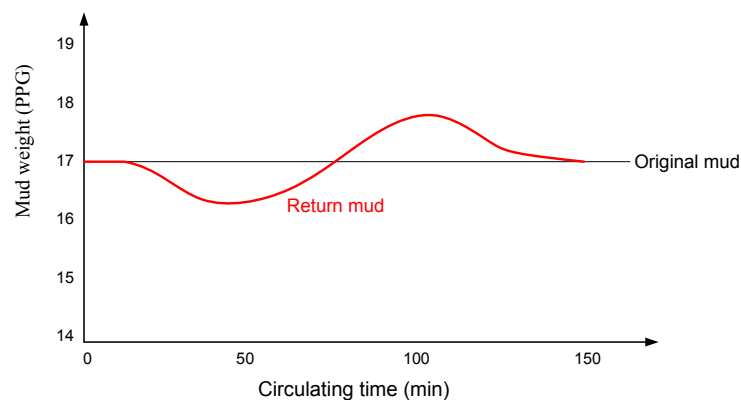


Figure 6-8: Density variation during circulation after a round trip caused by sagging in stillstanding mud.

The following summary of guidelines to obtain efficient hole cleaning is based on field experiences and on laboratory investigations:

6. Apply micro barite or equivalent. Such systems have an average particle size of 2 μm .
7. Use top drive rigs to allow for pipe rotation and redistribution of settling barite and cuttings while tripping and drilling (also with downhole motor).
8. Maximize fluid velocity during drilling and reaming by increasing pumping power and/or use large diameter drill string. This improves hydraulic and agitation of cuttings.
9. Design mud rheology so that it enhances turbulence in the annulus (if ECD allows). Turbulent flow will bring the cuttings and barite back into the flow stream if point 3 above “failed”.
10. Use various hole cleaning monitoring techniques including monitoring of drilled cuttings retrieval rate, drilled cuttings physical appearance, pressure while drilling, comparison of pick-up weight and slack-off weight (drag resistance) etc.
11. Perform frequent wiper trips.

7. Keeping wellbore within maximum and minimum pressure; ECD-control

Equivalent Circulating Density (ECD) represents the total actual bottom hole pressure exerted on the formation being penetrated and is usually presented in terms of equivalent density. ECD is the sum of the static density, the additional density increment due to the weight of drill cuttings contained in the annulus and the effect of pressure drop along the annulus. ECD effects are shown graphically in Figure 7-1, a figure that will increase the understanding of the phenomenon.

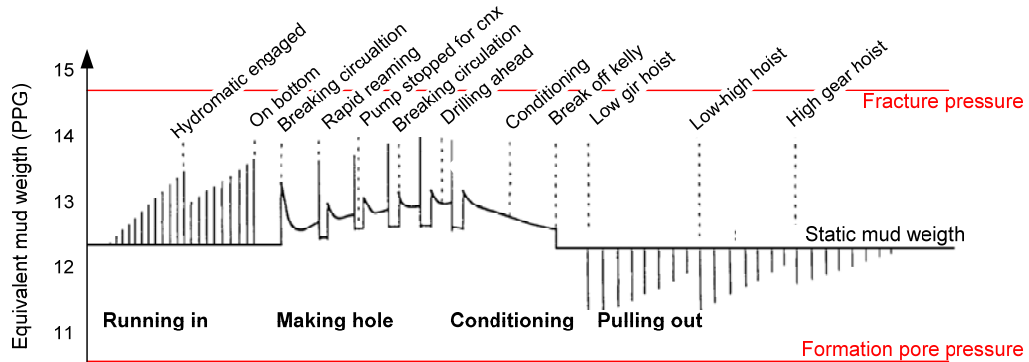


Figure 7-1: Graphical view of pressure variation during tripping and drilling.

The additional «weight» obtained as a result of the annular pressure drop may be of considerable importance when drilling through long and narrow well bores. In equation form, ECD can be expressed as:

$$ECD = \rho_{mud} + \frac{\Delta p_{annular\ friction} + \Delta p_{cuttings} + \Delta p_{surge\&\ swab} + \Delta p_{rotation} + \Delta p_{acceleration}}{gz} \tag{7.1}$$

ECD becomes more important in deeper wells as illustrated in Figure 7-2. Here the pressure window becomes narrower.

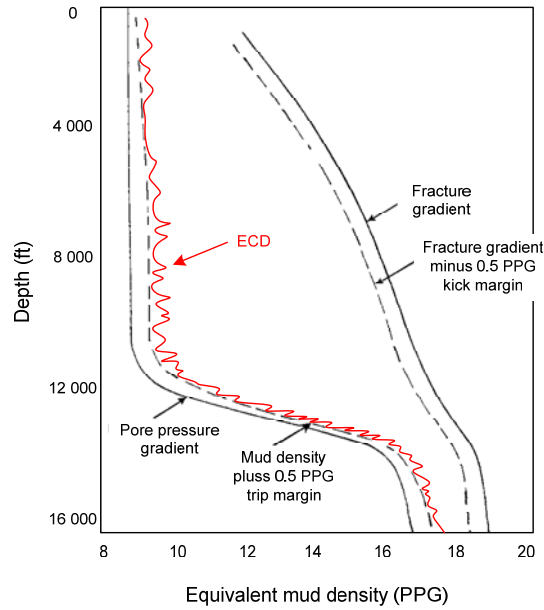


Figure 7-2: Equivalent pore- and fracture-density versus depth. Prevention of kicks, and loss of circulation, requires that down hole ECD remains within the given boundaries.

Before discussing the pressure variation in a well, we need to introduce how to produce a specific mud density.

7.1 Density control

There are two basic ways of increasing the density of water or oil; by adding Barite or salt.

Barite: The mineral barite can appear as an insoluble sediment (evaporite) Barium Sulphate, $BaSO_4$, with a specific density of typically 4.2 kg/l. The commercial product Barite is a fine powder with a medium particle size of 25 μm , but sieved to an upper particle size of 74 μm . Barite is insoluble in water and therefore said to be inert, unlike clay, polymer and salts, which all react with water.

Salt: When salt is added to water, its density is altered, and volume conversion tables must be consulted. Brines can be formulated over a range of densities as shown in Figure 7-3.

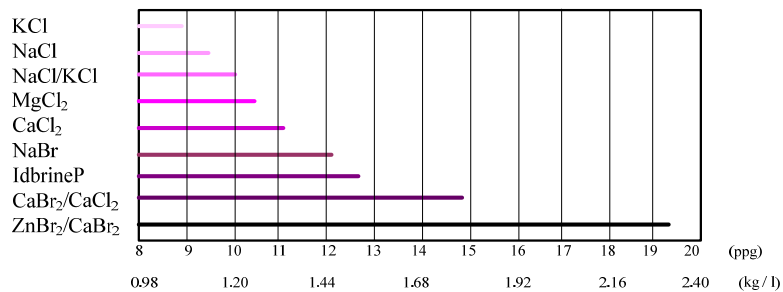


Figure 7-3: Different salts used to obtain brine density (in ppg and kg/l) when saturated at ambient⁶ conditions.

When inert components are added to the mud, they maintain their original volume, and are thus additive. For such components we can write a mass and volume balance:

$$m_1 + m_2 + \dots = \sum_{i=1}^n m_i \quad (7.2)$$

$$V_1 + V_2 + \dots = \sum_{i=1}^n V_i \quad (7.3)$$

Mass and volume of a substance are interrelated through its density:

$$\rho = \frac{\sum m}{\sum V} \quad (7.4)$$

Increasing or decreasing the density from ρ_1 to ρ_2 by means of an additive of density ρ_{add} , can be estimated through eqn (7.5):

$$\frac{V_{add}}{V_1} = \frac{\rho_2 - \rho_1}{\rho_{add} - \rho_2} \quad (7.5)$$

V_1 is the original volume of a fluid with density ρ_1 .

7.2 ECD factors

7.2.1 Mud density vs. temperature and pressure

Mud density is exposed to several effects:

- Increasing temperature, especially with increasing well depth
- Increasing hydrostatic pressure with increasing well depth
- Formation gas will expand substantially when approaching the surface and lower mud density. But the effect is negligible further down in the well since gas here is highly compressed

These density effects are all small and can for practical purposes be ignored. Pressure and temperature effects will normally neutralize each other.

Mud and especially OBM is very responsive to changes in pressure and temperature. This may affect the bottom hole pressure in cases whenever the two parameters change independently. Such situations do arise when the pump is shut off. Then a general increase in mud temperature will take place (more heating in lower part of the well than cooling in the upper part) leading to a decrease in the hydrostatic pressure. In static OBM columns, the complete heat transfer from the formation may take as much as a day. During tripping such slow density decrease combined with swabbing effects could cause kicks. Pressure testing or pressurizing the well during BOP tests or kick circulation cause compressible OBM to increase its density.

The following paragraph presents models for determining the effects of pressure and temperature on mud density.

Water and base oil (Clairsol) have been tested at a wide spectre of temperatures and pressures. The two fluids were curve fitted with respect to its individual dependency to temperature and pressure. The resulting linear curve fit to the measured data gave

$$\rho_w = 8.5 - 2.6 \cdot 10^{-3} T + 2.5 \cdot 10^{-5} p \quad (7.11)$$

$$\rho_o = 7.0 - 3.0 \cdot 10^{-3} T + 4.4 \cdot 10^{-5} p \quad (7.12)$$

Here T are in °F, p in psi and ρ in PPG. When increasing viscosity and solids concentration the constants increase by up to 50 %.

Oil based fluids are in general twice as compressible as water. The thermal expansion of OBM and WBM are less different. Another large difference between the two fluid types is the reaction time to temperature changes (due to difference in heat capacity); water reacts slower.

7.2.2 Annular friction

There is a dispute on which of the following rheological models that best describe the fluid viscosity; Newtonian, Bingham, Power law or Herschel Buckley. For the purpose of ECD estimation, we suggest simplifying by selecting only one rheological model (the best fitted) and base the estimation of constants...

7.2.3 Effect of cuttings

It is an almost impossible task to find the exact effect of cuttings on pressure. How is it possible to guess the amount of cuttings in suspension at any given time in an inclined wellbore? A rough guess is here suggested: We know how much cuttings is generated:

$$q_{\text{cuttings}} = \pi/4 \cdot d_{\text{bit}}^2 \cdot ROP \quad (7.13)$$

Most of it will settle out from time to time, some of it will be re-injected into the mud stream due to the rotation of the drill pipe; some will be lifted by the lift fore created by the mud flow. But how much? The following assumptions will bring us closer to the truth:

Cuttings beds occupy typically around 2-6 % of the cross sectional area in inclined wellbores. A rough assumption is therefore that 97 % of the generated cuttings come out at different times, the rest is deposited. When more cuttings is deposited, the flow area becomes smaller, mud velocity increases and bed erosion increases. There will be an equilibrium bed height (at least locally) for a given pump flow rate.

The original cuttings concentration at the bottom is a function of the flow rate:

$$c_{\text{cuttings,o}} = q_{\text{cuttings}} / (q_{\text{pump}} + q_{\text{cuttings}}) \approx q_{\text{cuttings}} / q_{\text{pump}} \quad (7.14)$$

In the vertical section ($I < 60^\circ$) the cuttings concentration increases due to slip, expressed through a Transport Ratio:

$$R_t = v_{\text{transport}} / v_{\text{ann}} = (v_{\text{ann}} - v_{\text{slip}}) / v_{\text{ann}} = 1 - v_{\text{slip}} / v_{\text{ann}} \quad (7.15)$$

In the vertical section the average cuttings concentration becomes:

$$c_{\text{cuttings,average}} = c_{\text{cuttings from the horizontal section}} / R_t \quad (7.16)$$

And the slip velocity is estimated through Stokes law from Chapter 6:

$$v_{\text{slip}} = d_p^2 * g (\rho_p - \rho_{\text{mud}}) / 6\pi \mu_{\text{eff}} * f_{\text{cuttings}} \quad (7.17)$$

Here the effect of concentration of cuttings is included. At high concentration there will be a hydraulic resistance to flow expressed in a satisfactory manner for our concentration range through eqn (7.18):

$$f_{\text{cuttings}} = 1 - 5 c_{\text{cuttings,average}} \quad (7.18)$$

In the horizontal section ($I > 60^\circ$) we simplify and assume that the average concentration in the mud fluctuates around the initial concentration as shown in Figure 7-4.

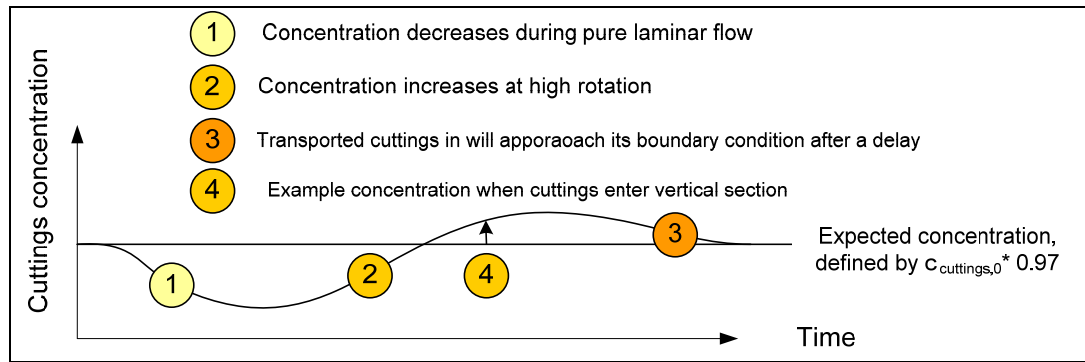


Figure 7-4: A suggested model of how to estimate cuttings concentration in the deviated part of the wellbore.

If the proposed concentration function becomes too complex, it is better to forget it and rely only on measured ECD. However, if measured ECD is not available, then you have to model it.

After constructing an average cuttings concentration function, the effect on well pressure is found by assuming that the density of cuttings is 2.3 kg/l. This is a good assumption: At shallow depths, the local sediment density may be as low as 2.0 kg/l, due to low compaction and accordingly high porosity. At large depths (> 5000 mTVD) porosity approaches zero, at which the matrix density is 2.8 kg/l for most sedimentary rocks.

Additional ECD effect in the vertical part of the well then becomes:

$$\Delta p_{\text{cuttings}} = \rho_{\text{cuttings,average}} \cdot g \cdot \text{TVD} \quad (7.19)$$

where

$$\rho_{\text{cuttings,average}} = \rho_{\text{mud}} (1 - c_{\text{cuttings, average}}) + \rho_{\text{cuttings}} \cdot c_{\text{cuttings,average}} \quad (7.20)$$

7.2.4 Surge & swab

When the drill string is hoisted up or lowered down, mud will flow in the annular space, as indicated in Figure 7-5, flow that results in pressure loss. Before applying formulas developed in the previous sub chapter, the resulting flow rate needs to be determined.

Pipe velocity, v_{pipe} , is the same as the speed of the travelling block. The resulting annular velocity, v_{ann} , becomes:

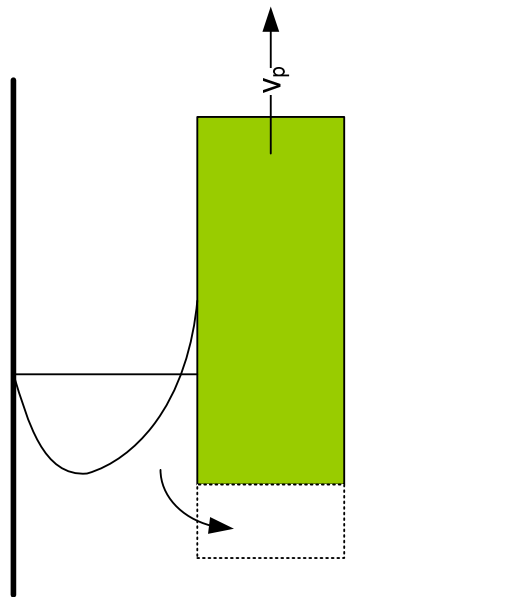


Figure 7-5: Upwards pipe movement causes downwards annular fluid flow.

$$v_{\text{ann}} = \frac{\text{rate of volume displaced}}{\text{flow area}} = \frac{v_{\text{pipe}} \cdot A_{\text{pipe}}}{A_{\text{annulus}}} \quad (7.21)$$

As indicated in Figure 7-5, the flow volume down is different from the removed volume, and must be adjusted. For this purpose we make simplifying assumptions. With uncertainty in wellbore diameter, the rudimentary are easy to accept. The two major assumptions are:

1. Closed pipe end: Assume the drill string is closed at the bottom. Displaced volume when running in hole (RIH) becomes larger than the theoretical one.
2. Clinging factor: The clinging factor d_{cling} makes mud move along the drill string as indicated in Figure 7-5, simply caused by the no-slip effect on the wall. It widens the pipe diameter. The widening effect varies with gap width vs. pipe ID. Until further notice assume that the clinging volume can be estimated by increasing the pipe diameter with 10 % of the gap:

$$d_{\text{cling}} = 1/10 * (d_{\text{bit}} - d_{\text{pipe}}) \quad (7.22)$$

Under these assumptions we obtain:

$$v_{\text{ann}} = \frac{A_{\text{pipe,eff}}}{A_{\text{ann,eff}}} \cdot v_{\text{pipe}} = \frac{(d_{\text{pipe}} + d_{\text{cling}})^2}{d_{\text{bit}}^2 - (d_{\text{pipe}} + d_{\text{cling}})^2} \cdot v_{\text{pipe}} \quad (7.23)$$

Now estimate the pressure loss along BHA in accordance with procedures in Chapter 4. The surge pressure will largely depend on the narrowness of the annulus. If the mud pump is turned on during tripping operations, which is rather unusual, v_{ann} must be adjusted accordingly.

7.2.5 Other effects

Effect of rotation: It is known that drill string rotation may have a significant impact on pressure drops in the annulus during fluid transport. During laminar flow, pipe rotation will induce an additional shear velocity component. And since drilling fluid is normally shear thinning, pipe rotation will increase total shear, reduce viscosity and thereby reduce the pressure drop.

If we solve for the rotational component in addition to the axial we may include the main features of these effects in a fundamental way. The transport equation for the rotational velocity for steady-state flow becomes:

$$0 = \frac{1}{r^2} \frac{\partial}{\partial r} \left(r^3 \mu_{\text{eff}} \frac{\partial}{\partial r} \left(\frac{v_{\theta}}{r} \right) \right) \quad (7.24)$$

The consequence of the solution of eqn (7.24) is that the effective strain rate (see Chapter 3) is increased and the effective viscosities are reduced. Hence, rotation will reduce the axial pressure drops. However, for laminar developed flows of Newtonian liquids, such effects do not exist, since viscosity is independent of shear rate.

Experience indicates that in real drilling operations the opposite often takes place; pump pressure increases with increasing pipe rotation. One explanation for this is the development of instabilities. A number of vortices develop in the radial-axial plane. Hence, rotation leads to axial-radial mixing which will have the same effect on momentum transport as turbulent mixing. Turbulent flow is shear thickening.

Effect of acceleration: Acceleration is experienced during tripping operations during pump rate manipulation, and also when a gas kick reaches the surface where expansion accelerates. High acceleration of the pipe should be avoided in critical situation, because of the acceleration pressure it creates in the corresponding fluid mass. Acceleration pressure caused by accelerating pipes, a_{pipe} , is estimated from eqn (7.25). Figure 7-5 indicates the importance of the effect of cross sectional area (d_{cling} is included).

$$\Delta p_{\text{acceleration}} = ma = \rho \cdot L \cdot a_{\text{pipe}} \cdot \frac{A_{\text{pipe,eff}}}{A_{\text{ann,eff}}} \quad (7.25)$$

Its magnitude is exemplified through running a 13 3/8" casing into a 17 1/2" hole. Let the pipe, at the depth 1000 m, accelerate 0.2 m/s². Drilling fluid density is 1200 kg/m³ and d_{cling} is 0.5". Pressure increase will then become:

$$\Delta p = 1200 \cdot 1000 \cdot 0.2 \cdot \frac{(13 \frac{3}{8} + 0.5)^2}{17.5^2 - (13 \frac{3}{8} + 0.5)^2} = 3 \cdot 10^5 \text{ Pa}$$

Effect of gelling: One more effect caused by pipe movement or pump start needs to be considered as a part of the ECD: Most mud types are time dependent and tend to build up a gelled structure when quiescent. By moving the drill string axially, extra pressure is needed to break the gel that has formed on the pipe surface. The surface shear stress relates to pressure:

$$\Delta p_{gel} = \frac{4\tau_w \cdot L}{ID_{pipe}} \quad (7.26)$$

It becomes much worse if the mud pump is used to break the gel. Then it must be broken first inside the drill string and then in the annulus along two surfaces; one surface is the drill string and the other is the wellbore. A 1000 m long 5" × 4.27" drill pipe (= 0.127 m × 0.108 m) has been at rest in a 12 1/2" (0.216 m) wellbore. The 10 minute gel strength = 50 lb/100 ft² = 50 · 0.4788 = 23.94 Pa. From eqn (7.26) we obtain: $\Delta p_{gel} = 19.6 \cdot 10^5$ Pa. This answer assumes that the fluid is completely incompressible and that the shear stress is broken simultaneously over the whole length.

However, in practice the drilling fluid is compressible, and compression and the resulting deformation of the long mud column would break the gel over a much shorter distance than the complete well length. Compressing a mud volume of 1000 l by one bar would compress it typically 0.1 liters. Such a small shrinkage would result in a deformation sufficiently large to break the gel locally. The effective length over which the gel is breaking simultaneously is shorter the higher the initial pressure. The gel breaking pressure is probably small and hidden in the acceleration pressure. Another effective method to break the gel structure in the annulus is simply to rotate the drill string.

The same reasoning must be applied when figuring out how high the drill string must be hoisted Δh before gravity force overcomes the gelled shear stress inside the drill string. Theory would show a high value, in accordance with eqn (7.27), where L is length of well:

$$\rho g \Delta h = \frac{4\tau_w \cdot L}{ID_{pipe}} \quad (7.27)$$

7.3 Temperature variation

7.3.1 Ocean and wellbore temperature profile

In order to estimate factors such as expansion of drilling fluids, change of fluid viscosity or variation in other fluid properties as a function of temperature, we need a model of the temperature variation in the well. A steady-state analytical model for computing circulating mud temperature profiles has been suggested through the API-model, a model that has gained general acceptance by the industry. Nevertheless, the model is not good enough for deep-water wells. The main reason is the cooling effect in the riser section in deep water wells as indicated in Figure 7-6.

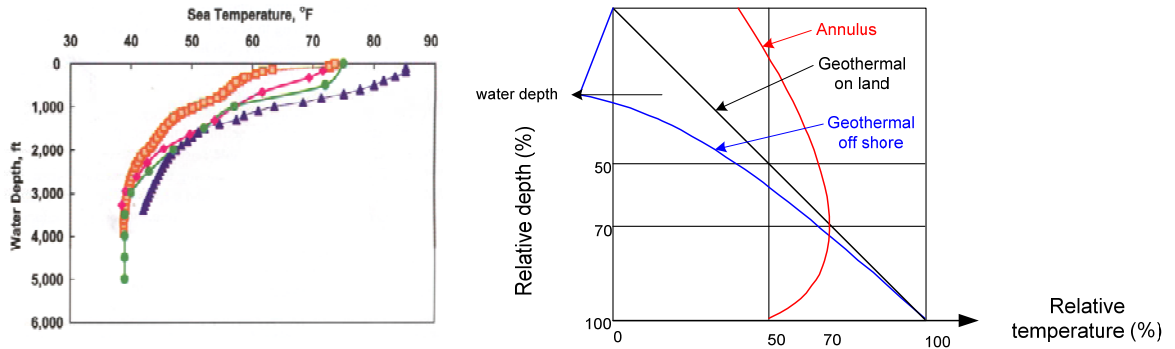


Figure 7-6: Sea temperature (left), principal wellbore temperature profile after long pumping period (right).

The heat capacity of water is high, and after shutting the pump off it may take a day, until the geothermal temperature profile is established.

When a drill string is lowered into a well and exposed to a temperature gradient, the resulting temperature distribution after pumping is initiated, assuming constant density and heat capacity, the resulting temperature is a result of convection and conduction of heat:

$$\rho c_p \cdot \frac{\partial T}{\partial t} = -\rho c_p u \frac{\partial T}{\partial z} - k \nabla^2 T \tag{7.28}$$

The first term in eqn (7.28) expresses the resulting rate or change of internal heat flux pr. unit area (W/m²). The second term expresses rate of change of convective flux (in the fluid), while the latter term expresses radially conducted heat from the material in contact with the fluid. The minus signs indicate positive flow towards a negative temperature gradient. In pipe flow both convection and conduction is involved in heat exchange on the interface between the pipe and the fluid. Our engineering task is now to find a heat transfer coefficient that is acceptable for both type of heat transfer.

The geometry of the drill pipe and the parameters involved are presented in Figure 7-7:

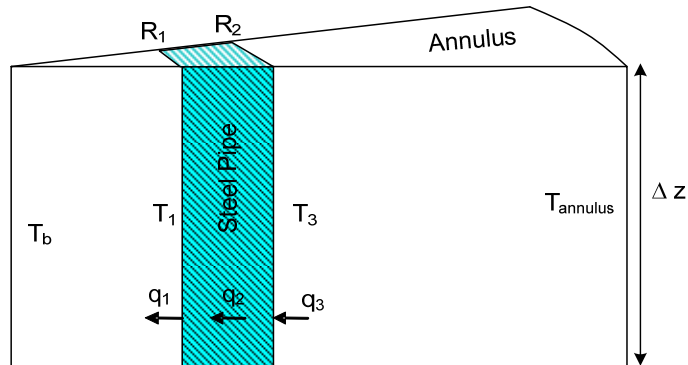


Figure 7-7: Heat transfer along and across the drill pipe steel wall (drill pipe centre to the left in the figure) from the annulus into the flowing liquid in the drill pipe. q_1 = convection (on surface)
 q_2 = conduction
 q_3 = convection (on surface)

In pipe flow heat is convected mainly through mass transport since water has a certain heat capacity. The two terms in eqn (7.1) will be discussed separately below:

7.3.2 Conduction

A simplified solution of the conductive heat transfer equation for steady state conditions, simplifies to (in Cartesian coordinates), expressed in terms of finite differences:

$$k\nabla^2 T = \frac{\partial}{\partial r} \cdot k \frac{\partial T}{\partial x} = k \left(\frac{\partial T}{\partial x} + r \frac{\partial^2 T}{\partial x^2} \right) \Rightarrow k \frac{\partial T}{\partial x} = k \frac{dT}{dx} \tag{7.29}$$

In cylindrical coordinates:

$$k\nabla^2 T = k \left(\frac{d^2 T}{dr^2} + \frac{1}{r} \frac{dT}{dr} \right) \Rightarrow \frac{k}{r} \frac{dT}{dr} \tag{7.30}$$

The final terms of eqn (7.29) and (7.30), where second order terms are neglected, represent steady state 1D conditions with constant k.

For estimation purposes we need to include the area. Annuli with small gaps can be assumed to be a flat wall of thickness r and length Δz :

$$q = -k A \cdot \frac{dT}{dr} = -2\pi r k \Delta z \frac{dT}{dr} \quad (7.31)$$

For small concentric pipes with large wall thickness, heat transfer becomes a function of the curvature. For a pipe wall, as in Figure 7-7, integrating from R_i to R_o yields:

$$q = -\frac{2\pi k \Delta z \Delta T}{\ln(R_2 / R_1)} \quad (7.32)$$

For most materials and liquids k varies 10-20 % for temperature ranges between 0 and 200 °C. Multilayer insulation will reduce conductivity by a factor of decades:

7.4.3 Convection

In Figure 7-8 heat is transferred from a flat plate of solid material into a flowing fluid. Temperature gradient (∇T) depends on how quickly heat is carried away by the fluid.

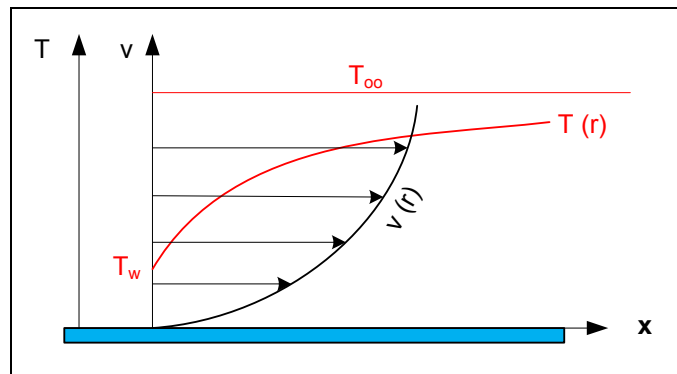


Figure 7-8: Velocity and temperature profile above a flat, cold plate.

Heat exchange (heating or cooling) of the liquid adjacent to the wall is expressed through Newton's law of convective cooling;

$$q = h A (T_w - T_\infty) \quad (7.33)$$

The convective heat transfer coefficient, h , must be determined experimentally. Holman (2001) shows how the heat coefficient can be arranged into a Nusselt Number for laminar pipe flow:

$$Nu = \frac{hd}{k} = 4.364 \quad (7.34)$$

For turbulent flow in smooth pipes, evaluated for bulk temperature, T_∞ , and valid for $0.6 < Pr < 100$ (i.e. liquids), the Nusselt Number becomes;

$$Nu = \frac{hd}{k} = 0.023 \cdot Re^{0.8} \cdot Pr^{1/3} \quad (7.35)$$

Eqn. (7.34) and (7.35) are empirical. Errors are in the order of $\pm 25\%$. Roughness (caused by tool joints etc.) must be corrected for through a higher Re-number.

If the convective heat transfer coefficient is unknown the approach is to eliminate T_2 and T_3 (the wall temperature in Figure 7-7) through the equations:

$$q_1 = q_2 = q_3 \quad (7.36)$$

7.4.4 Numerical solution

When simultaneous heat conduction and convection is taking place inside a control volume, it can be expressed on differential form:

$$\frac{\partial}{\partial t} \rho c_p T = - \frac{\partial}{\partial z} \rho u c_p T - \frac{k}{r} \cdot \frac{\partial T}{\partial r} \quad (7.37)$$

The explicit approach of finite differences is characterized by estimating the next time step on bases of information in the previous time step. If the time steps are sufficiently small a satisfactory accuracy will be maintained. Taking now the cylindrical volume ΔV as $2\pi r \cdot \Delta r \Delta z$, and assuming ρ and c_p are constants, an approximated integration of eqn. (7.37) yields;

$$2\pi r \Delta r \Delta z (\rho c_p) \frac{T(i, j, t+1) - T(i, j, t)}{\Delta t} = -2\pi r \Delta r \Delta z \cdot \rho u c_p \cdot \frac{T(i+1, j, t) - T(i, j, t)}{\Delta z} - 2\pi r \Delta r \Delta z \cdot \frac{k}{r} \cdot \frac{T(i, j+1, t) - T(i, j, t)}{\Delta r} \quad (7.38)$$

Solving eqn. (7.38) with respect to $T(i, j, t+1)$, you are on the track.

Conductivities and heat capacities for steel and water are presented in Table 7-1.

Table 7-1: Material constants for heat transfer.

Material		ρ (kg/l)	c_p (kJ/kg °C)	k (W/m °C)	Pr
Steel	20 °C	7.87	0.46	61	
Cement slurry	20 °C	2.5		0.29	
Granite	20 °C	2.64	0.82	1.7-4.0	
Cork	20 °C	0.05	1.88		
	40 °C	0.12		0.045	
Glass wool	40 °C	0.024	0.7	0.038	
Engine oil	20 °C	0.89	1.88	0.145	10400
	100 °C	0.84	2.22	0.137	
Water	20 °C	1.0	4.180	0.602	6.80
	100 °C	0.96	4.208	0.682	1.70

In liquid and solids we observe from Table 7-1 that the denser the material the higher the thermal conductivity.

8. Keeping the wellbore stable

8.1 Wellbore stability problems

Wellbore instability problems take many forms, and the most frequent ones are pointed out in Figure 8-1.

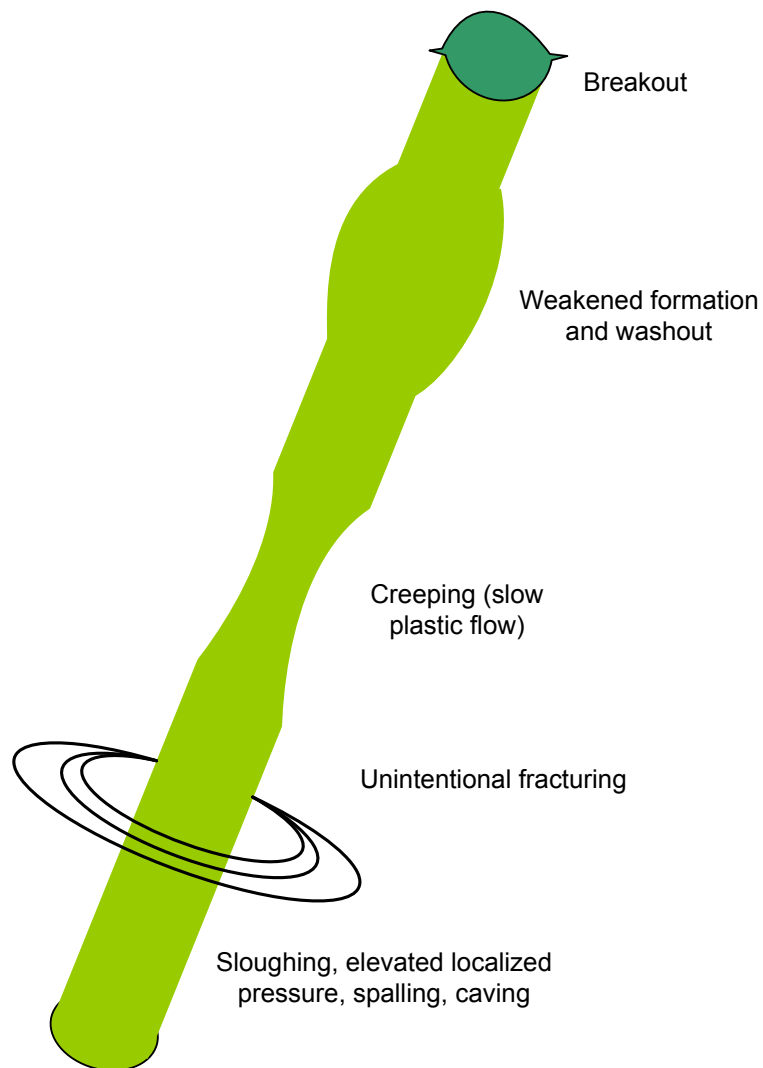


Figure 8-1: Possible wellbore instability problem during drilling.

Wellbore instability is experienced mainly in shale sections, induced by either high stress concentration or physical-chemical interactions of the drilling fluid with the shale, or a combination of both;

1. Mechanical stress-induced wellbore stability
2. Chemical related instability
 - a) Time-dependent drilling fluid-shale interaction
 - b) Time dependent water interaction with chalk, limestone, anhydrite, gypsum etc

Mechanical related stability problems are, besides minor erosion from turbulent flow and drill string interaction with the wall, governed by wellbore stresses. It is related to the vertical stresses created by the overburden. The overburden results in vertical compression / deformation, which create compressional stresses in the horizontal direction. Mechanical wellbore instability is a topic covered in courses of rock physics. In this book, mechanical wellbore instability will merely be pointed at, since it is inter-related to its chemical counterpart; water interaction with the sediments will have a negative influence on mechanical stability.

Chemical stability of the wellbore is related to water and its complex interaction with shale. The time dependency is related to the time it takes for water to be transported into the shale.

Reaction with chalk/limestone/anhydrite is related to dissolution of dissolvable material. Chalk, limestone and salt are all ionic compounds. Dissolution of them can lead to several problems:

- Flocculation of the colloidal phase of drilling fluid; clay or polymers (increasing viscosity) or aggregation of clay after ion-exchange (decreased viscosity)
- High solids content (disintegration of weakened cuttings)
- Hole enlargement (washout of weakened wall)

8.2 Filtration control

Darcy law governs filtration of liquids through porous media. However, fluid loss from the wellbore will decrease with time, since the permeability decreases continuously as particles make a tighter filter. In Figure 8-2, the spurt loss occurs at the start of a filter test, a test which is made on an initially clean filter paper. After the spurt loss, the filtrate volume becomes proportional to the square root of time.

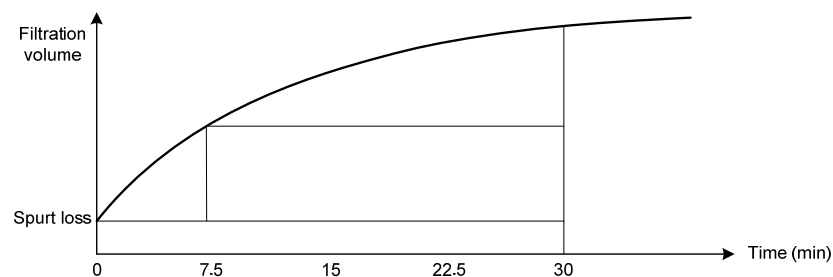


Figure 8-2: Filter press test results.

It is common to simplify laboratory procedures by decreasing test duration to 1/4 of the standard 30 minutes. The accumulated filtrate volume can be predicted from eqn (8.1);

$$q_{\text{filtrate}} = q_{\text{spurt loss}} + C \cdot \sqrt{t} \quad (8.1)$$

For example, the 30 minute filtrate volume is predicted by measuring the filtrate volume at 7.5 minutes, and doubling the value obtained, since $\sqrt{30} / \sqrt{7.5} = 2$.

In the well, spurts loss may be large when drilling through highly permeable rocks, unless the mud contains particles of the size required to bridge the pores of the rock, and thus establish an improved filter somewhat ahead of the bit. Only particles of a certain size relative to the pore size can bridge. Particles larger than the pore opening cannot enter the pores, and are swept away by the mud stream. Particles considerably smaller than the opening invade the formation unhindered. Particles of a certain critical size are caught in bottlenecks in the flow channels, and form a bridge inside the porous wall. Once a primary bridge is established, successively smaller particles, down to the fine colloids, are trapped, and thereafter only the filtrate (liquid) may invade the formation. The spurt loss period is very brief; it is a matter of seconds.

As a result of the process just described, three zones of mud particles are established in a permeable formation. This is shown in Figure 8-3.

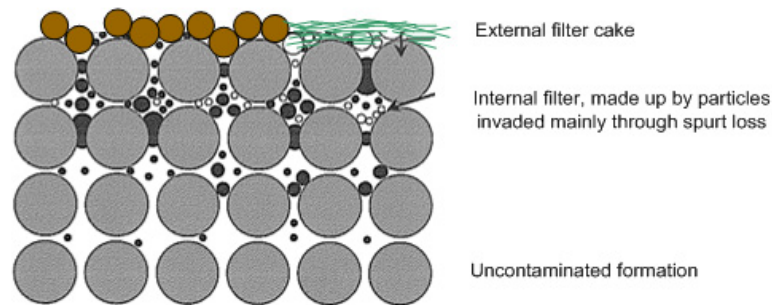


Figure 8-3: Invasion of a permeable formation by particles in the mud. The outer filter cake can be made by emulsified water droplets in oil based mud (left) and water based mud (right).

In the context of building a tighter filter it is important to supply the mud with a particle size distribution in relation to the pore size distribution of the porous formation to be drilled through. Mean particle size should be 1/3 - 1/7 of mean pore throat size. Barite and drilled particles, classified in Table 8-1, will always be available and perfect for filter building. However, at the same time these particles will interfere with the filter cake building process.

Table 8-1: Drilled solids classified by particle size.

1. Coarse	Particles greater than 2 000 microns
2. Intermediate	Particles between 250-2 000microns
3. Mediums	Particles between 74-250 microns
4. Fines	Particles between 44-74 microns
5. Ultrafine	Particles between 2-44 microns
6. Colloidal	Particles less than 2 microns

In the context of building a filter cake, a dispersed mud is the preferred mud state. Bentonite in flocculated state will experience high water loss and lead to a thick, soft filter cake. By the addition of a thinning agent (deflocculator or thinner) a thin, strong and low permeable cake will form. As a generalization, it may be said that cake permeabilities of flocculated muds are in the order of 10^{-2} mD, those of untreated fresh-water muds are in the order of 10^{-3} mD and filter cakes of muds treated with dispersants are in the order of 10^{-4} mD.

8.3 Mechanical stability

Mechanical instability can be classified into two groups;

- Stress related instability
 - o Creep: Wellbores that stays open for a long time (weeks), tend to close in.
 - o Tensile failure at high ρ_{mud} : Fractures are detected at the surface as lost circulation.
 - o Compression failure at low MW : Carvings, breakouts, leads eventually to total wellbore collapse

- Weakness in the formation
 - o Faults crossing the wellbore.
 - o Inter-bedded formations (between lithology changes, bedding angle close to wellbore angle)
 - o Naturally weak formations (coal beds, conglomerates, loose sands, etc)

To evaluate these types of instabilities we are dependent on information that can indicate what type of weakness has been encountered. Weakness in the formation, like sand and gravel often lack cementation material and are referred to as an unconsolidated formation, a problem that occurs mainly at shallow depths. The problem with unconsolidated formations is the fact that they cannot be supported by hydrostatic overbalance from the drilling fluid alone. For example, unconsolidated sand and pea gravel often fall into the hole and pack off around the drill string. Problems also occur if insufficient filter cake is deposited on loose, unconsolidated sand to prevent it from "flowing" into the well bore and packing off the hole. Solids-control equipment will be overloaded with large quantities of solids that do not correspond to the rate of penetration.

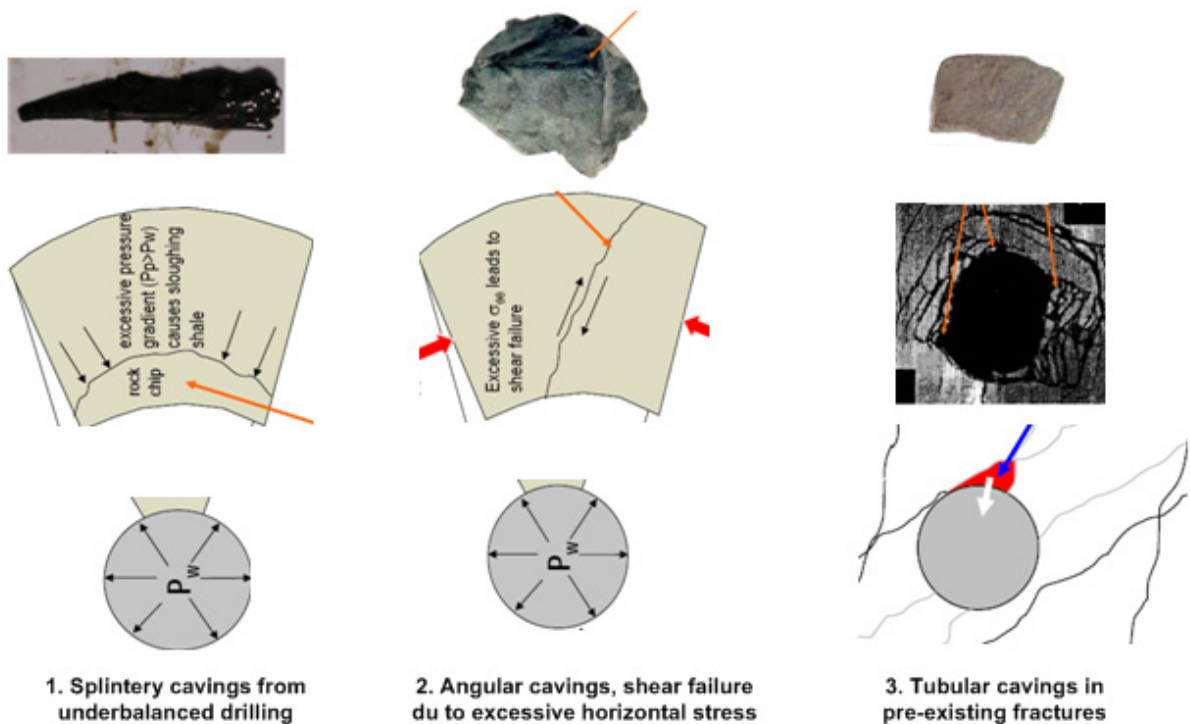
To drill such formations, the mud should provide a good-quality filter cake to help consolidate the formation so that hydrostatic pressure can "push against" and stabilize the annular wall. It is important to control the filtrate loss of the mud so that the water will not destabilize the formation. To minimize erosion, avoid any unnecessary reaming or turbulent flow opposite unconsolidated formations.

Stress related instability is related to the pore pressure and the hydrostatic pressure in the wellbore. It is also related to extraordinary in-situ stresses in the formation; historical tectonic activity in the area. Normally stressed basins are characterized by stresses in the vertical direction being the largest one. Too high wellbore pressure leads to fracture at the casing shoe, since the weakest point in the formation is located here.

By lowering the formation pressure below its collapse pressure, the formation will experience shear failure in the borehole wall resulting from high tangential stress. In older consolidated clay, which is hard and brittle, the wall will splinter under compressional stress and cave or slump into the hole. This leads to hole enlargement and possibly bridging when combined with inadequate hole cleaning. As the wellbore pressure drops further below the collapse pressure during the final stages of a gas blowout, the well will collapse and become packed with crushed wall material, and the blowout will eventually come to a stop.

During the initial stage of collapse, the cavings eventually arriving at the shale shaker can indicate what is causing the problem. The information that potentially can be gained from cabins are listed here, and also pointed out in Figure 8-4:

Geometrical Form	Cause	Countermeasure
1. Splintery cavings: Long, thin, concave surface	Drilling underbalanced in low permeable formations (shale)	- Increase MW - Monitor ECD/low trip speed - Reduce ROP
2. Angular cavings:	Un-normal stress regime vs. well path	- Optimize trajectory - Increase MW - Monitor ECD/low trip speed
3. Tabular cavings : Blocky shape with smooth, flat surfaces. Square shaped	Failure along bedding plane or cleavages in pre-existing fractures	- Improve fluid loss - Reduce hole vibration - Reduce surge / swab - Minimize back reaming



8.4 Chemical stability

Shale make up more than 75 % of the drilled formations, and more than 70 % of the borehole problems are caused by shale instability. Shale properties range from very soft to hard, and from very laminated to very compact. Shale destabilize when drilling fluid penetrate existing fissures, fractures and weak bedding planes. In addition to shale / fluid interaction, fluid invasion will also alter the pore pressure or effective stress state.

8.4.1 Swelling of shale

The term shale is used for an entire class of fine-grained sedimentary rocks that contain substantial amounts of clay minerals. The amount and type of clay content determine the shale's affinity for water. The Smectite shale type called Montmorillonite reacts strongly with water for one main reason; shale contains negatively charged clay minerals, and polar water is attracted to the mineral. Shale containing Smectite has a greater affinity for water than shale containing illite, mica, chlorite, zeonites or kaolinite.

Argillaceous rocks experience significant swelling, alteration, and degradation by adsorption of polar molecules (such as water) or ions (such as Na^+) onto weakly charged clay sites. Water is attracted to the surface of the mineral but also enters the opening between unit layers and may cause the distance between them to increase, a phenomenon called swelling. Swelling pressure can be predicted through the knowledge of the water activity in the shale and basic thermodynamic relationships. Swelling stress can be predicted by equation 8.2:

$$p_{swell} = -\frac{RT}{V} \ln\left(\frac{p}{p_o}\right) \quad (8.2)$$

Here R is the universal gas constant, V the partial molar volume of pure water, p the aqueous vapour pressure of the formation fluid, p_0 the aqueous vapour pressure of pure water. The quotient p/p_0 is very close to the value of the water activity of pore water.

When exposed to pure water, eqn (8.2) suggests that tremendous swelling pressures can be developed in relatively saline shale. Rupture tests have shown that shale sections exposed to water in a borehole can fracture if critical stress conditions exist.

To sum up, the swelling process is depending on these parameters:

- The salinity of the mud; the higher the salinity the lower the “water activity” (lower ability to react with the shale)
- The shale’s ability to swell depends on the amount of Montmorillonite in the shale
- The mechanical strength of the shale determines its ability to resist swelling

8.4.3 Bit balling

Attractive forces exist between two solid surfaces but the two surfaces do not normally adhere when pressed together, because the attractive forces are extremely short ranged (Angstroms), and the area of intimate contact is very small. Even two smooth, highly polished surfaces have microscopic irregularities, and contact is obtained only between highs, as shown in Figure 8-5.

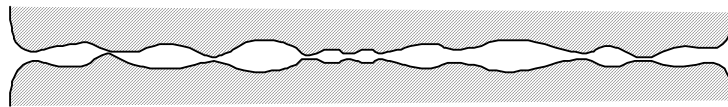


Figure 8-5: Microscopic section of two polished solid surfaces showing small area of contact.

Two plates of polished glass will stick together. It is the attractive van der Waal forces that are activated through the closeness of the two plates. And to separate the two plates a wedge must be forced in between them.

Solids can be bonded together if they are ductile enough to be forced into intimate contact. For instance, the old-time blacksmith welded two steel bars together by heating them white-hot, and hammering them together. For the same reason, shale, consisting of colloidal particles, has the ability of coming in intimate contact with the rock bit or the drill collars. Swellable, soft clays stick more easily to steel surfaces than stable clays since it is ductile and deformable, thus increasing the contact. One method of dealing with sticky gumbo is therefore to use inhibitive mud.

8.3.4 Downhole problems

In the upper formations the shale strength is lower. Shallow overburden is still relatively un-compacted, and it normally contains more Montmorillonite. In deeper sediments Montmorillonite transforms to Illite, which swell insignificantly. Some researchers claim that below 2500 m TVD, shale is chemically stable.

A typical problem in upper formation is: Shale swelling → weakened wellbore → erosion → expansion of the hole. Due to low permeability water penetrates shale very slowly. The driving force behind water transport in shale is either hydraulic pressure or osmosis. Hydraulic pressure can be excluded; the transport rate is extremely slow in shale. Only osmosis, through a salinity difference between pore water and mud, can explain water invasion leading to swelling. Swelled shale is soft and sticky. During tripping operations the expanded wellbore could possibly be scraped off by stabilizers and the bit. Material accumulated on the BHA during tripping may be observed in surface parameters as overpull and pack off (pack off is seen only when the pumps are on).

At shallow and medium depths: Typical problems at medium depths are weakening of the wellbore – erosion of the hole: The swelling process is a slow process. When one layer of shale has swelled, it is weakened, and therefore prone to erosion. The erosion could be both of hydraulic and mechanical nature. The longer the hole stays open, the higher the probability is that the wellbore has weakened. As soon as the wellbore has swelled, the erosion starts on the weakened layers, exposing new layers.

At larger depths: At greater depths the grains are eventually cemented together forming indurate shale and claystone. The problems become more related to mechanical stresses. Stresses in the wellbore of any kind leads to deformation, like creep or yielding of the wellbore material. Chemical interaction with the wellbore will in all cases lead to weakening of the formation, and therefore accelerating the instability caused by stress concentration. Cracks and permeable leads for water to attack the shale will support the weakening process.

8.5 Inhibitive muds

In the drilling fluids service industry the term «inhibition» has come to mean the suppression of hydration of clay, which means inhibit the water to transform the shale into swelled, soft, sticky shale.

8.5.1 Oil based muds (OBM)

In spite of the environmental related restrictions there are still many occasions when oil based mud of some kind is necessary. As yet, water based muds do not provide the levels of shale inhibition and lubrication offered by oil based muds. The viability of many offshore field developments depends on the ability to drill wells from a single central platform, with high lateral displacement. For many such wells, oil based muds are viewed as the only effective mud types to allow the targets to be safely and economically reached.

Oil based mud consists of these components:

- | | |
|-----------------------|------------------------------|
| 1. Base oil | - the continuous phase |
| 2. Water | - viscosifying droplets |
| 3. Emulsifier | - emulsify water in oil |
| 4. Wetting agent | - makes the wellbore oil wet |
| 5. Viscosifyer | - like in WBM |
| 6. Weighting material | - like in WBM |

The tree first items on the list make up the basic emulsion. When mixed together the result becomes like shown in Figure 8-6. Besides of lowering the interfacial tension, the emulsifier stabilizes the emulsion, because its molecules are adsorbed at the oil/water interface, forming a skin around the droplets. This skin acts as a physical barrier, preventing the droplets from coalescing when they collide with each other. The size of the droplets is in the colloidal size range. In order to create oil droplets in water or vice versa the surface tension between the two phases must be lowered, so that the droplet curvature increases and smaller droplets are formed. Two methods of measuring surface tension are presented next.

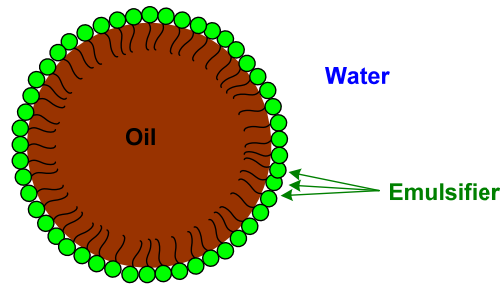


Figure 8-6: Protective skin of surfactants molecules around the surface of an oil droplet.

Figure 8-7 shows a capillary tube, where the height a liquid will spontaneously rise to is measured. At equilibrium, the contractile force of the meniscus is balanced by the hydrostatic head of the column of liquid, expressed through:

$$F = p \cdot A = \pi r^2 h \cdot \rho_{liquid} \cdot g = 2\pi r \cdot \cos \theta \cdot \sigma \tag{8.3}$$

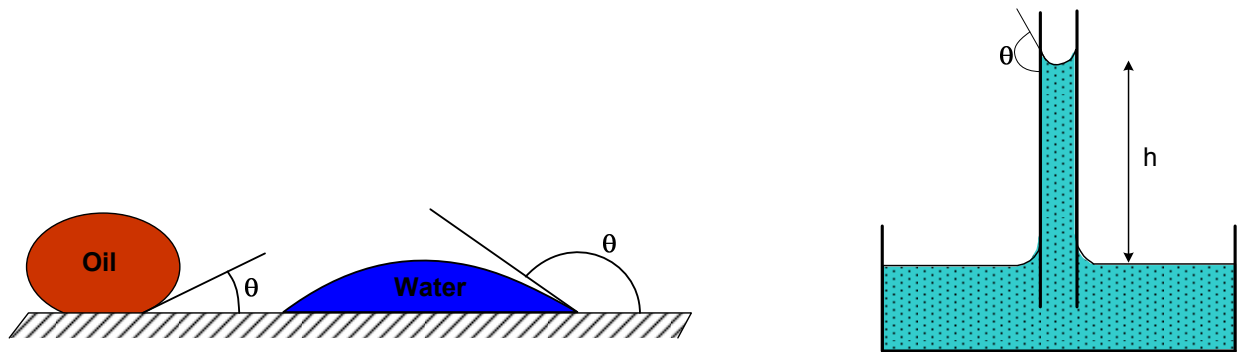


Figure 8-7: Contact angle (left). Capillary tube (right). Wetting when angle = $\theta > 90^\circ$ the solid is highly water wet.

σ is the surface tension, θ the contact angle, and r the radius of the capillary tube. The surface tension between the liquid and the contacting substance above the liquid is found by solving eqn (8.3):

$$\sigma = \frac{g h \rho_{liquid} r}{2 \cos \theta} \tag{8.4}$$

Solved for pressure ($p = \rho g h$), eqn. (8.4) takes the form:

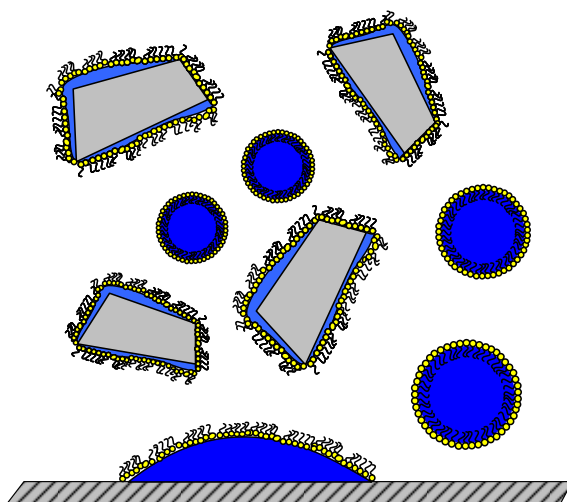
$$p = 2\sigma \cos \theta / r \tag{8.5}$$

If two immiscible liquids are juxtaposed on a surface, one liquid has preference over the other in wetting the surface, depending on the relative tension between the liquids and the solid, and on the interfacial tension. The angle θ indicates the preferential wettability. The interfacial tension between oil and water is very high, $\theta \approx 0^\circ$, so if the liquids are mixed together mechanically they separate soon after the agitation ceased, to maximize the interfacial area. Lowering the interfacial tension with a surfactant enables one of the two liquid to form very small droplets. The interfacial tension between mineral oil and water is about 50 dynes/cm, and a good emulsifier will lower it to about 10 dynes/cm.

To avoid water wetted solids or steel surfaces, add oil-wetting agents to the mud. Figure 8-8 presents the resulting condition in the wellbore.

The emulsion stability is tested with an Emulsion Stability Tester. The working principle is to determine at which voltage the currency will be short cut when immersed into the emulsion. As a rule of thumb, it is necessary with around 3 volume % of the emulsified phase to reach a maximum voltage. The stability of an emulsion increases with increasing viscosity (of the continuous phase) because the number of collisions between the droplets is decreased. Similarly, the stability decreases with increasing temperature because the number of collisions increases. The lower the interfacial tension can be made, the smaller the droplets become, and the more stable the emulsion.

Water (blue) is emulsified (yellow)
but wetting shale and cuttings (gray)



Wetting agent (red) is added

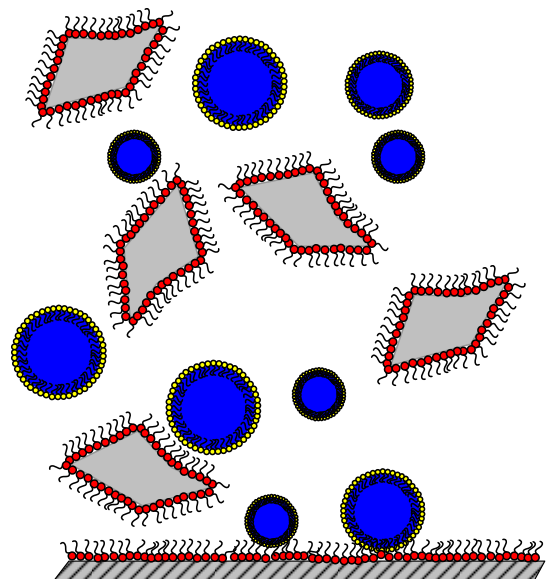


Figure 8-8: Water wetted solids (left) and oil wetted (right).

Pseudo oil based mud (POBM): The restrictions on the discharge of cuttings contaminated with mineral oil, led to the development of synthetic or natural derivative fluids which allowed synthetic oil based muds to be formulated with enhanced biodegradability and reduced bioaccumulation and toxicity, but which still possessed the high performance of mineral oil based muds. Pseudo-oil-based muds are made from:

Ester, ether, olefin and other extracts from plants and animals.

All the synthetic mud types have similar properties as mineral oil; they make emulsions (up to 50 % water in oil) by means of optimal emulsifiers, thus reducing cost and environmental impact; make wide ranges of densities and rheologies; tolerate contaminants; provide lubrication properties similar to mineral oil; similar compressibility/expansion ability as mineral oil; excellent return permeability; are thermally stable and are biodegradable.

8.5.2 Water based mud (WBM)

WBM allow water and thereby well pressure to penetrate into wellbore shale. Near wellbore pressure increases and thereby reducing the true overbalance. Without it, shear failure may occur. A perfect drilling fluid should create a high-osmotic-efficient membrane.



Although shale is almost impermeable, the osmotic flow is determined by chemical potential or water activity A_w in the mud and in the pore water. A_w is a measure of water's salinity

$$\begin{aligned} A_w, \text{ distilled water} &= 1.00 \\ A_w, \text{ saturated NaCl} &= 0.755 \\ A_w, \text{ saturated CaCl}_2 &= 0.295 \end{aligned}$$

When $A_w = 1$, the water has the lowest possible potential.

It is the difference in salinity that causes osmotic water flow, $\Delta A_w =$ chemical potential. When $\Delta A_w = 0$ between pore water and mud, there will be no osmotic flow of water, hence no swelling and accordingly no problems during drilling. Whenever there is a difference in A_w between clay and mud, the swelling pressure is defined as:

$$p_{\text{swell}} = - \frac{RT}{V_w} \cdot \ln \frac{A_{w, \text{clay}}}{A_{w, \text{mud}}} \quad (8.6)$$

Salt water muds are able to restrain the flow of water from the mud to the shale. This is accomplished by decreasing the concentration of free water molecules in the drilling fluid. In salt water muds, large quantities of NaCl or KCl are added to the mud system, and the water activity is largely reduced. When $A_{w, \text{clay}} = A_{w, \text{mud}}$, the formation will become stable. It has later become evident that also salt type must match pore water salt type to completely eliminate swelling. For limestone and salt formations this theory holds true.

One method of making a drilling fluid inhibitive is to exchange the ions present in shale to a less water absorbing ions; from the naturally occurring ions (Na^+) on clay to Ca^{++} or K^+ . Potassium is generally regarded as the most effective in making the clays less hydratable. And the geometry of Potassium ions is well suited for entering the space between Montmorillonite unit layers as indicated by Table 8-2.

Table 8-2: Diameter of some molecules (in Å).

	Not hydrated	Hydrated
H	1,6	1,6
O	1,3	1,3
H ₂ O	2,9	2,9
K ⁺	2,1	7,6
Na ⁺	1,8	11,2
Ca ⁺⁺	3,0	19,2
Na SiO ₂	6,1	6,1
Clay pore throat	10-100	

Cationic (+) polymer systems like PHPA, have proved to be very inhibitive and are excellent at minimizing problems associated with drilling massive amounts of reactive clays. PHPA have also good properties for inhibiting reactive shale. It is probably used on more wells for shale inhibition than any other polymer. Here are some popular water based systems.

PHPA + NaCl

PHPA + KCl

PAC/starch + KCl

Divalent soluble cations like calcium can react with exchange sites on two different clay platelets. They will form an «ion bridge» between the clays, and hence produce a flocculated structure. Calcium is often encountered in the form of gypsum, limestone and un-hydrated cement. If the clays in the drilling fluid are in the sodium form, then the contact with calcium ions will drastically alter the properties. Some mud systems overcome this problem by ensuring that the clays are already in the calcium form before the contaminant is encountered. Thus, lime or gypsum are added in excess to ensure a source of calcium is available. During preparation of the gyp-mud, flocculation is followed by mild aggregation of the clay; the viscosity of gyp mud is much lower than Bentonite mud.

9. References

Bourgoyne, A. T., Jr., Chenevert, M.E., Millheim, K.K. & Young, F.S., Jr.: "Applied Drilling Engineering", SPE Textbook Series, Vol. 2, 3rd edition, Society of Petroleum Engineers, Richardson (1991).

Casson, N.: "A Flow Equation for Pigment-Oil Suspensions of the Printing Ink Type", Rheology of Disperse Systems, Pergamon Press, New York, N.Y. (1959).

Chilingarian, G.V. and Vorabutr, P.: Drilling and Drilling Fluids, Elsevier Science Publishers, Amsterdam, Updated first edition (1983).

Classifications of fluids systems, World Oil (June, any year)

Darley, H.C.H. and Gray, G.R.: "Composition and properties of drilling and completion fluids", Gulf publishing company, Pittsburg, fifth edition, second printing (1991).

Drilling fluid engineering manual, Magcobar Division of Dresser Industries Inc., Houston (1982).

Drilling service companies:

Geosevices - <http://www.geoservices.com/>

Halliburton - <http://www.halliburton.com/>

M-I Swaco - <http://www.miswaco.com/> MI-Drilling Fluid Manual

Schlumberger - <http://www.slb.com/>

Google as dictionary; <http://www.google.no/language-tool/>

Govier, G.W. and Aziz, K.: "The Flow of Complex Mixtures in Pipes", E. Krieger Publishing Co., Malabar, Florida (1972).

Holman, J. P.: Heat Transfer. Eight SI Metric Edition, McGraw Hill, Printed in Singapore, 2001.

Kutasov, I.M.: "Correlation simplifies obtaining downhole brine density", Oil & Gas J. (Aug. 5, 1991) 48-49.

White, F. M.: Fluid Mechanics. International Edition, WCB/McGraw-Hill, Singapore, 1999.

Wikipedia as encyclopedia in 250 languages; <http://en.wikipedia.org/>

Aadnoy, B., Cooper, I., Miska, S., Mitchell, R. F. and Payne, M. L.: Advanced Drilling and Well technology, SPE, Richardson, 2009

10. Supportive information

10.1 Nomenclature

Latin:

A	cross sectional area	m^2
A	Angstrom, $1A = 10^{-10}$	m
c	concentration of volume fraction of particles	-
$c_{p,water}$	$= 4184 =$ specific heat, reasonably const. $[f(T)]$	$J/kg/^\circ K$
d	diameter	m
E	energy or work	W
F_R	reactive torque factor	-
f	fraction	-
G	gradient	
g	acceleration due to gravity	m/s^2
h	height	m
h_e	specific enthalpy $= c_p * T$	J / kg
h	convective heat transfer coefficient = film conduction	$W/m^2 / ^\circ K$
I	inclination of the well	$^\circ$
K	power law consistency index	Pas^n
K_L	coefficient for bit	-
k	specific thermal conductivity, k varies with p and T in similar manner as viscosity	$W/m / ^\circ K$
$k / (\rho c_p)$	thermal diffusivity	m^2s
L	length	m
m	mass	kg
m	exponent in Δp_d expression	-
M	momentum	Nm
N	number	-
n	exponent in power law (flow behaviour index)	-
Nu	Nusselt number $= h * \Delta l / k$	-
Pr	Prantl's number $= \mu c_p / k = \frac{\nu}{\alpha}$	-
p	pressure	Pa
Δp	pressure change	Pa
P	power or effect	J (W/s)
Q	heat flow $= q''A$	W
q	flow rate	m^3/s
mQ	heat flow $= q''A$	W
q''	heat flux pr. unit area $= -k \partial T / \partial x$	W/m^2
Q	heat	J
r	radial position	m

R	resistivity	-
R	radius of pipe	m
R	the gas constant = 8.31447	J/(°K*mol)
St	$Nu / (Re*Pr) = h/(\rho c_p u_\infty) =$ Strantons number	-
T	temperature	°K
V	volume	m ³
v	fluid velocity	m/s
x,y,z	Cartesian coordinates	m
\bar{v}	average fluid velocity	m/s

Greek:

α	thermal diffusivity = $k / \rho c_p$	
β	constant in Collins-Graves rheology model	-
ε	wall roughness	m
$\dot{\gamma}$	shear rate	s ⁻¹
η	high shear viscosity	Pas
μ_{app}	apparent viscosity	Pas
μ_{pl}	plastic viscosity (Bingham fluid)	Pas
π	3.1416	-
ρ	mass density	kg / m ³
σ	surface tension	Pa
τ	shear stress	Pa
θ	cylindrical coordinate (rad), readings in Fann viscometer	-
τ_o, τ_y	yield shear stress (yield point)	Pa
ν	kinematic viscosity = μ / ρ	

Subscripts referring to:

a, ann	annulus
app	apparent
bit	drill bit
c	cuttings
dc	drill collar
d	parasitic pressure drop minus Δp_{bit} in the circulating system
e	equivalent
eff	effective (viscosity)
F	Fanning
fl	fluid
h	hydraulic diameter ($d_o - d_i$)
i	initial or to arbitrary number or to inner
m	mud

M	Moody
max	maximum
mud	drilling mud
NL	no load
o	outer
p	pipe or parallel
r	radial position
Re	Reynold
s	sphere
w	water or to the wall of pipe

10.2 Abbreviations and explanations

1D	one dimensional
ADE	applied drilling engineering (SPE textbook)
BHA	bottom hole assembly
BHT	bottom hole temperature
CEC	Cation exchange capacity
CMC	Carboxyl Methyl Cellulose
CSG	casing
DC	drill collar
DP/DS	drill pipe/drill string
ECD	equivalent circulating density
GPM	gallons pr. minute
GYP	Gypsum (added to the mud)
HHP	hydraulic horse power
Hp	Horsepower
HTHP	high temperature high pressure
HWDP	heavy weight drill pipe
IADC	International Association of Drilling Contractors
ID	inner diameter
IF	impact force
LAB	linear alkyl benzene
LCM	Lost Circulation Material
Lithology	The description of a sedimentary rock. Sedimentary rocks can be classified according to grain size, color and hardness characteristic criteria to describe the lithology. A sandstone has river facies (appearance) when it has the typical litologic moves of river deposits.
MBT	Methylene Blue Test
MMS	mixed metal systems
MW	molecular weight, mud weight
MWD	measure while drilling
NS	North Sea
OBM	oil based mud, including LT(low toxic) and PO(pseudo oil) BM
OD	outer diameter
OFU	oil field units
O/W	oil water ratio
PAC	poly anionic cellulose
PDM	positive displacement motor
PHPA	partially hydrolyzed poly anion
PPB	pounds pr. barrel
PPG	pounds pr. gallon
R	Rest (of polymeric compounds)
Rheology	Rheology is the science of matter deformation and flow properties. Measuring quantities such as viscosity, elasticity and yield point. Viscosity describes the material flow behavior and elasticity describes the structure of the material.

ROP	Rate Of Penetration
SBM	synthetic oil based mud (= POBM)
SI	system international
SG	specific gravity (water = 1.00)
SPE	Society of Petroleum Engineers
TJ	tool joint
TVD	True Vertical Depth
WBM	water based mud
WOB	weight on bit
WOC	waiting on cement
WP	working pressure
YP	yield point

10.3 Definitions

moment	= torque = T (Nm)
momentum	= M (Nm)
energy	= work (W)
heat exchange rate	= Q
power	= $\dot{w} = P$ (W/s)
Isothermal process	= process at const T
Adiabatic process	= process where no heat is transferred
Isentropic process	= reversible, adiabatic (entropy is constant)
A priori	= valid independent on previous observations; non-analytic.
Ideal fluid	= a fluid where $\mu = 0$ and $\rho = konst$
$div a$	$= \frac{\partial a_x}{\partial x} + \frac{\partial a_y}{\partial y} + \frac{\partial a_z}{\partial z} = \nabla \cdot \vec{a}$ = divergence of a vector
$grad \varphi$	$= \vec{i} \frac{\partial \varphi}{\partial x} + \vec{j} \frac{\partial \varphi}{\partial y} + \vec{k} \frac{\partial \varphi}{\partial z} = \nabla \varphi$ = Gradient of a scalar field φ = a vector field
Natural convection	= heated fluid adjacent to the wall rises due to buoyancy.
Forced convection	= mass transferred heat when liquid is pumped through a pipe
Speed of sound in gas	$= c = \sqrt{k \frac{p}{\rho}} = \sqrt{kRT}$

$$\begin{aligned} \text{Speed of sound in liquid or solids} &= c = \sqrt{E/\rho} \\ \text{Elasticity or compressibility modulus} &= E_v = -V \frac{dp}{dV} = \rho \frac{dp}{d\rho} \quad (E_{\text{water}} = 2.1 \cdot 10^9 \text{ N/m}^2) \\ \text{Coefficient for thermal expansion} &= \alpha_T = \frac{1}{V} \cdot \frac{dV}{dT} = -\frac{1}{\rho} \frac{d\rho}{dT} \quad (\alpha_{T_{\text{water}}} = 1.53 \cdot 10^{-4} \text{ K}^{-1}) \end{aligned}$$

10.4 Continuity, momentum and energy equation in microscopic and macroscopic form

Continuity equation:

Microscopic

$$\text{General form} \quad -\frac{\partial \rho}{\partial t} = \nabla \cdot (\rho \mathbf{v})$$

$$\text{Cartesian coordinates} \quad -\frac{\partial \rho}{\partial t} = \frac{\partial}{\partial x}(\rho v_x) + \frac{\partial}{\partial y}(\rho v_y) + \frac{\partial}{\partial z}(\rho v_z)$$

$$\text{Cylindrical coordinates} \quad -\frac{\partial \rho}{\partial t} = \frac{1}{r} \frac{\partial}{\partial r}(\rho r v_r) + \frac{1}{r} \frac{\partial}{\partial \theta}(\rho v_\theta) + \frac{\partial}{\partial z}(\rho v_z)$$

Macroscopic

$$\frac{d \int v \rho dV}{dt} = -\Delta \rho \bar{v} A = \rho_1 \bar{v}_1 A_1 - \rho_2 \bar{v}_2 A_2$$

Momentum equation

Microscopic

$$\text{General form} \quad \rho \frac{D\mathbf{v}}{Dt} = \rho \mathbf{g} - \nabla p - \nabla \cdot \boldsymbol{\pi}$$

Cartesian coordinates
(only x-component)

$$\rho \left(\frac{\partial v_x}{\partial t} + v_x \frac{\partial v_x}{\partial x} + v_y \frac{\partial v_x}{\partial y} + v_z \frac{\partial v_x}{\partial z} \right) = -\frac{\partial p}{\partial x} + \mu \left(\frac{\partial^2 v_x}{\partial x^2} + \frac{\partial^2 v_x}{\partial y^2} + \frac{\partial^2 v_x}{\partial z^2} \right) + \rho g_x$$

Cylindrical coordinates
(only the r-component)

$$\begin{aligned} &\rho \left(\frac{\partial v_z}{\partial t} + v_z \frac{\partial v_r}{\partial r} + \frac{v_\theta}{r} \frac{\partial v_z}{\partial \theta} + v_z \frac{\partial v_z}{\partial z} \right) \\ &= -\frac{\partial p}{\partial z} + \mu \left[\frac{\partial}{\partial r} \left(\frac{1}{r} \frac{\partial}{\partial r} (r v_z) \right) + \frac{1}{r^2} \frac{\partial^2 v_z}{\partial \theta^2} + \frac{\partial^2 v_z}{\partial z^2} \right] + \rho g_z \end{aligned}$$

For steady state laminar flow, this expression reduces to

$$\frac{\partial p}{\partial z} = \frac{\mu}{r} \cdot \frac{\partial}{\partial r} \left(r \cdot \frac{\partial v_z}{\partial r} \right) + \rho g_z$$

Macroscopic
$$\frac{d}{dt} \int \rho dV = \rho_1 \bar{v}_1^2 A_1 - \rho_2 \bar{v}_2^2 A_2 + p_1 A_1 - p_2 A_2 - F + Mg$$

F is the resultant shear force acting on the system, M the total mass flow ($\int \rho dV$). The steady state, one dimensional pipe flow the macroscopic expression reduces to: $p_1 A_1 - p_2 A_2 - F = Mg \sin \theta$.



Energy equation

Microscopic

$$\text{Conservation of energy: } \frac{\partial Q}{\partial t} - k \nabla^2 T = 0 \text{ (for incompressible flow)}$$

Macroscopic

$$\left(\frac{p}{\rho g} + \frac{\bar{v}^2}{2g} + z \right)_{in} + h_{pump} = \left(\frac{p}{\rho g} + \frac{\bar{v}^2}{2g} + z \right)_{out} + h_{friction}$$

First bracket-term is called useful or total head. $\frac{p}{\rho g} + z$ is called the hydraulic head while $\frac{\bar{v}^2}{2g}$ the velocity head.

10.5 Hydraulic friction loss equations

	Newtonian model	Bingham model	Power law model
Lam. pipe	$\Delta p_p = \frac{32\bar{v}\mu L}{d^2}$	$\Delta p_p = \frac{32\mu_{pl} \cdot L \cdot \bar{v}}{d^2} + \frac{16L\tau_o}{3d}$	$\Delta p_p = 4K \left(\frac{8\bar{v}}{d} \cdot \frac{3n+1}{4n} \right)^n \cdot \frac{L}{d}$
Lam. annulus	$\Delta p_a = \frac{48\bar{v}\mu L}{(d_o - d_i)^2}$	$\Delta p_a = \frac{48\mu_{pl} \cdot L \cdot \bar{v}}{(d_o - d_i)^2} + \frac{6L\tau_o}{d_o - d_i}$	$\Delta p_a = 4K \left(\frac{12\bar{v}}{d_o - d_i} \cdot \frac{2n+1}{3n} \right)^n \cdot \frac{L}{d_o - d_i}$
Turb. Pipe. ann.	$\Delta p = \frac{0,092 \cdot \rho_m^{0,8} \cdot \bar{v}^{1,8} \cdot \mu^{0,2} \cdot L}{d_h^{1,2}}$	$\Delta p = \frac{0,073 \rho_m^{0,8} \cdot \bar{v}^{1,8} \cdot \mu_{pl}^{0,2} \cdot L}{d_h^{1,2}}$	$\Delta p = a \cdot N_{Re}^{-b} \cdot \frac{4L}{d_h} \cdot \frac{1}{2} \rho \bar{v}^2$ $a = (\log n + 3,93)/50$ $b = (1,75 - \log n)/7$
Eff. viscosity, pipe	$\mu_{eff} = \mu$	$\mu_{eff} = \mu_{pl} + \frac{\tau_o d}{6\bar{v}}$	$\mu_{eff} = \left(\frac{8\bar{v}}{d} \cdot \frac{3n+1}{4n} \right)^n \cdot \frac{Kd}{8\bar{v}}$
Eff. visc. ann.	$\mu_{eff} = \mu$	$\mu_{eff} = \mu_{pl} + \frac{\tau_o (d_o - d_i)}{8\bar{v}}$	$\mu_{eff} = \left(\frac{12\bar{v}}{d_h} \cdot \frac{2n+1}{3n} \right)^n \cdot \frac{Kd_h}{12\bar{v}}$
Shear rate pipe	$\dot{\gamma} = \frac{8\bar{v}}{d}$	$\dot{\gamma} = \frac{8\bar{v}}{d} + \frac{\tau_o}{3\mu_{pl}}$	$\dot{\gamma} = \left(\frac{8\bar{v}}{d} \cdot \frac{3n+1}{4n} \right)$
Shear rate ann.	$\dot{\gamma} = \frac{12\bar{v}}{d_y - d_i}$	$\dot{\gamma} = \frac{12\bar{v}}{d_o - d_i} + \frac{\tau_o}{2\mu_{pl}}$	$\dot{\gamma} = \left(\frac{12\bar{v}}{d_o - d_i} \cdot \frac{2n+1}{3n} \right)$
General Re_{pipe}	$Re = \frac{d^n \cdot \bar{v}^{2-n} \cdot \rho}{K_p \cdot (8^{n-1})}$	$K_p = K \cdot \left(\frac{3n+1}{4n} \right)^n$	Fanning $f_{lam} = 16/Re$
General Re_{ann}	$Re = \frac{d^n \cdot \bar{v}^{2-n} \cdot \rho}{K_a \cdot (12^{n-1})}$	$K_a = K \cdot \left(\frac{2n+1}{3n} \right)^n$	Fanning $f_{lam} = 24/Re$

10.6 Determine Rheological Constants – Regression Analysis

Generally, the best fit is evaluated through the least squares method. In this method, the best fit is considered to be that instance of the model for which the sum of squared of the difference between an observed value and the value given by the model has the lowest value.

Regression analysis can broadly be divided into two categories – linear regression and nonlinear regression. In linear regression, a straight line is fitted to the observed data values while a nonlinear model is fitted in case of nonlinear regression.

For the project, linear regression is used for the Newtonian and the Bingham plastic model while nonlinear regression is used for the Power Law and the Herschel-Bulkley model to calculate the rheological constants.

Tools for Regression Analysis:

Specialist programs such as Microcal Origin, Sigma Plot or Graphpad Prism are available for regression analysis. These programs are capable of fitting user-input functions to data. However these programs are expensive. Also these programs are difficult for the novice to learn as they are aimed at experienced users with mathematical background.

An alternative method to fit non-linear functions is to use Microsoft Excel. Excel is included in the computer package as part of the Microsoft Office and hence requires no additional expense.

Excel offers a user friendly interface, flexible data manipulation, built-in mathematical functions and instantaneous graphing of data.

Excel also contains the SOLVER function which can be used to fit data with non-linear functions. In addition, Excel can directly be used for linear regression analysis.

Linear Regression Using Excel:

For linear regression analysis using MS Excel, the data have to be put in the spreadsheet using two columns – one for the independent variable and the other for the dependent variable: shear rate and shear stress respectively. Afterwards ‘Data Analysis’ has to be chosen from the ‘Tools Menu’ and the option ‘Regression’ has to be selected from the dialog box for performing linear regression.

In linear regression, a linear function is used to describe the relationship between the independent and the dependent variables. The linear function can be in the following form:

$$y = mx + c$$

The parameters m and c are calculated by:

$$m = \frac{n \cdot \sum xy - \sum x \cdot \sum y}{n \cdot \sum x^2 - (\sum x)^2}$$

$$c = \frac{\sum y \cdot \sum x^2 - \sum x \cdot \sum xy}{n \cdot \sum x^2 - (\sum x)^2}$$

The coefficient of determination (denoted by r^2 for linear regression and R^2 for nonlinear regression) expresses the proportion of variance in the dependent variable explained by the independent variable and is defined as:

$$r^2 = 1 - \frac{\sum (y - y_{model})^2}{\sum (y - y_{mean})^2}$$

The closer the r^2 value is to 1, the better the fit. It is to be noted that for determining apparent viscosity for the Newtonian model using linear regression provided by the MS Excel the 'Constant is zero' box in the 'Regression' dialog box has to be checked. For the Binghamian model, this need not to be done since the intercept in this case is not zero.

Nonlinear Regression Using Excel⁷:

A method called 'Iterative Nonlinear Least Squares Fitting' can be used for nonlinear regression analysis. Like linear regression, this minimizes the value of the squared sum (SS) of the difference between data and fit. However unlike linear regression, it is an iterative or cyclical process. In this case, an initial estimate of the parameter values is made based on prior experience of the data or a sensible guess based on knowledge of the function used to fit the data.

The first iteration involves computing the SS based on the initial parameter values. The second iteration involves changing the parameter values by a small amount and recalculating the SS. This process is repeated many times to ensure that changes in the parameter values result in the smallest possible value of SS.

Several different algorithms can be used in non-linear regression including the Gauss–Newton, the Marquardt–Levenberg, the Nelder–Mead and the steepest descent methods. However, SOLVER uses another iteration protocol. It is based on the robust and reliable generalized reduced gradient (GRG) method.

All of these algorithms have similar properties. They all require the user to input the initial parameter values and use these values to provide a better estimate of the parameters employing an iterative process. All of these methods should yield the same parameter values with the same set of data.

For determining the rheological constants using nonlinear regression analysis, the initial values of the constants are determined by using the field approach. Nonlinear regression has been used for the Power Law and the Herschel – Bulkley model.

The procedure for nonlinear regression using MS Excel is outlined as follows:

- Insert the experimental values for shear rate and shear stress in two columns of the spread sheet
- Calculate shear stress using the formula for the corresponding model (i.e. Power Law or the Herschel – Bulkley model) in the third column using the rheological constant values those were calculated by adopting the field approach
- Calculate the mean of the experimental shear stress
- Calculate the degrees of freedom by subtracting the number of parameters or rheological constants in the model from the number of data points
- Calculate the standard error in shear stress by using the following formula:

$$S.E = \sqrt{\frac{\sum (y - y_{model})^2}{df}}$$

In Excel this formula must be expressed as an array formula by pressing Ctrl+Sift+Enter.

- Calculate the R² value
- Calculate the confidence interval (CI) of the fit at a significance level of 95 % by inserting the following built in formula for the critical *t* value:
- `tinv(0.05,df)`
- Calculate the upper confidence limit by adding CI to y_{model} and lower confidence limit by subtracting CI from y_{model}
- Open the solver function and iterate to maximize R² by changing the parameter values

Figure 10-1, 2 and 3 show images of the spreadsheet which has been used for regression analysis to determine the rheological constants taking data for all the six rotational speeds of the Fann viscometer into consideration. In addition, it also shows the improved curves obtained from the regression analysis.

Experimental Results		Shear Rate		Shear Stress		Initial values of rheological constants using field approach:				
Rotor Speed	Dial Reading	(s ⁻¹)	(Pa)	Bingham	Power Law	Herschel-Bulkley				
RPM	degree	τ_0 (Pa)	μ_p (cp)	τ_0 (Pa)	k	τ_0 (Pa)	k	τ_0 (Pa)	2.2839	
600	38	1021.80	19.29	7.11	0.43					
300	26	510.90	13.20	12	0.5475				0.2019	
200	22	340.60	11.17					m	0.6398	
100	15	170.30	7.61							
6	5	10.22	2.54							
3	4	5.11	2.03							

Bingham Model (Linear regression)		Using Regression Analysis		Model Shear Stress	R ²
Shear Rate	Shear Stress	τ_0 (Pa)	μ_p (Pas)	(Pa)	
(s ⁻¹)	(Pa)				0.945
1021.80	19.29	3.57102	0.01671	20.64	
510.90	13.20			12.11	
340.60	11.17			9.26	
170.30	7.61			6.42	
10.22	2.54			3.74	
5.11	2.03			3.66	

Figure 10-1: Data and regression analysis of the Bingham model.

Power Law Model (Nonlinear regression)		Model Shear Stress		Upper CI	Lower CI	K	0.67127
Shear Rate	Shear Stress	(Pa)	(Pa)			m	0.48211
(s ⁻¹)	(Pa)	(Pa)	(Pa)			Mean	9.305
1021.80	19.29	18.96	19.31	18.60		df	4.000
510.90	13.20	13.57	13.93	13.21		SE	0.483
340.60	11.17	11.16	11.52	10.80		R ²	0.996
170.30	7.61	7.99	8.35	7.63		Critical t	0.741
10.22	2.54	2.06	2.42	1.70		CI	0.358
5.11	2.03	1.47	1.83	1.12			

Herschel-Bulkley Model (Nonlinear regression)		Model Shear Stress		Upper CI	Lower CI	τ_0	1.15069
Shear Rate	Shear Stress	(Pa)	(Pa)			k	0.36165
(s ⁻¹)	(Pa)	(Pa)	(Pa)			m	0.56477
1021.80	19.29	19.26	19.42	19.10		Mean	9.305
510.90	13.20	13.39	13.56	13.23		df	3.000
340.60	11.17	10.89	11.05	10.73		SE	0.212
170.30	7.61	7.73	7.90	7.57		R ²	0.999
10.22	2.54	2.49	2.66	2.33		Critical t	0.765
5.11	2.03	2.06	2.22	1.90		CI	0.162

Figure 10-2. Regression analysis of Power-Law and Herschel-Bulkley model.

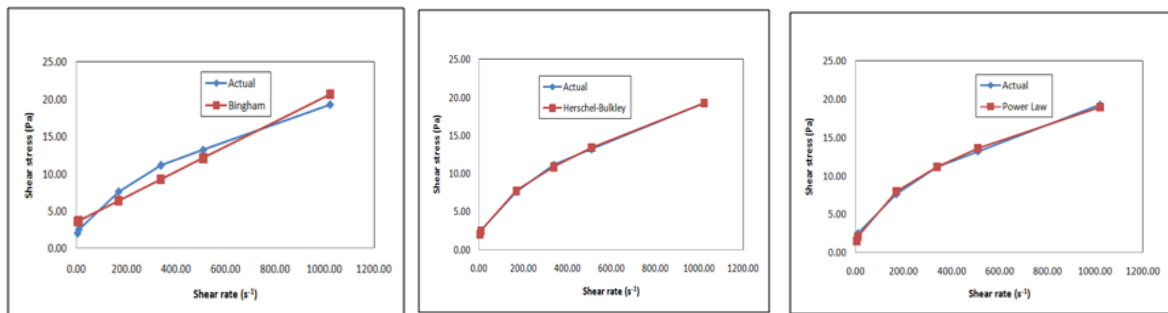


Figure 10-3: Regressed results for Bingham model, Power-Law model and Herschel-Bulkley model

10.7 Unit conversion factors

Variable	Symbol	Oil Field Units	Engineering	SI	OFU * factor = SI	
Fluid	Mass	m	lb	kg	kg	0.4536
	Density	ρ	lb/gal (PPG)	kg/l	kg/m ³	119.8264
	Viscosity	μ	cP	cP	Pa*s	10 ⁻³
	Yield Point	τ_y	lb/100 ft ²	m bar	Pa	0.4788026
	Additives		lb/bbl (PPB)	g/l	kg/m ³	2.853010
Geo- metry	Depth	D	ft	m	m	0.3048
	Diameter hole	d_{well}	in	mm	m	0.0254
	Diameter nozzle	d_{nozzle}	1/32nd in	mm	m	.00079375
	Volume	V	ft ³	l	m ³	2.8315*10 ⁻⁵
	Volume	V	gal	l	m ³	3.785412*10 ⁻³
	Volume	V	bbl	l	m ³	0.158987
Opera- tional	Flow rate	q	gal/min (GPM)	l/min	m ³ /s	6.309020*10 ⁻⁵
	Velocity	v	ft/min	m/min	m/s	5.08*10 ⁻³
	Force	F	lb _f	kg _f	N	4.448
	Force	F	dyne		N	10 ⁻⁵
	Force	F	kilogram-force	kilopond	N	9.81
	Pressure	p	psi	bar	Pa	6894.76
	Power ⁸	P	Hp	KW	W	745.7
	Power ⁹	P	Hp	Hp	W	735.5
Temperature	T	°F	°C	°K	(°F-32)/1.8	

10.8 Viscosity and density of liquids vs. temperature

Table 10.3: Absolute density and viscosity of water at 1 atm and different temperatures.

T, °C	ρ , kg/m ³	μ , Pa*s (*E-3)
0	1000	1.788
10	1000	1.307
20	998	1.003
30	996	0.799
40	992	0.657
50	988	0.548
60	983	0.467
70	978	0.405
80	972	0.355
90	965	0.316
100	958	0.283

Endnotes

¹ A list of general references are found in Chapter 9.

² Gyp = gypsum. A list of abbreviations are presented in Chapter 10.2

³ CEC is a relative measure of water-shale reactivity and a measure of clay amount in mud

⁴ SI = System Internasjonale

⁵ Since there are 3 unknown we need 3 data points

⁶ 15 °C and 1 bar_a.

⁷ This section was written by D. Chowdhury in his MSc thesis at NTNU, Trondheim, 2009.

⁸ In OFU: 1 Hp = 550 lb_f * 1 ft/s

⁹ In SI units: 1 Hp = 75 kp * 1 m/s